2015

Detection, identification and localization of R/C electronic devices through their unintended emissions

Vivek Thotla

Department: Electrical and Computer Engineering

DETECTION, IDENTIFICATION AND LOCALIZATION OF R/C ELECTRONIC DEVICES THROUGH THEIR UNINTENDED EMISSIONS

by

VIVEK THOTLA

A DISSERTATION

Presented to the Faculty of the Graduate School of the

MISSOURI UNIVERSITY OF SCIENCE AND TECHNOLOGY

In Partial Fulfillment of the Requirements for the Degree

DOCTOR OF PHILOSOPHY

In

Electrical Engineering

2015

Approved by:
Dr. Maciej J. Zawodniok, Advisor
Dr. Jagannathan Sarangapani
Dr. Mohammad Tayeb Ahmad Ghasr
Dr. Steve Grant
Dr. Sriram Chellappan

PUBLICATION DISSERTATION OPTION

This dissertation consists of four articles prepared in the style prescribed by the journals in which they were published.

Pages 8-35, “Detection of Super-Regenerative Receivers Using Hurst Parameter”, were published in IEEE Transactions on Instrumentation and Measurement, in Nov. 2013. An earlier conference version of this paper was published in Proc. SPIE 8359, (2012).

Pages 36-69, “Detection and Localization of Multiple R/C Electronic Devices Using Array Detectors”, were published in IEEE Transactions on Instrumentation and Measurement, in Jan.2015. The conference version was published in Instrumentation and Measurement Technology Conference (I2MTC), 2012 IEEE International, May 2012.

Pages 70-96, “Detection of Multiple R/C Devices Using MVDR and Genetic Algorithms”, were resubmitted with minor revisions in IEEE Transactions on Instrumentation and Measurement. The conference version was published in Instrumentation and Measurement Technology Conference (I2MTC), 2014 IEEE International, May 2014.

Pages 97-124, “UAV based detection of R/C devices”, will be submitted to IEEE Transactions on Instrumentation and Measurements. Earlier work on this paper was submitted to Proc. SPIE 8387, Unmanned Systems Technology XIV, 83870H, May 1, 2012 and Instrumentation and Measurement Technology Conference (I2MTC), 2013 IEEE International , May 2013.

ABSTRACT

The accurate and reliable detection of unintended emissions from radio receivers has a broad range of commercial and security applications. This thesis presents detection, identification, and localization methods for multiple RC electronic devices in a realistic environment. First, a Hurst parameter based detection method for super-regenerative receivers (SRR) has been used for detection. Hurst parameter based detection method exploits a self-similarity property of the SRR receiver emissions to distinguish it from background noise. Second paper presents a novel detection and localization scheme of multiple RC electronic devices called Edge-Synthetic Aperture Radar (Edge-SAR). It employs cost-effective, mobile antenna-array detectors. Two types of RC devices are considered: SRR with H parameter method and super heterodyne receivers (SHR) with peak detection method. Third paper improves detection of multiple devices by proposing a dynamic antenna-array processing method called VIVEK-MVDR-GA. It combines multi-constrained genetic algorithm (GA) and minimum variance distortion-less response (MVDR) method to increase accuracy of detection and localization of multiple devices. Finally, a 4-element array mounted on an unmanned aerial vehicle (UAV) is proposed to overcome multipath and reflection due to environmental surroundings and improve the response time in compromised scenarios. Also, a time based correlation method is proposed for array detectors to identify the line of sight (LOS) and non-line of sight (N-LOS) signals. A normalized error correlation function has been implemented to improve the estimation of angle of arrival (AOA) in the presence of strong non-line of sight (N-LOS) signals.

ACKNOWLEDGMENTS

"Guru Brahma Gurur Vishnu, Guru Devo Maheshwaraha

Guru Saakshat Para Brahma, Tasmai Sree Gurave Namaha"

First and foremost, I would like to extend my heartfelt and sincere thanks to my advisor Dr. Maciej Zawodniok for having the faith in me and giving me this opportunity to work for him as a PhD candidate. Dr. Z, as I call him, is the best advisor anybody could ask for. I really appreciate the time, energy and funds he invested in me in order to make my experience as a PhD candidate productive, fun and full of learning. His support as an advisor and a mentor is unmatched and priceless. I would also like to extend my sincere thanks to Dr. Jagannathan Sarangapani who has been a true inspiration for me. He has been the light guiding me through everything. His advice on research and life has proven to be very helpful and will remain with me for the rest of my life. I would also like to thank Dr. Tayeb for mentoring me during my PhD. I have learned a lot from him. The knowledge I have acquired working with him has helped me excel as a PhD candidate. I would like to thank my committee members Dr. Steve Grant and Dr. Sriram Chellappan for their extraordinary feedback that helped me improve the standard of my dissertation. Finally, I want to thank my parents Amar Prakash Thotla and Padma Thotla who are above everyone in my life. They have been my biggest support system throughout and I can't thank them enough for all the sacrifices they've made so I can concentrate on my work. Special thanks to Sneha for being the best companion ever. She has been a great moral support through my toughest times. My time at Missouri S&T was made memorable and enjoyable in large part due to the many friends that became a part of my life. I am thankful for all the help, fun times, late nights and memorable trips.

TABLE OF CONTENTS

Page

LIST OF ILLUSTRATIONS

PAPER I

PAPER II

LIST OF TABLES

1. INTRODUCTION

Detection, identification and localization of multiple R/C electronic devices through their unintended emissions have many applications in security and surveillance. There are two common type of radio frequency (RF) based receivers: 1) a super-heterodyne receiver (SHR), and 2) super-regenerative receivers (SRR). The SHR employs a crystal oscillator that determines the operating frequency. Walkie-talkies and cell phones are examples of such SHR based devices. SRR are low-cost and low bandwidth devices when compared to SHR. Also, they are easily reconfigurable. SRRs are found in a number of electronic circuits such as RC cars, wireless doorbells, garage door openers etc. In contrast to SHR, SRR contains a feedback loop that acts as a quench oscillator.

Theoretically any R/C device with a switching network emits unintended emissions. These emissions are low power and mostly masked by noise. The major challenge is detecting the emissions from the devices under high noise conditions. In practical situations there might be multiple of such devices. Detection of multiple devices and being able to differentiate between line of sight (LOS) and non-line of sight (NLOS) is another major challenge. After detection of the unintended emissions a localization method is required to determine the exact location of the devices under practical conditions. The development of a process to solve the above mentioned major challenges in detection, identification and localization through unintended emission is presented in this dissertation.

Initial work on detection of unintended emissions used a signal to stimulate the emissions from a SRR. A matched filter was used for detection of these stimulate

emissions. The use of a lookup table with the spectrum of known devices was also suggested. Based on the lookup table method a neural network was designed and trained to identify devices with known emission characteristics. The trained neural network was then used to match unknown emissions to the closest receiver type. In general, these existing detection methods require prior knowledge of frequency, bandwidth and profile of the device. Also, environmental noise plays a major role in detection of devices. These existing methods fail when power of emissions from the receiver is low, at or below the noise level.

The first paper presents a novel second order self-similarity based method to detect the unintended emissions from a super regenerative receiver (SRR). SRR contains a feedback loop that acts as a quench oscillator. The unintended emissions are a shaped response of noise caused by the filter in the SRR. When SRR receives a signal, its internal quench oscillator modulates the received signal. Modulation leaks from the quench oscillator results in unintended emissions. The quench signal allows for detection and identification of SRRs. Also, previous study indicates that a sinusoidal stimulating signal enhances the emissions of the SRR. The self-similar property of these emissions is used for detection of these devices. Self-similarity is a phenomenon that displays the long range statistical similarities of a process.

Hurst parameter is used to quantify the self-similarity property of the emissions. Rescaled adjusted range (R/S) method is used for the estimation of H parameter. Hurst parameter is also used to determine the range of detection instead of traditional received signal strength (RSS) based methods. It is shown that Hurst parameter based method

detects the signal when the signal fades into the noise floor (RSS methods fail in this condition).

The main contributions of the first paper are: (1) mathematical modeling of a super regenerative receiver with a sawtooth quench signal, (2) analysis of the frequency spectrum of unintended emissions for self-similarity, (3) analysis of the variation of H parameter for ideal SRR emissions and in the presence of Gaussian noise, Brownian noise, and (4) experimental validation of the simulations with a doorbell, (5) analysis of the variation of H parameter with distance for a doorbell.

One of the major challenges in detection of R/C devices is multiple device detection. Previous studies present different methods for detection of devices using their passive emissions. However, analysis of detection of multiple devices and interference due to multiple devices has not been adequately addressed. Also, localization of single device and multiple devices is considered a topic of significant interest.

Array processing has been used previously for detection of multiple active sources. An antenna array gives angle of arrival (AOA) information of the signal and also the signal strength. This allows for spatial differentiation of emission sources. With the presence of multiple devices, emissions can interfere with each other causing errors in detection and ranging. Spatially differentiating emissions from multiple devices is a challenge when several devices are present.

In the second paper, a cost effective mobile 4-element array detector has been designed with phased array processing for detection of multiple super heterodyne receivers (SHR). Angle of arrival information from peak detection method is obtained from the measurements of 4-element array that can be used for localization. It has also

been shown that 4-element array increases the range of detection compared to a single antenna detector. The proposed architecture for the array detector employs wide band antennas to detect devices with emissions of different frequencies and to distinguish among multiple devices with similar profiles. Hurst parameter based method is also combined with 4-element array based detector for detection of multiple super regenerative receivers (SRR). Furthermore, a bigger array (8-element array) has been utilized to increase the range of detection.

A 2-D array has also been proposed for localization of devices with SHRs using the angle of arrival. A new synthetic aperture radar (SAR)-based scheme called edge synthetic aperture radar (ESAR) is also introduced in this paper for localization. The results for localization and error in localization are analyzed and a comparison of these methods has also been presented. The ESAR method reduces the error in localization up to 75% and increases accuracy in detection of multiple devices.

The main contributions of the second paper are: (1) performance evaluation of array processing based detection and localization of multiple devices with passive emissions in terms of detection range, detection of multiple devices, and point of failure for varying number of antenna elements, (2) design of a new detection and localization scheme called Edge SAR (ESAR), and (3) analysis of error in detection for different non-uniform topologies of 4-element arrays. Experimental results are included herein to demonstrate the performance of the proposed schemes.

Some of the major problems for detection of multiple devices using array detectors are 1) multiple reflections, 2) multipath, 3) correlated sources and, 4) closely spaced devices. Reflections, multipath propagation, and scattering create phantom

sources of signal. Also, interference due to presence of multiple closely spaced devices results in errors and false detection. It is important to overcome the interference due to other devices by jamming the signal for accurate detection. Previously, various adaptive array-processing techniques have been used for detection of multiple entities like partition linear interference canceller (PLIC), auto-focusing algorithm using steepest descent (SD) and minimum variance distortion-less response (MVDR). Steepest descent has been used for iteratively changing the focusing angles for beamforming and MVDR is used to null stationary and non-stationary interferences. Also, gain from a particular angle of arrival can be enhanced. Nulls applied to jam signals from a particular direction can be used to reduce interference. Previous methods assume different noise models and use received signal strength for detection of active sources. These methods fail in the presence of multiple coherent sources and closely spaced sources. MVDR fails when direction of main beam is closer to the direction of null.

Genetic algorithms (GA) have been used for search and optimization. GA can be applied to any cost function with multiple constraints to obtain a solution. The concept of GA has been extended to array processing with the array factor as the cost function and the position of peaks and nulls as constraints to obtain an optimized set of weights. This can be used to increase the directivity in one direction while jamming signal from other directions.

The novel detection scheme presented in the third paper combines self-similarity and received signal strength indicator (RSSI) based detection with minimum variance distortion-less response (MVDR) method. Also, detection accuracy is improved using multi-constrained genetic algorithms. RSSI method detects multiple devices from

received signal strength and Hurst parameter identifies self-similar SRR devices. MVDR improves detection of multiple devices by jamming unwanted signals and signals from known angle of arrival (AOA). Regularization reduces variation in detection due to environmental noise. Multi-constrained genetic algorithm is implemented in cases where MVDR fails.

The main contributions of the third paper are: (1) study of major challenges in detection of multiple SRR's, (2), analysis of failure for MVDR based detection, (3) developing a novel detection scheme that combines RSS, Hurst parameter, MVDR and GA and, (4) analysis of detection for the proposed approach under different conditions. Experimental results for real time data are also included.

The methods presented in the papers above are ground based detection methods. The sensors (antennas/arrays) are usually attached to vehicles or other installations on the ground. Reflections and multipath are the major reasons for detection errors. Obstacles / installations in the environment are the prime reason for reflections. Detection can be improved by having maximum line of sight (LOS) detection. One of the best ways to eliminate the effect of the reflections and obtain LOS is by using UAV (unmanned aerial vehicle) based detection. Unmanned aerial based vehicles (UAV) have been used for surveillance and many other security applications. It is predicted that the use of UAV's for different applications will be dominant in the near future. One of the major advantages of UAV's is the low risk factor in its applications. UAV's can be guided remotely and can be used for sensitive applications involving detection and identification. The UAV can easily be used to do a first step surveillance over a given area. Detection using a UAV eliminates many reflections due obstacles on the ground and have a higher

probability for line of sight (LOS) detection. Also, a normalized error correlation function is used to identify LOS signals under strong non-line of sight NLOS conditions.

PAPER

I. DETECTION OF SUPER REGENERATIVE RECEIVERS USING HURST PARAMETER

ABSTRACT

The accurate and reliable detection of unintended emissions from radio receivers has a broad range of commercial and security applications. This paper presents and analyzes Hurst parameter-based detection method for super-regenerative receivers (SRR). Super regenerative receivers are low cost, easily manipulated, and widely used in common remote devices including doorbells, garage door openers, and remote controlled (R/C) toys. By design the SRR is a passive device that should only receive an RF signal. However, it also emits a low power, unintended electromagnetic signal. Such unintended emissions are enhanced by the presence of a known stimulating signal. Also, the emission is referred to as a device signature since it can uniquely identify the devices. The proposed detection method exploits a self-similarity property of such emissions to distinguish it from background noise. Hurst parameter quantifies the self-similarity. It is employed to detect and identify the SRR-based devices even if the signal fades into a noise.

1. INTRODUCTION

Detection of unintended emissions from low cost receivers has many potential applications. Such low cost receivers of employed in a number of consumer products where detection and tracking of such devices, for example on an airplane, improves safety and security. Furthermore, such low cost and low power devices would be ideal for localization and tracking applications. We have studied and observed the unintended emissions of such devices in their inactive state. These emissions are low power and have a signature specific to the receiver. The unintended emissions can be used to detect and identify the presence of a particular device in the environment [1]–[7]. Moreover, unintended emissions of receivers can be enhanced by a stimulating signal to increase the efficiency of detection [2][7].

There are two, common types of radio frequency (RF) based receivers: 1) a superheterodyne receiver (SHR), and 2) super-regenerative receivers (SRR) [8][9]. The SHRs are expensive and operate on a wide range of frequencies. The SHR employs a crystal oscillator that determines the operating frequency. Walkie-talkies and cell phones are examples of such SHR based devices. In the past, a stimulated signal was used to enhance emissions from a superheterodyne receiver and a matched filter was used for detection [5][7]. Other detection methods characterized unintended emissions and a cascading cross correlation method for detecting passive emissions from the device [2]. Also, a look up table method with the spectrum of known devices was used to identify the receiver. Artificial neural networks were trained in other methods [3]–[7] using signatures of emissions from a set of known receivers. The trained neural network then matches unknown emissions to the closest receiver type. In general, these existing

detection methods require prior knowledge of frequency, bandwidth and profile of the device. Also, environmental noise plays a major role in detection of devices. Finally, the existing methods fail when power of emissions from the receiver is low, at or below the noise level.

Super regenerative receivers (SRR) [8][9] are low-cost and low bandwidth devices when compared to superheterodyne receivers (SHR). Also, they are easily reconfigurable. SRRs are found in a number of electronic circuits such as RC cars, wireless doorbells, garage door openers etc. In contrast to SHR, SRR contains a feedback loop that acts as a quench oscillator. The unintended emissions are a shaped response of noise caused by the filter in the SRR. When SRR receives a signal, its internal quench oscillator modulates the received signal. Modulation leaks from the quench oscillator results in unintended emissions. Harmonics in the received emissions determine the quench signal of SRR. The quench signal allows for detection and identification of SRRs. Also, previous study indicates that a sinusoidal stimulating signal enhances the emissions of the SRR.

In this paper, the proposed detection method of SRR utilizes statistical properties of its frequency spectrum. Mathematical modeling and simulations of SRR justifies the inherent self-similar property of the emissions. Measure of self-similar property of the received emissions forms the metric for detection of SRR based devices.

Self-similarity is a phenomenon that displays the long range statistical similarities of a process. It can also be defined as a property in which a part of the process is similar to the overall process. The degree or measure of self-similarity is defined via Hurst parameter (H). Mandelbrot (1965), Mandelbrot and Wallis (1969) originally introduced

the concept of self-similarity and its estimation for communication systems. Rescaled adjusted range (R/S method) [12][13] is one such method that was used to estimate 'H'. Beran[11] extended the concept of self-similarity and R/S method to data analysis including Ethernet/Internet traffic. Other methods for estimation of the Hurst parameter include a periodogram method [13], aggregate variance method [13], and variance time plot [13][14]. A similar method [1] was used for detection of a SRR, where a second order self-similarity model was used in time domain. In [1] there is no profound analysis on mathematical modeling of SRR and self-similarity method for detection. The paper considers only a few cases of measurements of an SRR. Whereas, in the proposed paper an in-depth analysis of self-similarity estimation of super regenerative receivers is presented along with the variation of Hurst parameter with distance. An ideal case of SRR is simulated from the mathematical model and H parameter is estimated with different noise components added to it. Furthermore, the probability of detection is estimated for different range measurements and also some interesting observations have been put forth.

The main contributions of the paper are: (1) mathematical modeling of a super regenerative receiver with a sawtooth quench signal, (2) analysis of the frequency spectrum of unintended emissions for self-similarity, (3) analysis of the variation of H parameter for ideal SRR emissions and in the presence of Gaussian noise, Brownian noise, and (4) experimental validation of the simulations with a doorbell, (5) analysis of the variation of H parameter with distance for a doorbell.

2. OVERVIEW

A brief overview of the method and its operation is presented in this section. Figure 2.1 shows a block diagram of the proposed approach. A doorbell with a low cost super regenerative receiver is considered for the following experiments. The super regenerative receiver is first stimulated with a sinusoidal signal at its operating frequency. The stimulating signal results in enhanced unintended emissions from the SRR. The unintended emissions due to quench modulation are then captured by the receiving antenna. The signal-processing unit filters and amplifies the emissions. Finally, R/S method is used to calculate Hurst parameter of the frequency spectrum of processed emissions.

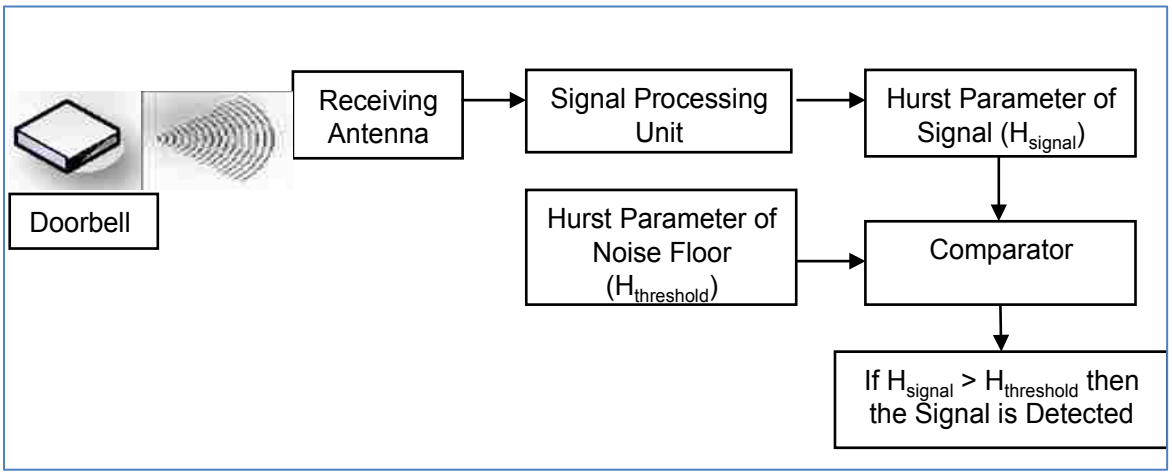

Figure 2. 1. Block diagram for Hurst parameter based detection

The detection threshold for Hurst parameter is determined based on the variation of the Hurst parameter for the background noise in the given area. First, we calculate the range of H values for the noise signal. Then, we determine the maximum H for the background noise. The threshold is equal to the maximum H for noise. The threshold can

be determined offline for the given area or calculated online using a moving window of measurements. The latter will adapt to changing environment but could fail to detect a slow approaching device that slowly increases the threshold.

The existence of self-similar emissions from a SRR device increases Hurst parameter of the frequency spectrum compared to the Hurst parameter of background noise. This increase in H parameter reveals the presence of SRR device. Ideally, self-similarity of frequency spectrum of the signal from the device (e.g. a doorbell) is independent of signal power. Hence, detection using Hurst parameter (Second Order Self Similar Property) is more accurate when compared to the traditional methods including received signal strength (RSSI) based detection, cross correlation.

3. MATHEMATICAL MODELING

In this section, the mathematical model of the super-regenerative receiver (SRR) emissions and R/S method of Hurst parameter calculation are presented. In particular, Section 3.1 derives the mathematical model of the unintended emissions generated by the super-regenerative receiver (SRR). Subsequently, in Section 3.2, the effect of SRR emissions on the Hurst parameter value is analyzed theoretically by applying the R/S method to the derived SRR signal model.

3.1 SUPER REGENERATIVE RECEIVER.

Super-regenerative receivers (SRR) have been used for many years and have the most popular receiver design. The SRR characteristics include high gain, low cost, low power consumption, simplicity, and a self-similar profile in frequency domain due to usage of the quench oscillator. Another notable property of the SRR is its constant demodulated output for different stimulating signals.

The closed feedback loop of a SRR alternates between periods of oscillation resulting in quenching. Quench oscillator determines length of the interval for the oscillations. It has also been modeled as a selective network with a feedback amplifier. The feedback amplifier has a variable gain $K_a(t)$ controlled by the signal from quench oscillator. The feedback helps in controlling the regenerative actions and the quench signal controls the period of stability and instability of the system. The block diagram model of a generic SRR is shown in Figure 3.1 and Figure 3.2.

Figure 3. 1. Circuit of a doorbell used for experiment

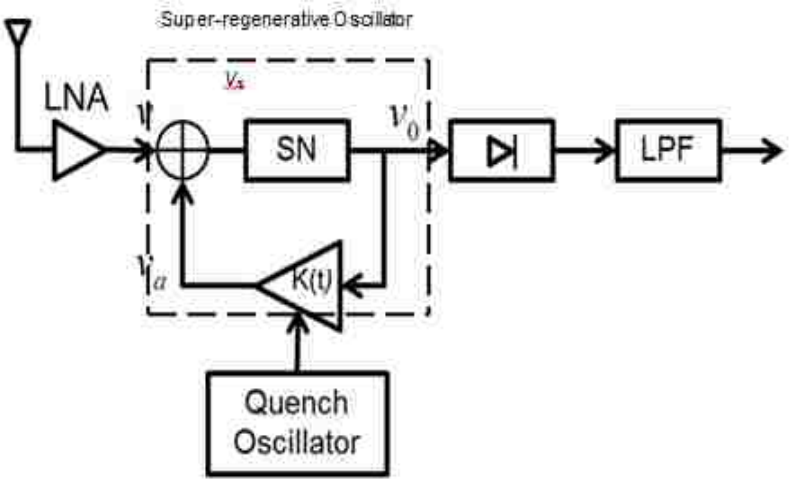

Figure 3. 2. Block diagram of SRR

The emitted SRR response is derived from the SRO for one quench cycle, *(t_a, t_b)*. [8] [9]. For analyzing self-similarity of the unintended emission we employ the following response model:

$$v_O(t) = VK_0K_sK_rp(t)\cos(\omega_0 t + \phi) \quad (3.\ 1)$$

where K_0 is the maximum amplification, ω_0 is the frequency of oscillations, $\emptyset$ is the initial phase. Other terms in (3.1) include:

The super regenerative gain given by

$$K_s = e^{-\omega_0 \int_0^{t_b} \varsigma(\lambda) d\lambda} \tag{3. 2}$$

The regenerative gain for a constant quiescent damping factor ς_0 , is expressed as

$$K_r = \varsigma_0 \omega_0 \left[\int_{t_a}^{t_b} p_c(\tau) s(\tau) d\tau \right] \tag{3.3}$$

The normalized envelope of the SRO output is described by

$$p(t) = e^{-\omega_0 \int_{t_b}^{t} \varsigma(\lambda) d\lambda} \tag{3.4}$$

The sensitivity curve is given by

$$s(t) = e^{\omega_0 \int_0^{t} \varsigma(\lambda) d\lambda} \tag{3.5}$$

The instantaneous damping factor of the SRO with $K_a(t)$ denoting the gain of the buffer amplifier is given by

$$\varsigma(t) = \varsigma_0 (1 - K_0 K_a(t)) \tag{3.6}$$

In summary, the response is a product of the envelope of the SRO and the cosine wave at the tuned resonant frequency, assuming V and K = K_0 K_s K_r as constants.

3.2 RESCALED RANGE METHOD FOR CALCULATION OF HURST PARAMETER.

Beran [10] stated that a self-similar stochastic process is precisely or closely similar to a part of the rescaled process. Hurst parameter H, determines the degree of self-similarity. A Hurst parameter value H of a process, that satisfies 0.5< H < 1 is self-similar. A value below 0.5 implies that the process is not self-similar. For a stochastic

process '*x'* defined at discrete instances, the rescaled range of *'x'* over an interval 'N' is defined as the ratio R/S.

$$\frac{R}{S} = \frac{\max_{1 \le j \le N}\left[\sum_{k=1}^{j}(X_k - M(N))\right] - \min_{1 \le j \le N}\left[\sum_{k=1}^{j}(X_k - M(N))\right]}{\sqrt{\frac{1}{N}\sum_{k=1}^{N}(X_k - M(N))^2}} \tag{3.7}$$

where M(N) is a sample mean over the period *N*.

$$M(N) = \frac{1}{N}\sum_{j=1}^{N} X_j \tag{3.8}$$

The numerator (R) in (3.7) measures the Rescaled or dynamic range of the process and the denominator (S) is the Standard deviation. For large values of *N*, the Hurst Parameter is related to R/S ratio by the following equation:

$$\frac{R}{S} \sim (N/2)^H \quad ; when\ H > 0.5 \tag{3.9}$$

In logarithmic scale (3,7) is expressed as

$$log[R/S] \sim H\log(N) - H\log(2) \tag{3.10}$$

The slope of the first order curve fitting for a plot of $log[R/S]$ versus *N* on a log-log graph determines the value of H parameter.

4. ANALYSIS OF DETECTION

Theorem: For an ideal SRR, R/S method detects the self-similarity of its response with Hurst parameter close to 1.

Proof: In this section the expressions for ideal case of SRR with R/S method applied to the periodogram or frequency spectrum of the response is derived. Consider fq as the sawtooth quench signal of SRR, assume an activating signal at frequency (fc) and the maximum gain to be 1, the response of the SRR from (3.1) is:

$$v_O(t) = s(t)\cos(wt) \tag{4.1}$$

$$w = 2 * \pi * fc \tag{4.2}$$

where $s(t)$ is the sawtooth waveform of frequency fq. With the sampling frequency fs, the condition fq<fc<fs holds good for equations (4.3) and (4.4).

The sawtooth waveform in time domain can be written as [16]

$$s(t) = t - \lfloor t \rfloor \tag{4.3}$$

The discrete form of the above response (after sampling) is expressed as:

$$v_O(n) = [nT_s - \lfloor nT_s \rfloor] * \left[\cos\left(2\pi f_c(nT_s)\right)\right] \tag{4.4}$$

The Hurst parameter of the frequency spectrum of the signal is estimated using the R/S method. Taking the FFT of $v_O(n)$ results:

$$X_k = \sum_{n=0}^{N-1} v_0(n) e^{\frac{-i2\pi nk}{N}}; N = \frac{T_q}{T_s}, T_q = \frac{1}{f_q} \tag{4.5}$$

In equation(4.4), ‘fc’ is assumed to be an even multiple of ‘fq’. This assumption reduces the computation complexity of FFT. With “fc = even multiple of fq” the FFT of one period (period of quench cycle) is same for all other time periods.

The value of $v_O(n)$ is replaced by (4.4):

$$X_k = \sum_{n=0}^{N-1} nT_s \cos(w_c nT_s)\, e^{\frac{-i2\pi nk}{N}} \tag{4.6}$$

For $0 < nT_s < 1$, $[[nT_s]] = 0$. The cosine term is replaced by exponential terms using the Euler's formula:

$$X_k = \sum_{n=0}^{N-1} \frac{nT_s}{2} \left[e^{iw_c nT_s} - e^{-iw_c nT_s}\right] e^{\frac{-i2\pi nk}{N}} \tag{4.7}$$

$$X_k = \frac{T_s}{2}\left[\sum_{n=0}^{N-1} \left[ne^{in(w_c T_s - w_N k)} - ne^{-in(w_c T_s + w_N k)}\right]\right] \tag{4.8}$$

The following relation can be used to simplify (4.8):

$$\sum_{i=0}^{n-1} iZ^i = \frac{Z - nZ^n + (n-1)Z^{n+1}}{(1-Z)^2} \tag{4.9}$$

where $w_N = 2\pi/N$, and $\sum X_k$ is the process tested for self-similarity.

Figure 4.1 shows the ideal response of SRR with Gaussian noise. Rescaled range (R/S) method calculates the difference between maximum and minimum value of the variance in the bursts of signal considered and is divided by its standard deviation. With increase in burst size of the ideal SRR signal, R/S value of the signal increases. This is due to increase in variance of the signal for more sample points.

The emissions from an ideal SRR (quench signal) have a frequency spectrum with a Hurst parameter of 1. In general noise is not a self-similar process. Hence, emissions from SRR distorts in the presence of noise thus decreasing the Hurst parameter below 1. However, the response still remains self-similar (i.e. H>0.5) till the noise becomes significantly stronger than the self-similar component.

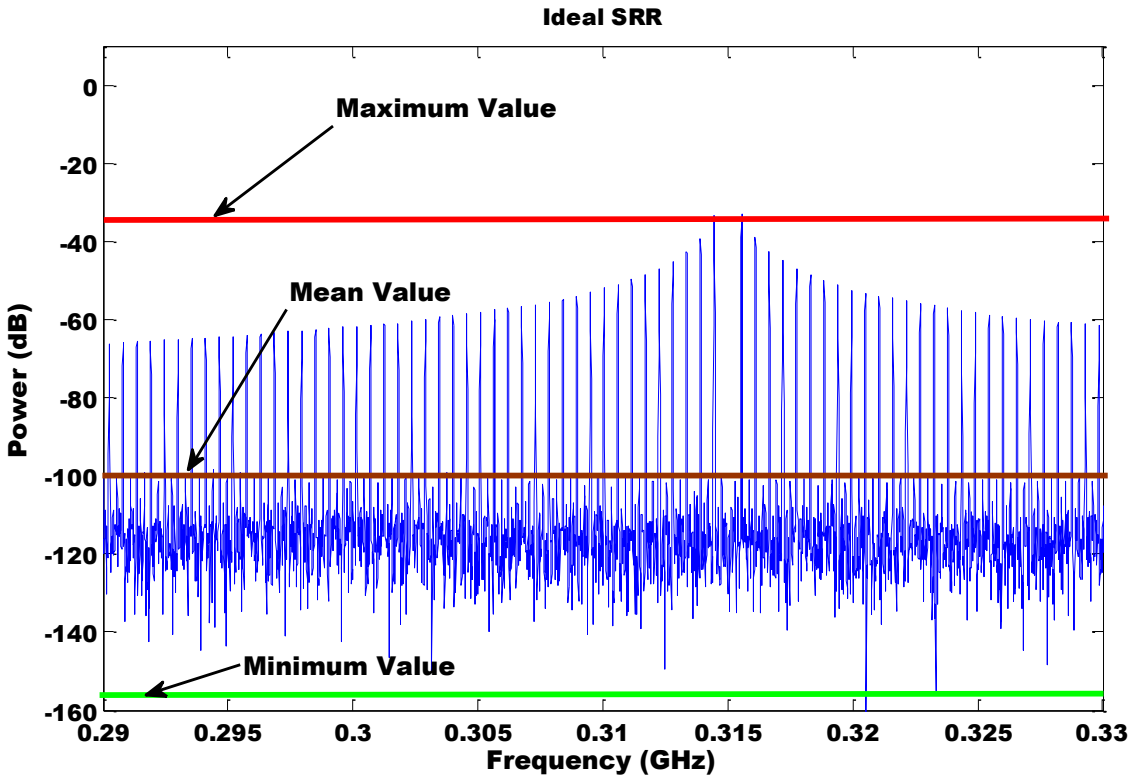

Figure 4. 1. Ideal response of SRR with Gaussian noise

Three applications of Hurst parameter for SRR are considered in this paper: (a) detection, (b) ranging, and (c) probability of detection.

4.1 DETECTION.

The presence of SRR device is detected when the Hurst parameter exceeds a detection threshold. The threshold is equal to the maximum value of Hurst parameter of a background noise. For simulations, the frequency spectrum of response to a stimulating signal of an ideal SRR is tested for self-similarity using R/S method. Also, the Hurst parameter of the response of ideal SRR is calculated for different SNR values and noise components. Adding Gaussian noise to the ideal SRR signal (4.10) results in a combined signal represented by [16].

$$v_O(t) = s(t)\cos(wt) + n(t) \tag{4.10}$$

The frequency spectrum of equation (4.11) is described by

$$V_O(f) = S(f) + N(f) \tag{4.11}$$

$$H_O = H(V_O(f)) \tag{4.12}$$

$$H_N = H(N(f)) \tag{4.13}$$

where H(.) represents the Hurst parameter value of the process. H_o greater than H_N confirms the presence of the device.

4.2 ESTIMATION OF MAXIMUM RANGE OF DETECTION.

Range of detection plays a major role in many security applications. The detection of security threat from larger distances increases the chances for safe neutralization of the threat. For estimation of maximum range the device is placed at different distances from the receiving antenna. Hurst parameter is then estimated for each of the distances. The distance at which Hurst parameter of the received signal is same as that of threshold value, determines the maximum range of detection. For simulations, the SNR of the signal is varied and Hurst parameter is calculated. Friss transmission equation gives the relation between power variation (SNR) and distance [16].

$$Measured\ Power\ \propto \frac{1}{D^2} \tag{4.14}$$

$$SNR = \ P_S/P_N \tag{4.15}$$

$$SNR_{Max} = \frac{Max\ (P_S)}{R^2 P_N} \tag{4.16}$$

$$SNR_{dB} = SNR_{Max} - 20\log D \tag{4.17}$$

where P_S is the signal power and P_N is the noise power and D is the distance from the detector.

4.3 PROBABILITY OF DETECTION.

Probability of detection determines the reliability of a method. It can be calculated by taking the ratio of successful detections to total number of trials where the device was placed (at a particular point). Probability of detection varies with the distance from the receiver. When the device is close to the receiver the received signal is strong and hence the probability of detection is the maximum, i.e equal to 1. [16]

$$Probability\ of\ Detection = \frac{N_{detected}}{N_{total}} \tag{4.18}$$

where $N_{detected}$ is the number of successful attempts and N_{total} is the total number of attempts when the device is placed at a point. For probability of detection calculation, multiple measurements have been made at different distances and the graph for probability of detection with distance has been plotted in the later section.

5. EXPERIMENTAL SETUP

This section gives an overview of the experimental setup employed in validation of the proposed detection scheme. Figure 5.1 gives a pictorial representation of the setup used to collect measurements. The setup consists of two wideband bi-conical antennas (20MHz – 2.2 GHz) for transmitting the stimulating signal and receiving the response, an Agilent MSO6104A oscilloscope that acts as a receiver (collects the data) and an Agilent N5182A signal generator to send the stimulating signal. The stimulating signal is a sinusoid at 315MHz with amplitude of -40dbm. A 40dB low noise amplifier (HILNA-G2VIR, NuWaves) is connected between receiving antenna and the oscilloscope to amplify weak unintended emissions. The oscilloscope is controlled by a base station with labview interface to store the data and to be used for Hurst parameter calculation. A basic wireless doorbell operating at frequency of 315MHz is used as a device under test (DUT).

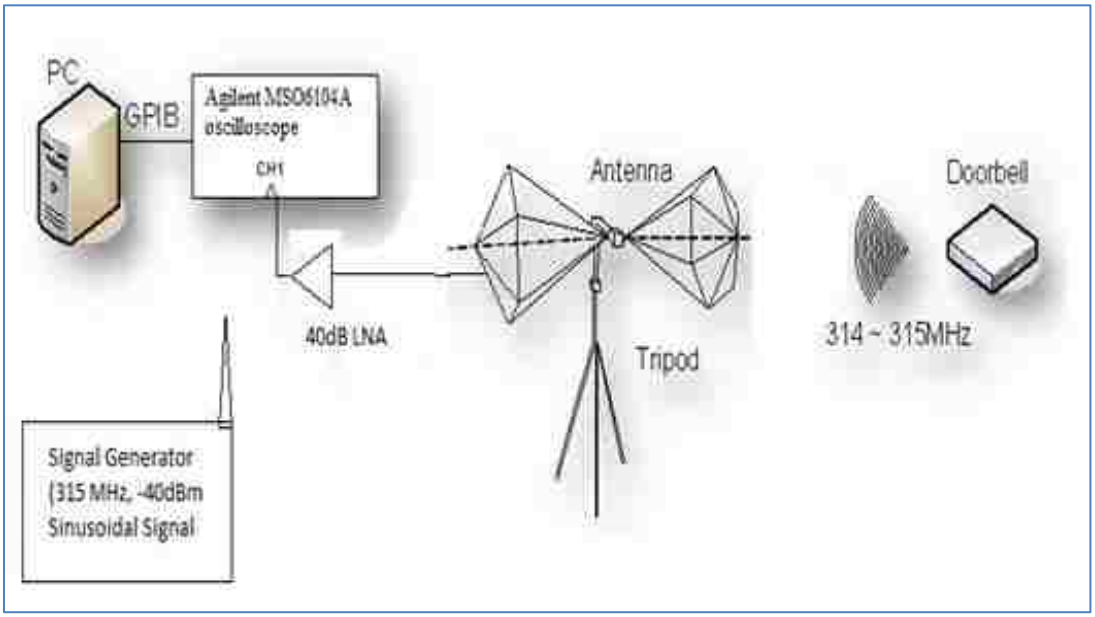

Figure 5. 1. Experimental setup for detection of doorbell

Initially the doorbell is switched off and measurements are made to estimate the Hurst parameter of noise floor. Multiple measurements of background noise are considered and an average Hurst parameter value is fixed as the threshold for detection. The doorbell is then switched on and placed at different distances for estimation of Hurst parameter and determination of range. Multiple measurements at the same point are recorded for averaging and to calculate the probability of detection.

6. RESULTS AND DISCUSSION

Simulation and experimental results of the proposed SRR detector are discussed in this section. Simulation results validate the detection performance in presence of various noise signals. The experimental analysis validates the scheme in realistic scenarios and evaluates the detection accuracy and standoff distance. The results are compared with the traditional RSS peak detection approach.

6.1 MODELING OF SRR.

In this section the response of the SRR obtained from mathematical modeling is studied. The response of a doorbell under active stimulation is also plotted for comparison.

The equations (3.1) – (3.6) define the mathematical model for the response of SRR. Figure 6.1(a) illustrates the ideal response of the SRR obtained by the mathematical model. Noise is added to the ideal response and is filtered to make the response identical to the actual response Figure 6.1(b). Addition of brownian noise makes the signal self-similar thus causing error in Hurst parameter based detection.

The response of the mathematical model of the SRR is compared to the actual response of the doorbell. Harmonics of the emissions are enhanced under active stimulation. Frequency separation between these harmonics determines the quench signal of the receiver. Each of the harmonics of wireless doorbell are separated by integral multiples of a constant value $\Delta f = 550KHz$ around the stimulating frequency. Since the response contains all the integral harmonics, it can be concluded that the quench oscillator signal is a sawtooth waveform and the frequency difference between the consecutive harmonics is the frequency of the sawtooth.

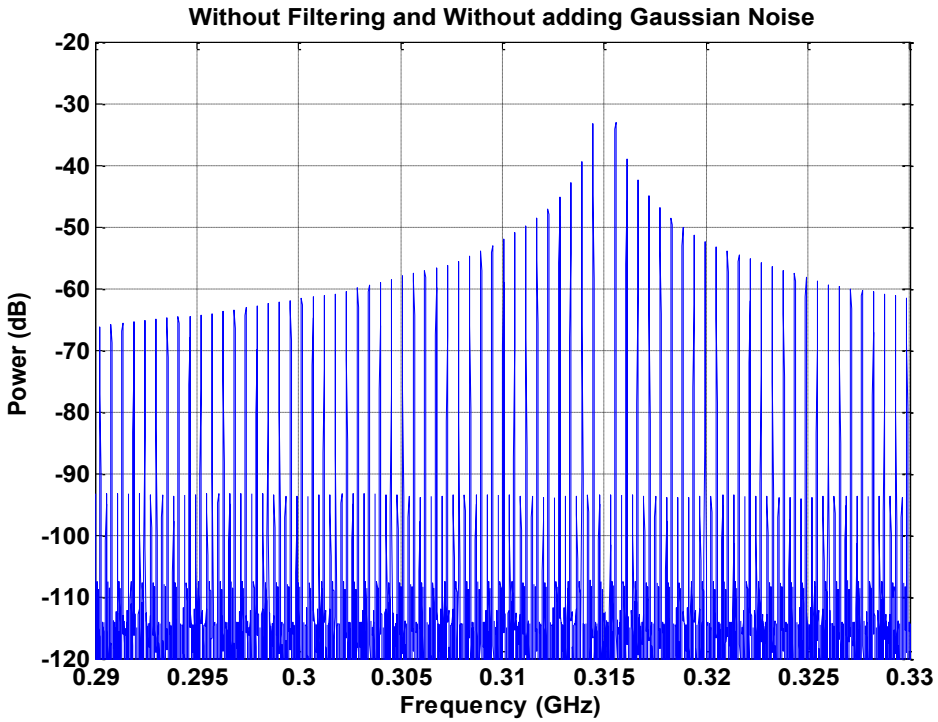

Figure 6.1 (a). Response of SRR Ideal

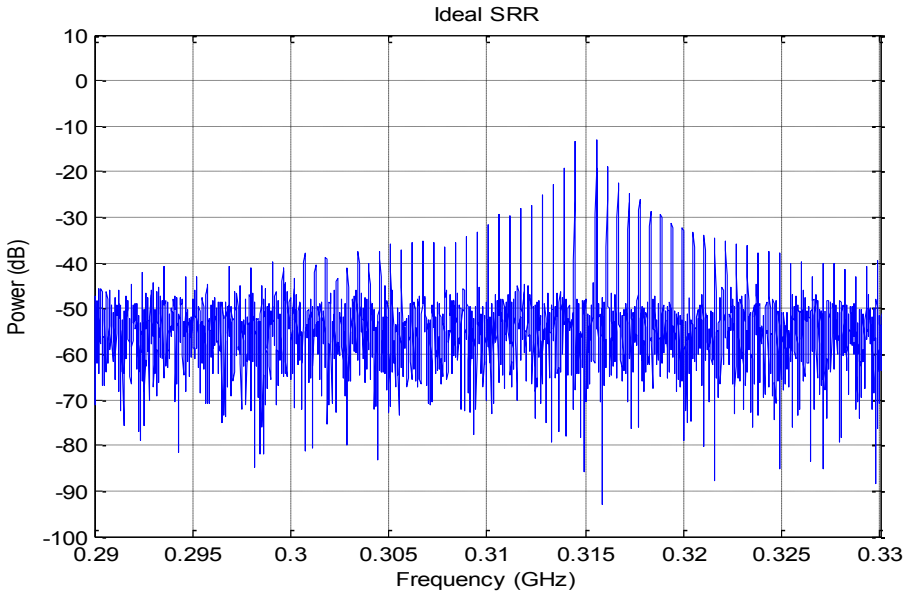

Figure 6.1 (b). Response of SRR with Brownian noise

Figure 6. 1: Response of SRR: (a) ideal (no noise) and (b) with Brownian noise

The value of Δf from the above graphs is used to generate an ideal SRR response. The stimulating frequency is set to 315 MHz and the frequency of the quench oscillator is set to 550 KHz. The generated response is plotted and Gaussian noise is added to the ideal SRR. The similarity between the ideal SRR with a sawtooth quench signal and the doorbell placed at 1.5m (5ft) is shown in Table 6.1 and Figure 6.2.

Table 6. 1. Summary of Harmonic Frequencies for SRR Receivers

Harmonic Number	Frequency of a Harmonic of Ideal SRR	Frequency of a Harmonic of Doorbell
1	315.6 MHz	315.6 MHz
-1	314.4 MHz	314.4 MHz
2	316.1 MHz	316.2 MHz
-2	313.9 MHz	313.8 MHz
3	316.7 MHz	316.8 MHz
-3	313.3 MHz	313.2 MHz
4	317.2 MHz	317.3 MHz
-4	312.8 MHz	312.7 MHz
5	317.7 MHz	317.9 MHz
-5	312.3 MHz	312.1 MHz

*Negative harmonic number represents harmonic on left side of the carrier frequency

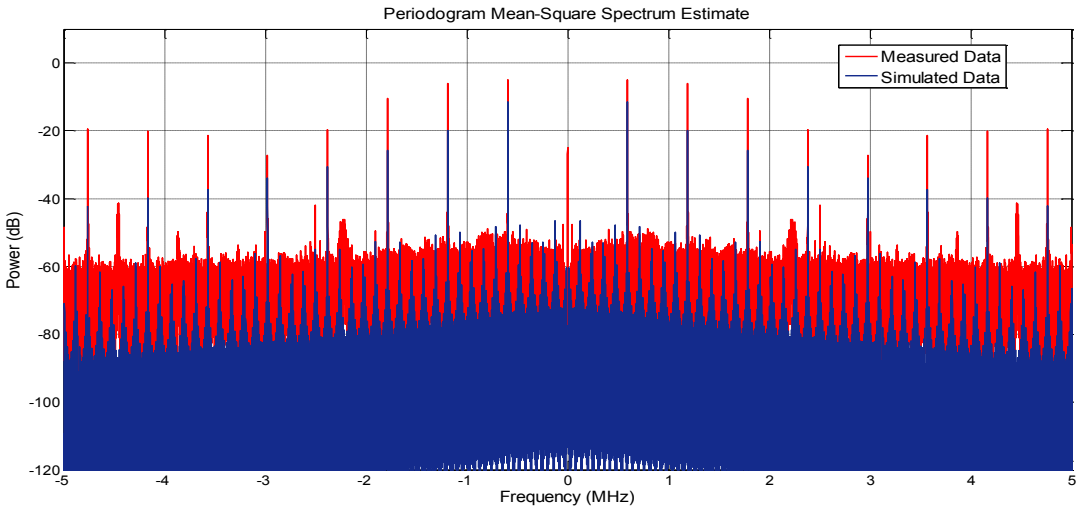

Figure 6. 2. Figure shows the overlap of simulated response to measured response of doorbell

6.2 HURST PARAMETER.

Hurst parameter for ideal case of SRR is compared with experimental results for doorbell. For the ideal response of SRR and response of doorbell, Hurst parameter is calculated using the method shown in section 3.2. Hurst parameter for ideal SRR is estimated as 1 from Figure 6.3, which implies that in the ideal case the response, is self-similar. Gaussian noise is then added to the signal with high SNR and it is shown that the Hurst parameter has decreased to 0.6.

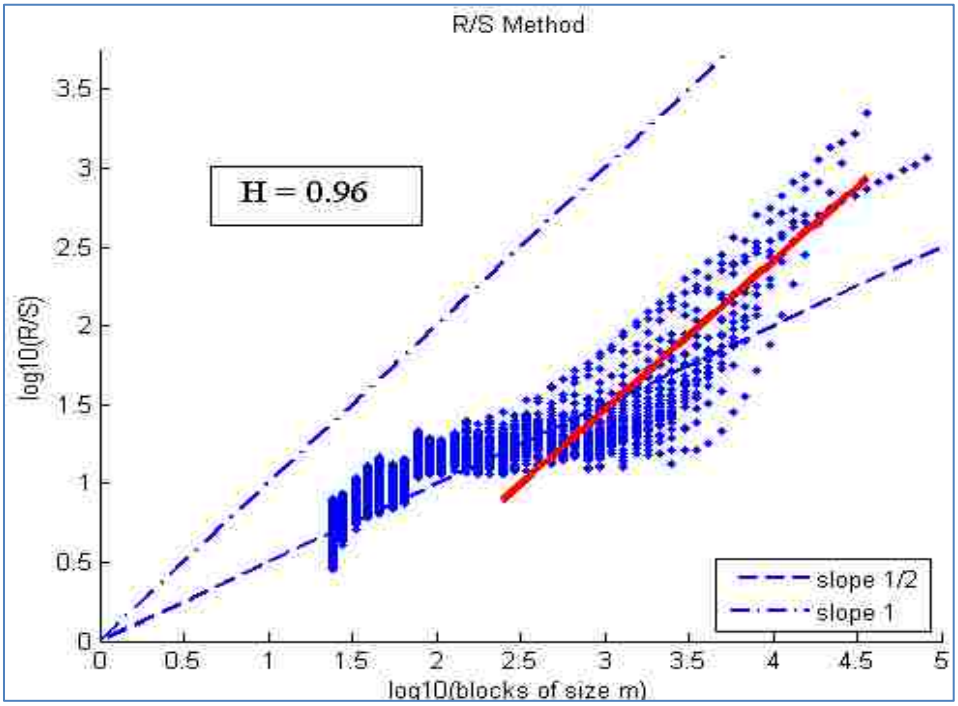

Figure 6. 3. Hurst parameter of ideal response of SRR

The rescaled range method calculates the dynamic range of the process for different bursts of data. For ideal case of SRR, the response maintains a similar dynamic range for all bursts of the response. The addition of noise and other non-similar

components reduce the Hurst parameter. The Hurst parameter for the signal obtained from the doorbell at different distances is also calculated.

Equations from Section 4 can be used to plot an approximate relation between Hurst parameter and distance assuming only the presence of Gaussian noise for different values of SNR.

Figure 6.4 compare the performance of Hurst parameter and the received signal strength (RSS) based detection schemes with standoff distance. RSS is a typical method used for detection where the received signal strength is compared to strength of the noise floor. The RSS method is completely dependent on power of the received signal. Strength of the received signal above noise floor confirms the presence of a device. RSS method has many problems with impulsive signals, multipath fading, reflection, etc. In contrast, Hurst parameter method overcomes the dependency of received signal strength. Hence, there is an increase in the maximum detection range compared to the RSS method.

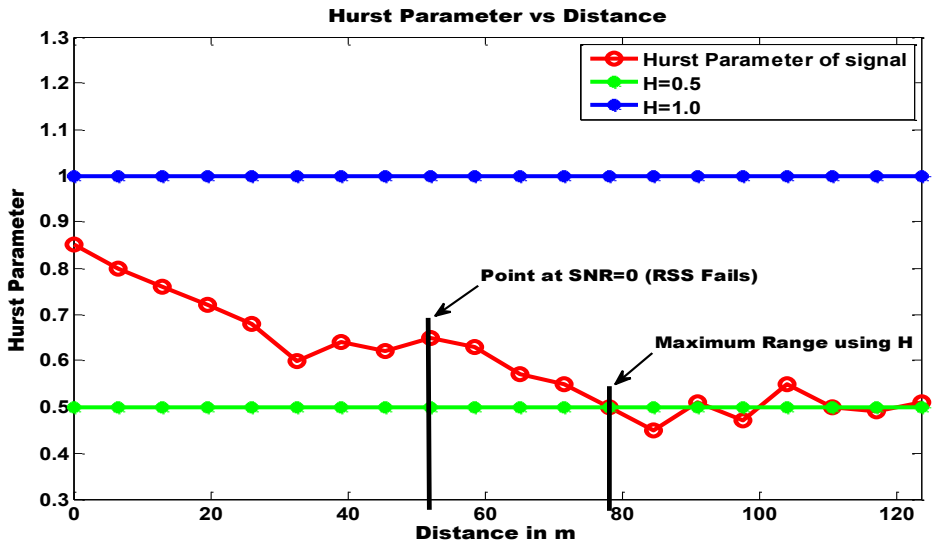

Figure 6. 4. Hurst parameter with distance for ideal SRR with Gaussian noise (Max SNR (SNR at 0m) = 40dB) compared with RSS based detection

Hurst parameter method fails in the presence of dominant self-similar noise (e.g. Brownian noise). Even with decrease in SNR of the signal, H parameter remains almost constant due to the presence of Brownian noise. Figure 6.5 shows variation of Hurst parameter with distance for the case of Brownian noise. Even at low signal power, Hurst parameter of the signal is high resulting in false detection.

A combination of Brownian noise and Gaussian noise is also considered to test the variation of Hurst parameter. Figure 6.7 shows the variation of Hurst parameter with both Brownian and Gaussian noise added. Though the Hurst parameter is less compared to Figure 6.5, it remains constant due to the presence of dominant Brownian noise. This case also results in false detection.

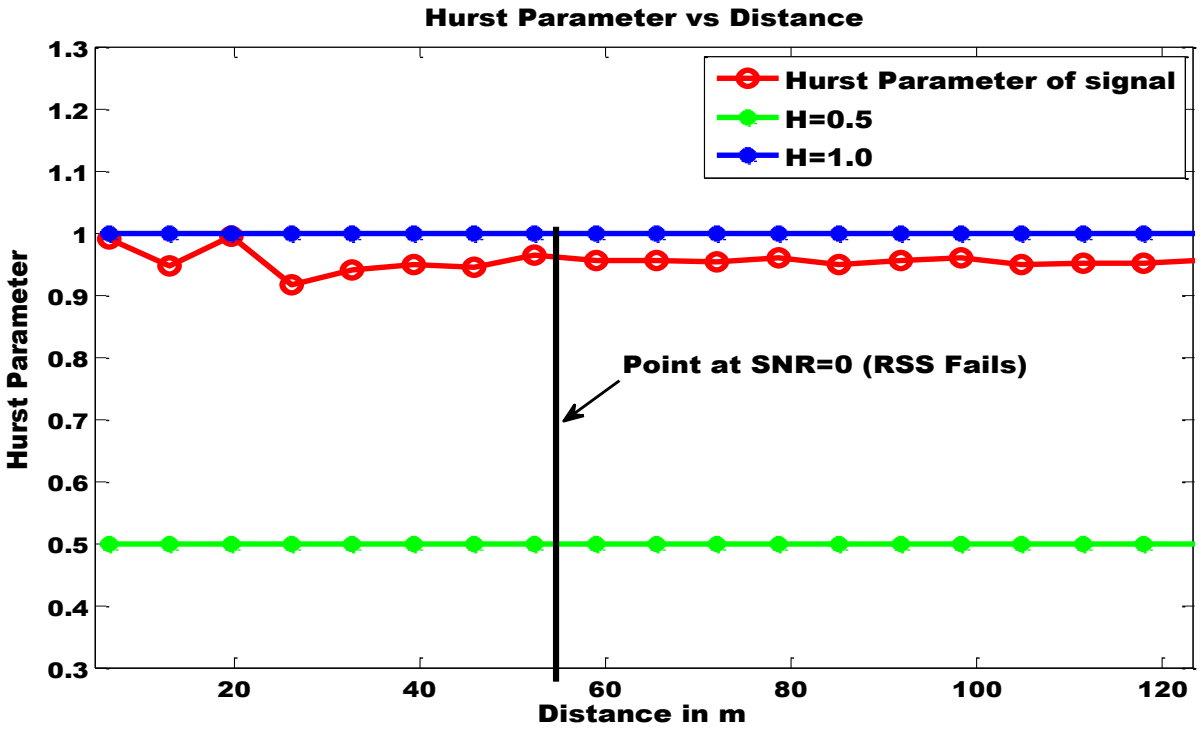

Figure 6. 5. Variation of Hurst parameter with distance in presence of dominant Brownian noise

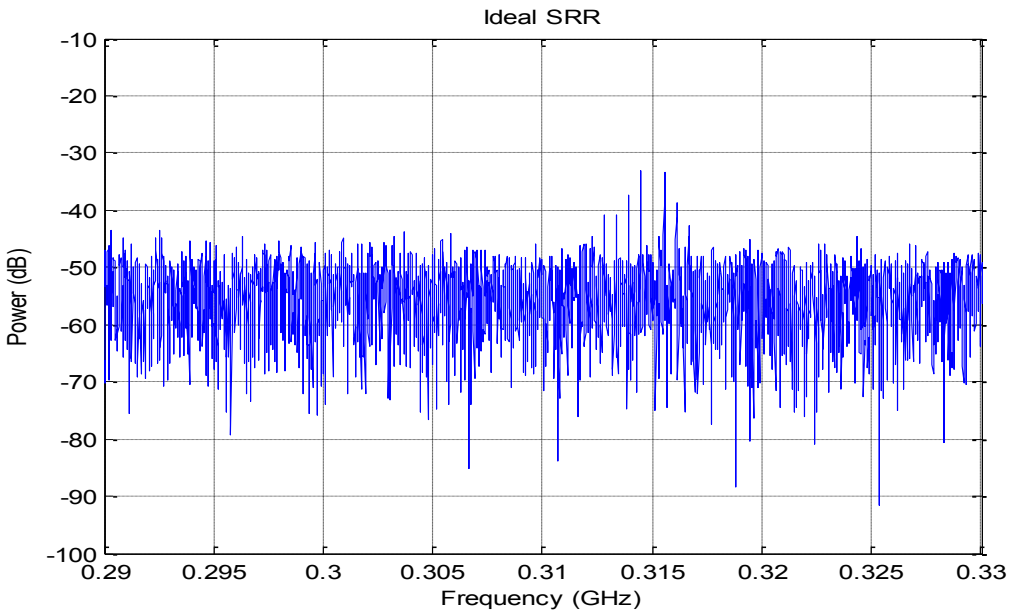

Figure 6. 6. Ideal SRR with Brownian noise at low SNR

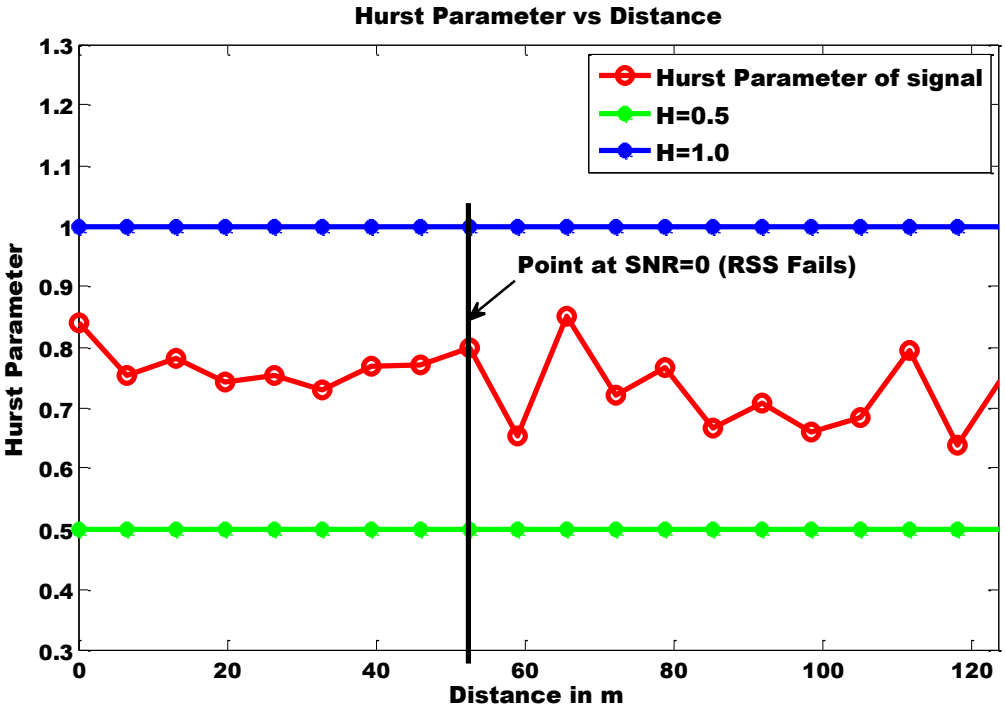

Figure 6. 7. Variation of Hurst parameter with distance for a combination of Brownian noise and Gaussian noise

The Hurst parameter is now tested for a real environment with a doorbell (SRR). Figure 6.8 shows the Hurst parameter variation with distance for the doorbell. The signal strength from doorbell goes below noise floor after 15.24m (50ft) and thus RSS method fails after 15.24m (50ft). However, Hurst parameter of the emissions from doorbell remains above Hurst parameter of noise floor at 15.24m (50ft). Hence, H parameter method detects the signal after its strength goes below noise floor. Range of detection is further increased by 70% (26 m) when compared to RSS method.

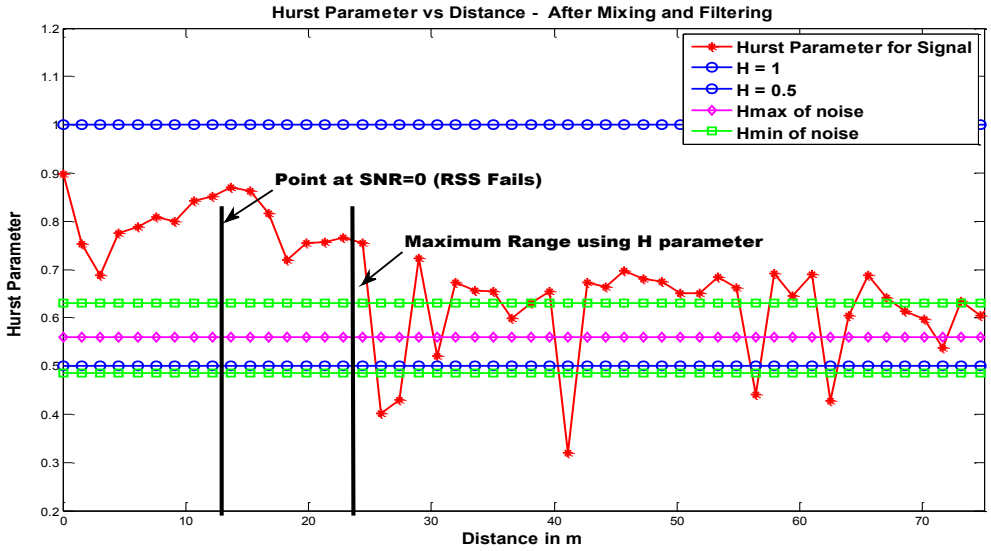

Figure 6. 8. Hurst parameter of doorbell vs distance

6.3 PROBABILITY OF DETECTION.

Probability of detection (PoD) is a measure of reliability and success rate of detection. It is estimated by making multiple iterations at different distances and checking whether or not the device is detected using Hurst parameter or RSS method. PoD is estimated for RSS and Hurst parameter method for 10 iterations at each point. Hurst parameter method not only improves the range of detection, it also improves the

probability of detection. Figure 6.9 shows the variation of probability of detection as the distance increases. The probability of detection decreases with distance for both schemes. However, the Hurst parameter method can reliably detect SRR devices at larger distance than the RSS-based method.

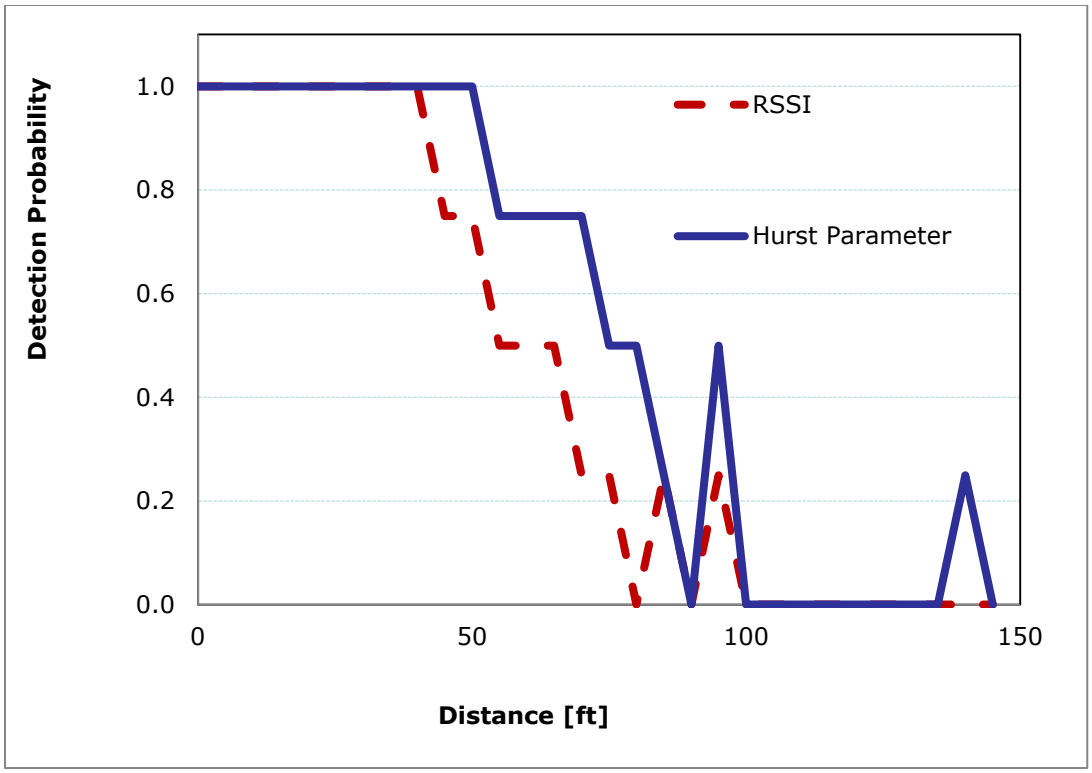

Figure 6. 9. Probability of detection for Hurst parameter

6.4 OBSERVATIONS FOR FUTURE SCOPE.

Further observation of the harmonics of emissions reveals some important characteristics. The strength of harmonics remains almost constant with the variation in stimulating signal power. In contrast, the frequency of the first harmonic varies (up to +/- 200KHz) with the power of the stimulating signal. Hence, the doorbell can be kept active

even at small signal powers Figure 6.10. The variation of frequency will be a point of great interest for future analysis of SRR.

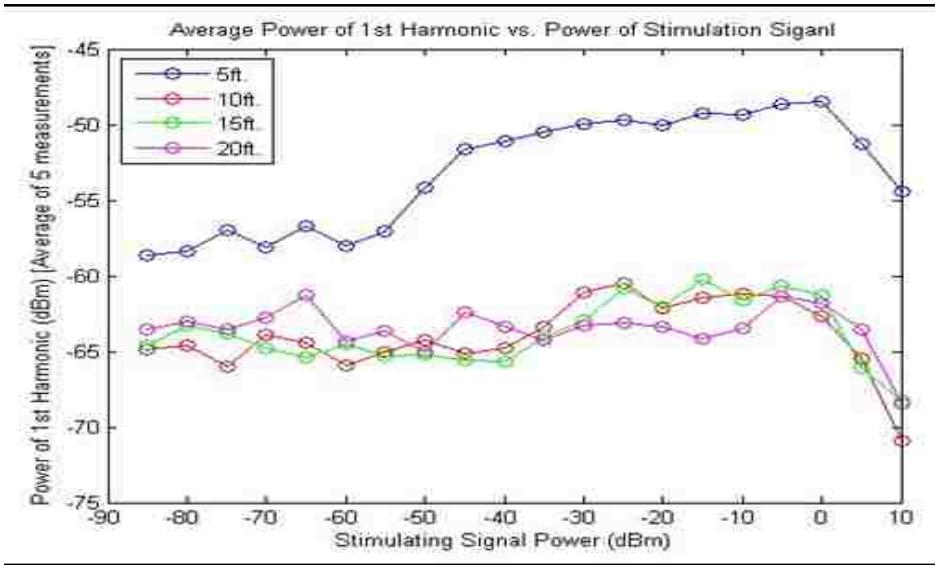

(a) Power of 1st Harmonic vs Stimulating signal power

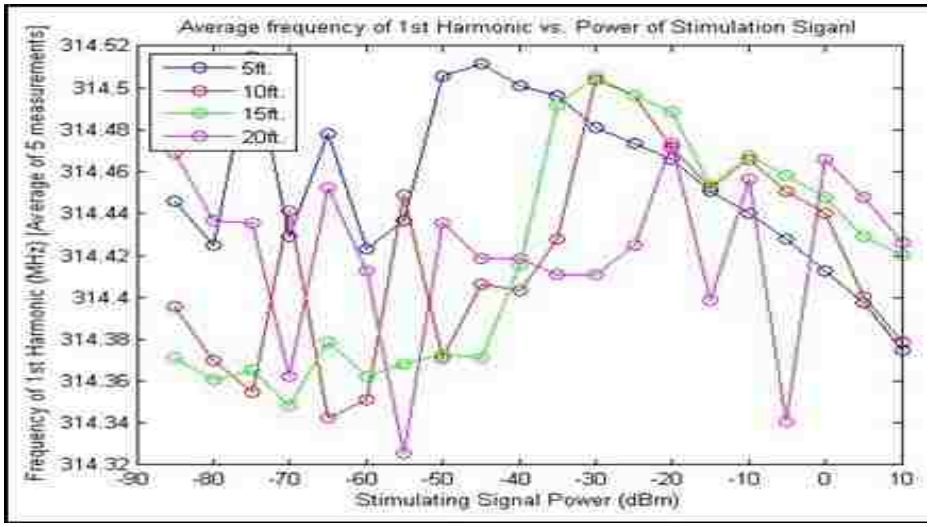

(b) Frequency of 1st harmonic vs Stimulating signal power

Figure 6. 10. Variation of harmonics (a) power and (b) frequency with stimulating signal power

7. CONCLUSIONS

The proposed Hurst parameter based detection of SRR is successfully validated through a comprehensive mathematical, simulation, and experimental analysis. The self-similar property of the SRR signal spectrum is shown for R/S method of Hurst parameter calculation both in theory and using experimental setup. The proposed scheme successfully detects devices with SRR circuitry even if the signal power faded into a noise, i.e. SNR<1.

The proposed detection scheme outperforms the traditional, RSS-based peak power detection approach. It improves the range of detection by 70% over the RSS based schemes (15.24m for RSS and 26m for H parameter). Moreover, it increases the probability of detection when compared to the traditional RSS based detection. Also, the variation of Hurst parameter has been shown for different noise inputs. In general, the proposed scheme falsely detects a device in the presence of self-similar Brownian noise, which in real life corresponds to environment with sources of self-similar signal, e.g. multiple SRR devices.

Hence, the future work should address this weakness by exploring other self-similar properties of the emissions. Also, the variation of signal strengths and harmonic frequencies will be studied for multiple-device scenarios.

8. REFERENCES

[1] S. Jagannathan and J. Hertenstein, "Detection of Unintended Electromagnetic emissions from Super Regenerative Receivers". Proc. SPIE 8017, 80170F (2011); doi:10.1117/12.883223

[2] S. Seguin, "Detection of Low Cost Radio Frequency Receivers Based on their Unintended Electromagnetic Emissions and an Active Stimulation". Ph.D dissertation, Missouri University of Science and Technology, Rolla, MO 2009.

[3] X. Dong, H. Xiao Weng, D.G. Beetner, T.H. Hubing, D.C. Wunsch, M. Noll, H. Goksu, and B. Moss, "Detection and identification of vehicles based on their unintended electromagnetic emissions". Electromagnetic Compatibility, IEEE Transactions on, 48(4):752-759, Nov. 2006.

[4] H. Xiao Weng, X. Dong, Xiao Hu, D.G. Beetner, T. Hubing, and D. Wunsch, "Neural network detection and identification of electronic devices based on their unintended emissions". In Electromagnetic Compatibility, 2005. EMC 2005. 2005 International Symposium, volume 1, pages 245-249, August 2005.

[5] A. Shaik, H. Xiao Weng, Xiaopeng Dong, T.H. Hubing and D.G. Beetner. "Matched filter detection an identification of electronic circuits based on their unintentional radiated emissions". In Electromagnetic Compatibility, 2006. EMC 2006. 2006 IEEE International Symposium on, volume 3, pages 853-856, August 2006.

[6] D. Beetner, S. Seguin and H. Hubing, "Electromagnetic emissions stimulation and detection system", U.S. Patent 7 464 005, Dec. 9, 2008.

[7] C. Stagner, A. Conrad, C. Osterwise, D.G. Beetner and S. Grant,. "A Practical Superheterodyne-Receiver Detector Using Stimulated Emissions". IEEE Transactions on Instrumentation and Measurement, Vol. 60, No. 4, April 2011.

[8] R. Feick, O. Rojas. "Modeling and Simulation of the Superregenerative Receiver. IEEE Transactions on Consumer Electronics", Vol. 43, No. 2, May 1997.

[9] U.L. Rohde, A.K. Poddar. "Super-Regenerative Receiver". Microwave Journal. Sarnoff Symposium, April 2008 IEEE.

[10] J. Beran. "Statistics for Long-Memory Processes", Chapman and Hall, 1994.

[11] J. Beran, Robert Sherman, Murad S. Taqqu, and Walter Willinger. "Long-Range Dependence in Variable Bit-Rate Video Traffic". IEEE Transaction on Communications, Vol. 43, No. 2/3/4, February/March/April 1995.

[12] William Stallings. "High-Speed Networks and Internets, Performance and Quality of Service", Second Edition. Chapter 9.

[13] Will E. Leland, Murad S. Taqqu, W. Willinger, and D.V. Wilson. “On the Self-Similar Nature of Ethernet Traffic (Extended Version)”. IEEE/ACM Transactions on Networking. Vol. 2, No. 1, February 1994.

[14] H.F. Zhang, Y.T. Shu and O. Yang. “Estimation of Hurst Parameter by Variance-Time Plots”. IEEE 1997.

[15] C.A. Tudor and F.G. Viens. “Statistical Aspects of the Fractional Stochastic Calculus”. The Annals of Statistics. 2007, Vol. 35. No. 3, 1183-1212. Institute of Mathematical Statistics, 2007.

[16] Vivek Thotla, M. T. A Ghasr, M. Zawodniok, S. Jagannathan, S. Agarwal. “Detection and Localization of R/C Electronice Devices Using Hurst Parameter”. Proc. SPIE 8359, 835915 (2012).

[17] B. B. Mandelbrot. “Self-Similar Error Clusters in Communication Systems and the Concept of Conditional Stationarity”. IEEE Trans. Communications Technology COM-13, 71-90, 1965.

II. DETECTION AND LOCALIZATION OF MULTIPLE R/C ELECTRONIC DEVICES UISNG ARRAY DETECTORS

ABSTRACT

Accurate detection and localization of unintended emissions from multiple radio controlled (RC) electronic devices has a wide range of security applications. First, this paper introduces a cost-effective mobile array detector. Subsequently, a novel scheme is presented for detection and localization of multiple devices emitting unintended passive emissions. Peak detection is used for detection of devices with superheterodyne receivers. Experimental results demonstrate that the proposed scheme outperforms traditional methodologies with single antenna. A 2-D array is also proposed in this paper for localization of devices with superheterodyne receivers using AOA (Angle of Arrival). A new, SAR-based scheme called ESAR (Edge Synthetic Aperture Radar) is also introduced in this paper for localization. Finally, the results for localization and error in localization are analyzed. Edge SAR method reduces the error in localization by 75% and increases accuracy in detection of multiple devices.

1. INTRODUCTION

All electronic devices emit unintentional electromagnetic (EM) radiations. Regulatory standards limit the level of these emissions; however, some unintended radiations will always be present. Typical radio controlled (RC) devices have either superheterodyne [1-5] or super-regenerative receivers [6-7]. These devices emit unintended emissions that can be used to identify and locate an RC device. Unfortunately, these emissions are weak, when compared to background RF noise, and thus difficult to detect. The emissions are weakened further when the device is placed on the ground.

Studies have indicated that unintended passive emissions from a superheterodyne receiver can be detected by using a stimulated source [1-2]. A second-order self-similarity representation was utilized to detect the emissions generated by a super-regenerative receiver [6-7] of an unknown device. However, detection of multiple devices has not been adequately addressed in the literature and is considered a topic of significant interest. In addition, localization of the devices is not sufficiently presented.

Detection methods described in [2-8] use a single antenna and a single device. The angle of arrival (AoA) information is also not available with single antenna detectors. With the presence of multiple devices, emissions can interfere with each other causing errors in detection and ranging. Spatially differentiating emissions from multiple devices is a challenge when several devices are present.

Therefore, this paper addresses the challenges in detection, and localization of multiple devices. An antenna array is used in this paper to spatially discriminate emissions from multiple devices. Also, array processing increases the measurement gain

resulting in a better estimate of signal strength. The increased gain results in a larger signal-to-noise ratio, which is utilized for improving the range of detection.

Array processing techniques and array detectors have been utilized previously to detect the presence of multiple devices [9]. These installations are large and non-mobile. Therefore, a cost-effective mobile array detector is more desirable. The proposed architecture for the array detector employs wide band antennas to detect devices with emissions of different frequencies and to distinguish among multiple devices with similar profiles.

In addition to detection, the paper proposes localization schemes based on the angle of arrival (AoA) technique and our edge synthetic aperture radar (ESAR) method. Angle of arrival method is implemented on the two-dimensional array for localization based on received signal strength (RSS). Synthetic aperture radar (SAR) [14-16] on the other hand, is a form of radar used for generating high resolution images using coherent radar signals. The primary motive for SAR is to generate optical quality images of bigger areas under different environmental conditions [16]. A matrix of synthetic sensors generated from relative motion between the sensor and target is usually utilized for SAR processing. Narrow band and wide band signals are used to illuminate the targets. Coherent summation of the received signals is utilized to improve spatial resolution [15, 16] to resolve targets that are closely spaced. Monostatic and bistatic aperture radar imaging are special cases of SAR used for detection [22]. These methods are based on Fourier analysis of data from synthesized array. Single frequency and wide band holographic image reconstruction is a combination of backward wave image reconstruction and SAR [22].

In this paper a two dimensional array is created with sensor only on the edge and single frequency backward wave image reconstruction SAR processing is applied on the unintended emissions from the superheterodyne receiver to localize the receiver. Furthermore, a comparison of error in localization is also presented for these two methods.

First, this paper describes the array detector used to implement the proposed detection and localization scheme. Second, a two-dimensional detector is proposed for detection of multiple devices using angle of arrival (AOA) and ESAR. Then, the experimental setup used for real time measurements is described. Detection and point of failure for different cases with multiple devices is further analyzed. The array detector results in a substantial increase in the range of detection. The performance of this array detector is also compared to that of a single antenna detector. The size of the array antenna is further increased to 8-elements and the range of detection is compared to the 4-element array and single antenna detector.

The main contributions of the proposed work are: (1) performance evaluation of array processing based detection and localization of multiple devices with passive emissions in terms of detection range, detection of multiple devices, and point of failure for varying number of antenna elements, (2) design of a new detection and localization scheme called Edge SAR (ESAR), and (3) analysis of error in detection for different non-uniform topologies of 4-element arrays. Experimental results are included herein to demonstrate the performance of the proposed schemes.

2. BACKGROUND

First, the phased array processing is briefly introduced for reference. It is basic methodology in array-based angle of arrival detection and localization schemes. Depending on distance from the objects, near-field and far-field models for array processing are employed. The widely accepted threshold for the far-field is equal to $2\,d^2/\lambda$, where d is the longest dimension of the antenna [13]. Please note that the actual difference between closest point of detection and far-field is of the order of 5 ns. Table 2.1 shows the difference in time delays under near field and far field conditions for a 4-element uniform array and a source placed along the center of the array. Difference in time for emissions to reach center of array and its elements for near field and far field distance is compared in this table. In context of both the considered application and realistic measurement equipment, the final difference in time is small enough to be ignored and far field conditions can be assumed.

Table 2. 1. Time difference for actual distance to array element and far-field distance for 4-element array

Distance from center of array	Time difference for first element from center of array	Time difference for second element from center of array
1.524 m	0.2 ns	0.5 ns
3.048 m	0.1 ns	0.3 ns
30.048 m	0.01 ns	0.03 ns

Consider a signal R_n from the antenna element A_n, where $n=1,2,3,..,N$ is antenna number. Phased array processing provides for a coherent summation of the received signals from each individual array element R_n:

$$S(t,\theta) = \sum_{n=1}^{N} R_n(t) * e^{j*(n-1)*\Psi} \quad (2.1)$$

where θ is the angle at which the antenna beam is directed for signal measurement and Ψ represents the progressive phase of each array element referenced to the previous one [10].

$$\Psi = K * d * \cos\theta \quad (2.2)$$

$$K = 2\pi/\lambda \qquad d = \lambda/2 \quad (2.3)$$

where d is the distance between the antennas, and $\theta \in [0, \pi]$. The signal power is obtained by integrating the signal at the frequency of interest over a period of time T and is given by

$$P(\theta) = \int_0^T S(t,\theta) * e^{-j2\pi f t}\, dt \quad (2.4)$$

Equations (2.1) – (2.4) display the relationship between power and angle of measurement for an N-element array. A plot of equation (2.4) reveals the AOA information.

Computationally intensive methods like MLE (maximum likelihood estimator) [23] and MUSIC (multiple signal characterization) [24] use other signal parameters for estimation of AOA. Spectral properties of the signals and noise are used to generate a covariance matrix to find the maximum likelihood estimator. This method requires explicit knowledge of the noise spectral properties. Most MLE method assumes the noise process to be known. Unfortunately this is a limited assumption leading to error in estimation.

MUSIC on the other hand uses orthogonal relationship between the signal and noise. Eigen vectors of the covariance matrix determine the estimation of AOA. Different variations of MUSIC have been formulated based on correlation between sources and noise.

3. METHODOLOGY

The overview of detection and localization process is depicted in Figure 3.1 and Figure 3.2. For AOA based method, presence of a device at a given bearing with respect to the antenna is detected as an increase in received power (peak). The plot of amplitude vs theta (θ) is analyzed to determine the presence of a device and an angle at which it is located. The device is detected when the amplitude exceeds a minimum threshold, which is calculated based on ambient noise level.

Furthermore, AOA and power information can be used to localize the devices. The main challenge in localization is accurate estimation of AOA. Error in AOA may result in large localization errors. This challenge is addressed by employing Edge SAR signal processing proposed in this paper.

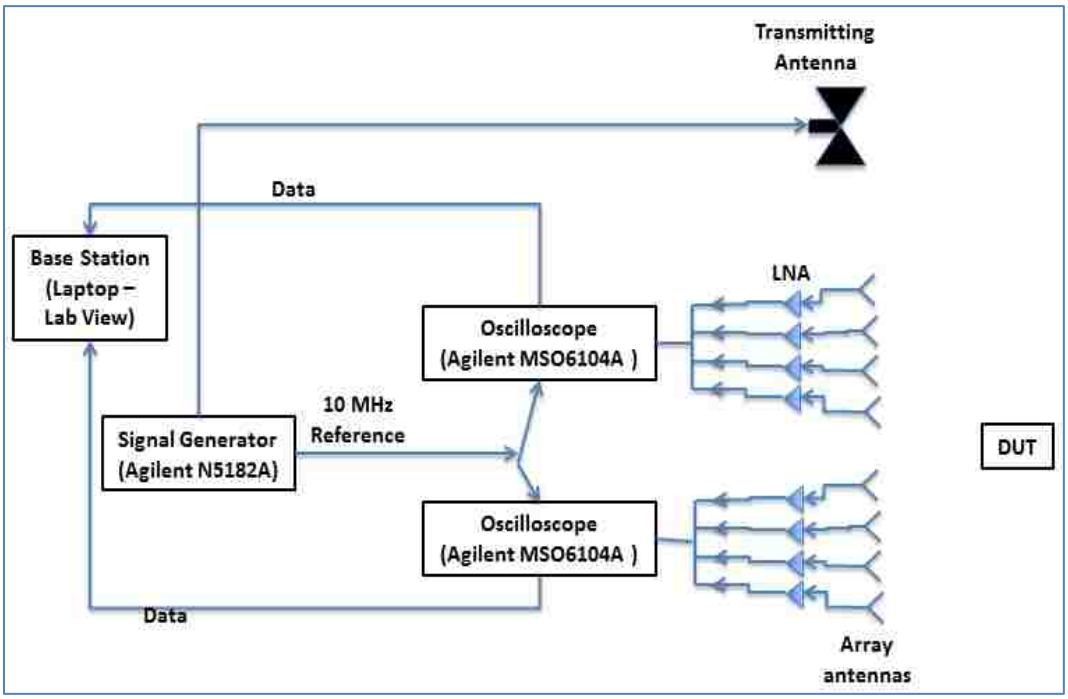

Figure 3. 1. Architecture of uniform array processing

Note, that the proposed method is most suitable for detection and localization of super heterodyne receivers (SHRs). SHRs have a built in crystal oscillator at a fixed carrier frequency. The narrowband oscillator signal leaks out of these devices and is identified as a peak in the frequency spectrum.

3.1 TWO DIMENSIONAL DETECTION WITH TWO 4-ELEMENT ARRAYS.

Figure 3.3 illustrates a basic localization scenario that is considered in this paper with two antenna arrays. The arrays are placed in a 2D, orthogonal configuration that improves localization accuracy. Increasing the number of elements in a linear array improves detection accuracy and detection range. However, adding more antenna elements has diminishing effect on localization accuracy. Consequently, a two dimensional orthogonal array is considered as shown in Figure 3.3. Each of the two four-element arrays is placed along the X-axis and Y-axis respectively. Two different targets are placed at multiple locations and the unintended emissions are measured. The measurements are evaluated for localization using two different methods: 1) angle of arrival (AOA) based estimation and 2) a newly proposed, two-dimensional Edge SAR.

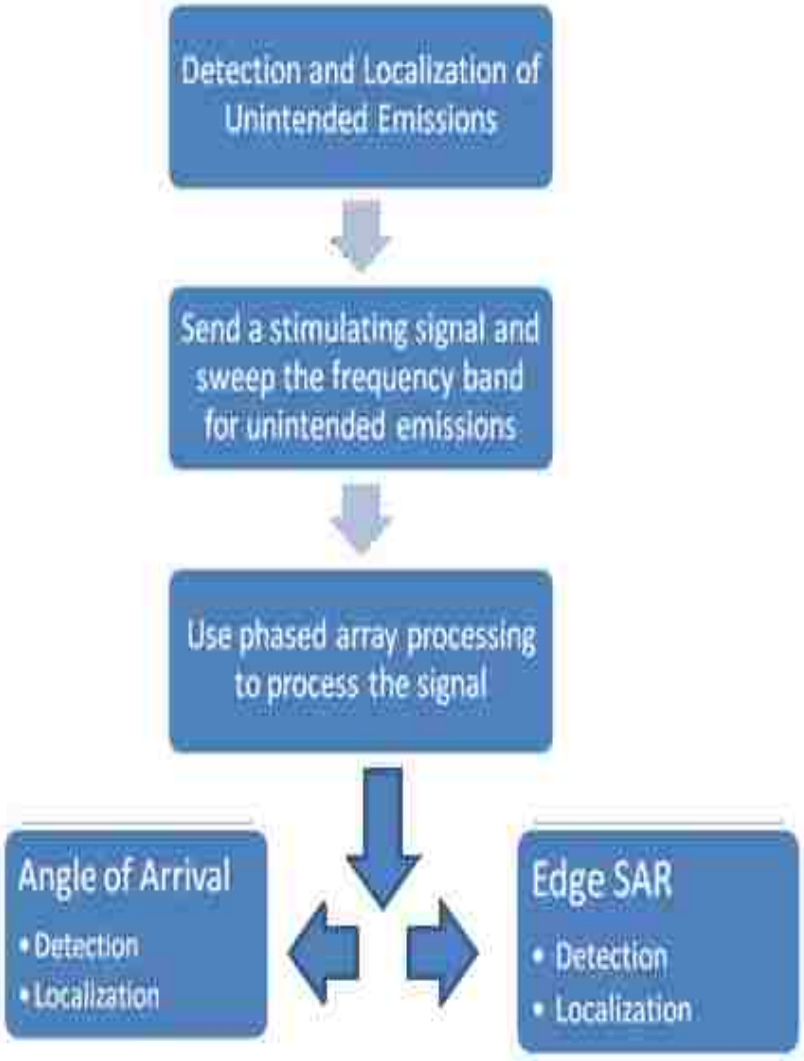

Figure 3. 2. Overview of detection and localization

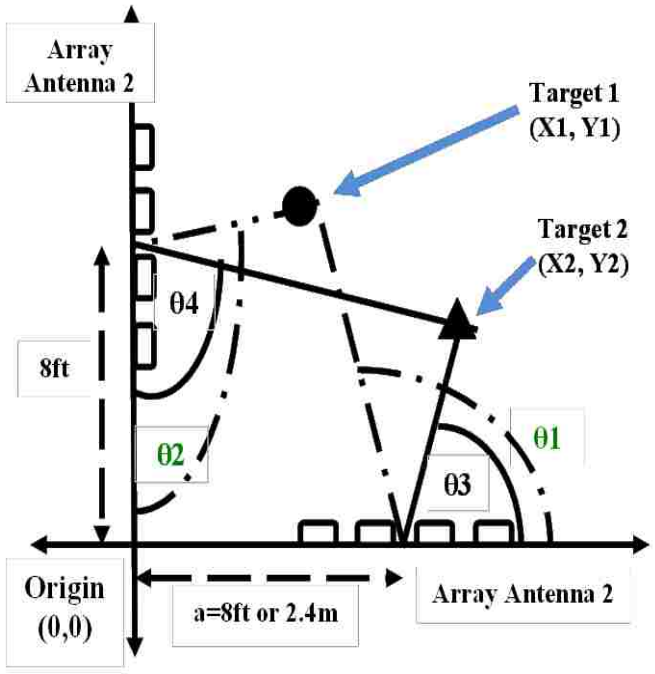

Figure 3. 3. Experimental setup for 2-dimensional array and multiple targets

1) Angle of arrival (AOA) based localization. Localization using AOA uses the phased array processing approach discussed in Section 2. Intersection of AoA's from the antenna arrays estimate the location. Coordinates of the four-element arrays and their respective AOA's are used to calculate the coordinates of the targets as follows.

Consider two targets Target1 and Target2 placed at (X1, Y1) and (X2, Y2) respectively. The center of the array antennas are at (a, 0) and (0, b). Let θ1 and θ2 be the estimated angle of arrivals for Target 1 w.r.t array antenna 1 and array antenna 2 respectively. Let a=b=2.4m. Simple coordinate geometry can be used to estimate X1 and Y1.

$$\tan(180° - \theta 1) = \frac{Y1}{a - X1} \tag{3.1}$$

$$\tan(180° - \theta 2) = \frac{X1}{Y1 - b} \tag{3.2}$$

Position coordinates can be calculated by solving (3.1) and (3.2) with respect to X1 and Y1. Similarly for Target 2, the angles of arrival, θ3 and θ4, are the estimated w.r.t the antenna array 1 and 2 respectively. Coordinates of Target 2 (X2, Y2) are determined from (3.3) and (3.4).

$$\tan(\theta 3) = \frac{Y2}{X2-a} \tag{3.3}$$

$$\tan(\theta 4) = \frac{X2}{b-Y2} \tag{3.4}$$

2) Edge Synthetic Aperture Radar (SAR) based Localization. Edge SAR (ESAR) is a new alternative localization approach proposed to improve detection and localization accuracy. In contrast to the traditional SAR method [14-16] and backward wave reconstruction [22, 23], ESAR uses antenna arrays placed on edges of the area rather than collecting measurements as a grid of synthetic array. It generates heat maps – or images – for each of the antenna arrays 1 and 2. Next, the images are combined to give the final SAR image. Placing arrays only on the edges reduces computational complexity compared to the usual SAR processing.

Consider a general point on the sensor *(x', y')* and a general point on the target *(x, y)* shown in Figure 3.4. The emissions from the target vary in space by a function *f(x, y)*. The response at the sensor is a coherent summation of the field from each point on the target. The edge SAR case is formulated as a superposition of two arrays placed on X and Y axis.

$$s(x', y') = \int\int f(x, y)\, e^{-jk\sqrt{(x-x')^2+(y-y_0)^2}}\, dx\, dy \tag{3.5}$$

A 2D flat domain is considered where the target location is on a plane and the arrays are located on the edge of the plane. The wave number is given by k=ω/c, where ω

is the angular frequency and c is the speed of light. Amplitude decay with range has little effect on the image for near ideal case. The exponential component in equation (3.5) can be replaced by a combination of plane wave components travelling in *y* direction.

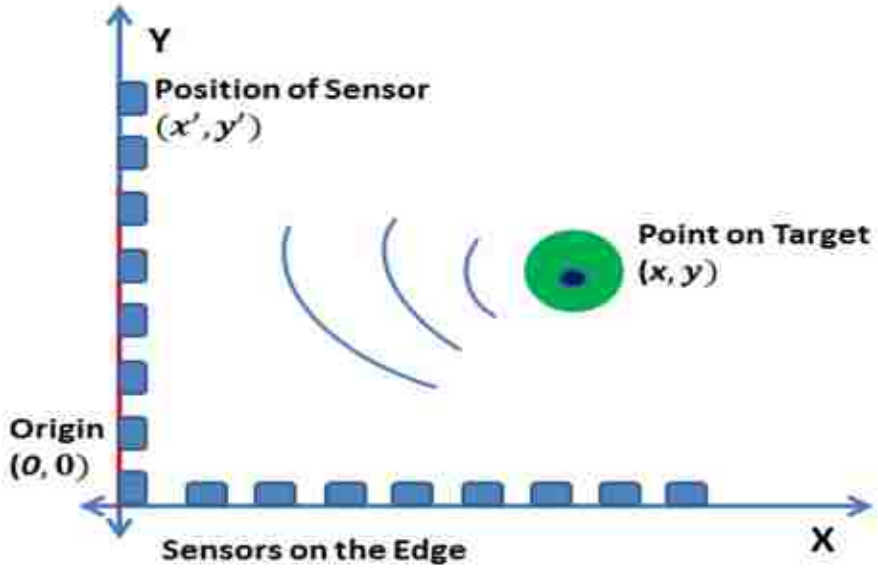

Figure 3. 4. Setup for E-SAR

$$e^{-jk\sqrt{(x-x')^2+(y-y_0)^2}} = \int e^{jk'_x(x'-x)+jk'_y(y_0-y)} dk_{x'} \tag{3.6}$$

where k'_x and k'_y are the wave numbers for x' and y' and $K^2 = K_x^2 + K_y^2$.

$$s(x', y') = \int\left[\int f(x,y)\, e^{-j\left(k'_x x + k'_y y\right)}\, dx\, dy\right] \tag{3.7}$$

The Fourier transforms of $f(x, y)$ along X axis is given by:

$$F\left(k_x, k_y\right) = \int f(x,y) e^{-j\left(k_x x + k_y y\right)} dx \quad = FT\{f(x,y)\} \tag{3.8}$$

Using the above equations for Fourier transform

$$s(x,y) = \int F\left(k_x, k_y\right) e^{j\left(k_x x + k_y y\right)}\, dk_x \tag{3.9}$$

Inverse Fourier transform is given by:

$$f(x,y) = \frac{1}{2\pi}\int F\left(k_x, k_y\right) e^{j(k_x x)}\, dk_x =$$

$$= FT^{-1}\left\{F\left(k_x, k_y\right)\right\} \tag{3.10}$$

$$s(x,y) = FT^{-1}\left\{F\left(k_x, k_y\right)\right\} \tag{3.11}$$

$$F\left(k_x, k_y\right) = FT\{s(x,y)\} \tag{3.12}$$

$$f(x,y) = FT^{-1}\left[FT\left\{s(x,y_0)e^{jy\sqrt{K^2-K_x^2}}\right\}\right] \tag{3.13}$$

ESAR image along Y-axis is also generated similarly. The final image for ESAR is given below:

$$ESAR = \sum f(x_i, 0) + \sum f(0, y_i) \tag{3.14}$$

The electric field due to the emissions from a source in far-filed varies with *R (distance vector)* as shown in equation (3.15).

$$E = \frac{1}{|R|}e^{-jkR} \tag{3.15}$$

where $k = 2\pi/\lambda$, λ is the wavelength of the emissions. SAR image is obtained by coherent summation of the spatial Fourier transform of E and reverse mapping to the measurement coordinates. The SAR image generated by antenna array 1 and 2 are added to obtain higher resolution in localization. A generalized version of the backward wave propagation algorithm is discussed in [22].

4. EXPERIMENTAL SETUP

The uniform linear array shown in Figure 4.1 is designed to operate at 450 MHz with a spacing of λ/2 between the elements. The array elements are omnidirectional, lightweight, unobtrusive, and wideband antennas with an operating bandwidth in the range of 225 – 2500 MHz. Each of the antennas is connected to a 20 dB low-noise amplifier (HILNAG2VIR, NuWaves) and output of the amplifier is connected to an oscilloscope. The oscilloscope acts as a receiver. Outputs of the amplifiers are connected to four channels of the oscilloscope for measurement and data collection. Two of the Agilent MSO6104A oscilloscopes that act as receivers are used and an Agilent N5182A signal generator is used to send the stimulating signal. The oscilloscope is controlled from a laptop using LabView interface to acquire and store data. Noise floor for all cases is estimated by an average of multiple measurements of the environmental noise over a period of the experiment. Block diagram of the experimental setup is shown in Figure 4.1.

The AoA estimation accuracy is evaluated by placing the walkie-talkies at known angles. Additionally, phased array processing is compared to other complex methods like MUSIC and MLE (maximum likelihood estimator).

Figure 4. 1. Experimental setup

Also, the detection range is studied. The device under test (walkie-talkie) is placed on the ground at 90^{o} w.r.t the array antenna. The walkie-talkie is then moved away from the antenna with multiple measurements at each location. Mean amplitude of the emissions is plotted with distances. The maximum detection range corresponds to the distance where the signal strength decreases to the noise level (threshold).

Localization of multiple devices is evaluated for two methods: (a) angle of arrival (AOA) based localization and (b) ESAR based localization. Two walkie-talkies of the same kind are placed in different locations and multiple measurements are recorded. A comparison between the two methods is also presented in the paper.

5. RESULTS AND DISCUSSION

The four-element and eight-element array detectors have been used to detect walkie-talkies. Passive emissions from the local oscillator (LO) of a walkie-talkie are measured and processed. Prior knowledge of the communications channel makes it easier for detection. Spectrum scan is used for detecting signals in unknown frequency channels. Note that the array spacing is not changed for detection of devices at different frequency channels. Change in wavelength for frequencies (462MHz to 467 MHz) of the walkie-talkies considered for the experiment is small. Though an exact ideal sampling is not achieved, it serves the purpose by being either slightly over sampled or under sampled.

This experiment employs channel 8 (FRS) of the walkie-talkie. A continuous wave (CW) signal at 467.5625MHz with a power of -40dBm acts as a stimulating signal to prevent walkie-talkie from periodic switching between standby and power-saver mode. It also keeps the LO on continuously [2]. Note that the stimulating signal does not turn on the walkie-talkie. Moreover, the stimulating signal is not necessary in general case; however, in its absence, the detector has to listen to the channel for a longer time to "catch" at least one "on" period. The walkie-talkie has a fixed IF (Intermediate Frequency = 21.7 MHz). This can be used to estimate the frequency of the unintended emissions. The power of the emissions can be calculated by match filter detection [1, 3].

A) Range Estimation. Increasing the range of detection is a major issue for passive detection due to the low signal strength of the unintended emissions. Moreover, when the device is placed on the ground or on other large surface, the signal radiation is significantly reduced. Therefore, in this paper the worst-case scenario is evaluated with

the device placed on the ground. The walkie-talkie is placed at an angle of 90^{o} (i.e., in front of the antenna array) and measurements are made at different distances.

During the experiments, the device is periodically turned off and the noise floor is measured at f_{LO}. These noise measurements are used to determine the detection threshold. Thresholds shown in the figure are estimated by a mean of multiple iterations taken through the course of the experiment. Overall, the choice of threshold depends on application and desired receiver operating characteristics (missed detection, false alarms, etc.) Measurements are made for 4-element array and 8-element array. Moreover, the results are compared with analogous measurements with a single antenna detector.

Figure 5.1 shows the relationship between measured amplitude and distance for the array detectors. The noise floor is measured and plotted as a baseline. The amplitude of the measured signal above the noise floor confirms the presence of a walkie-talkie. The detection range is determined based on the distance at which the signal strength fades into the noise floor.

The amplitude of the signal detected in Figure 5.1 decreases and fades into maximum noise floor at 18m. Although there are other distances at which the signal is above the noise floor, detection can no longer be guaranteed. The variation of signal amplitude is due to reflections and multipath fading. In summary, the reliable standoff distance for the eight-element array is 18m and four-element array is 10m.

Additionally, Figure 5.1 shows the graph for a single antenna detector. The range for the single antenna detector is 4m. The array processing and diversity gains improve the signal-to-noise ratio by increasing the signal strength. As a result, the antenna array increases the effective detection range.

B) Angle of Arrival (AOA). The performance and accuracy of the AoA method has been evaluated using a single device. Measurements were made with the walkie-talkie placed at angles 0^o, 45^o, 90^o, 135^o, and 180^o. Synthetic beam-forming was implemented using equations (2.1)-(2.4) to obtain power received with the angle of arrival [1]. Figure 5.2 shows the power received vs angle for a walkie-talkie placed at the predefined five angles.

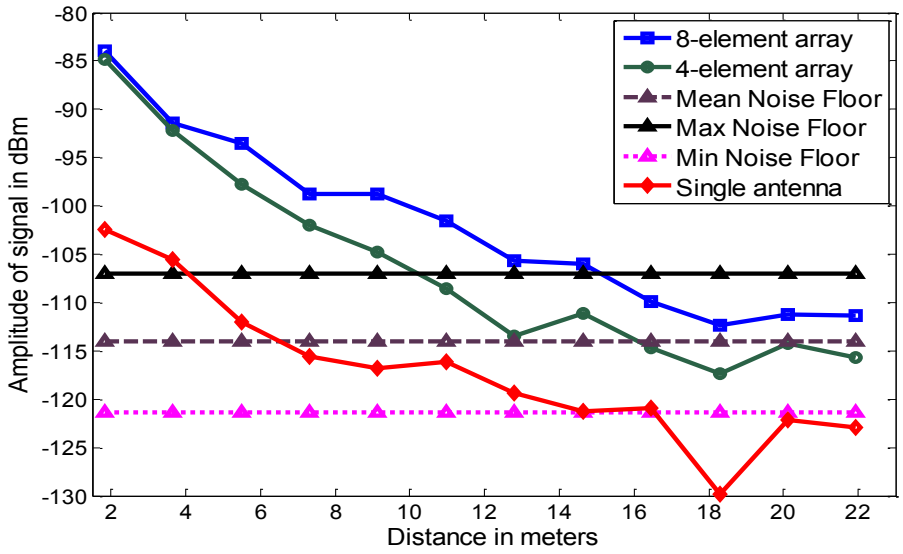

Figure 5. 1. Estimation of range for 4-element array and 8=element array

The performance of the antenna array degrades for AoA approaching 0 and 180 degrees. This is a direct consequence of directionality of antenna elements. The nulls occur at 0 and 180 degrees. Therefore, signals arriving from such angles are significantly attenuated such that they fade into the background noise. Omni-directional antennas can be employed to overcome this problem at the expense of gain at 90 degree, which will reduce effective detection range.

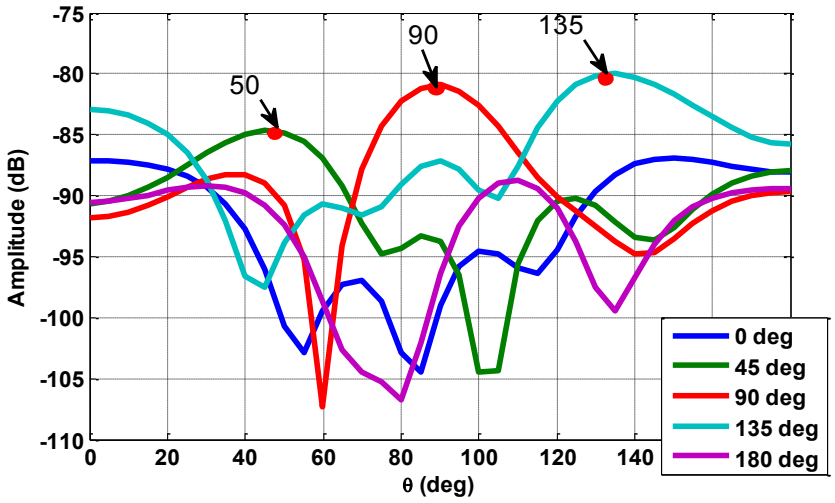

Figure 5. 2. Angle of detection for a single device placed at different angles

C) Detection of Multiple Devices. The AoA-based detection scheme is now extended to the detection of multiple devices. Two walkie-talkies are placed at 90^{o} and 130^{o}. Passive emissions from the devices are measured and amplitude vs. angle is plotted similarly to the case of angle detection. The peaks observed in Figure 5.3 affirm the presence of two devices. Peaks in the graph also represent the angle at which the devices have been placed. Also, performance of phased array processing is compared to other methods like MUSIC and MLE.

D) Detection of Multiple Devices at Different Frequencies. Walkie-talkies at different channels or different operating frequencies are also detected using the array. Walkie-talkie 1 at the Family Radio Service (FRS) channel 8 (467.5625 MHz) and walkie-talkie 2 at FRS channel 14 (467.7125 MHz) are used. The operating frequencies are separated by a 150kHz band. A sinusoidal sweep signal generated by the signal generator is used to stimulate the walkie-talkies. If the frequency of the walkie-talkie

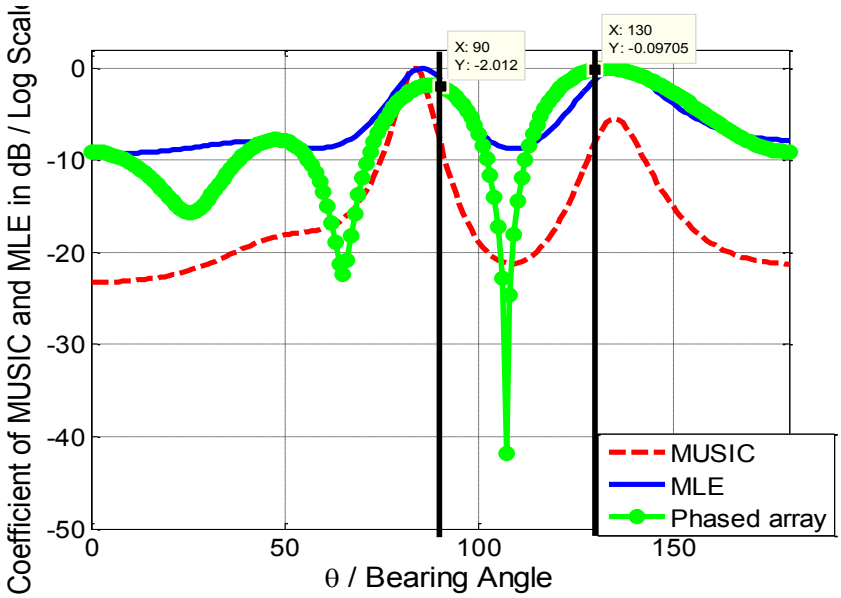

Figure 5. 3. Angle of arrival detection for two angles
(21.7 MHz) can be used to estimate the frequency of unintended emissions.

Measurements are made with walkie-talkie 1 placed at 60^{o} and walkie-talkie 2 is placed at 90^{o} and operating at two different channels. Amplitude vs angle is plotted for measurements at two different frequencies. The presence of two devices is detected as two different peaks at 60^{o} and 90^{o}, as shown in Figure 5.4. Two different lines indicate different operating frequencies for the walkie-talkies.

E) Analysis of Multiple Device Detection. The major limitations of phased array processing for detection of multiple R/C devices are: 1) devices placed close to each other appear as one peak using a 1-dimensional array and phased array processing; 2) phased array processing cannot be used to differentiate between line of sight and non-line sight (reflections/multipath) signals; 3) Devices placed towards the corners of the

array antenna are hard to detect; 4) Gain pattern of the uniform array antenna plays a major role in detection of angle of arrival.

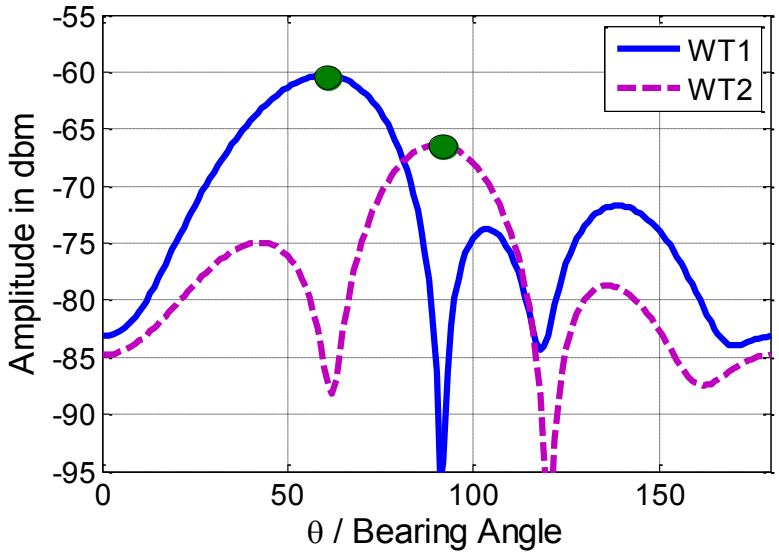

Figure 5. 4. Angle of detection for two walkie-talkies operating at two different frequencies

Resolution of the array antenna depends on half power beam width and distance of target from the array. Increasing number of elements decreases the half power beam width of the array. Array antenna with a smaller beam width can be used to detect devices placed closer to each other. Half power beam width of a uniform array antenna is given by equation (5.1) and resolution by equation (5.2) [13].

$$\theta_h = \cos^{-1}\left(\frac{1.391\lambda}{\pi N d}\right) \tag{5.1}$$

$$\delta y = 2R \sin\left(\frac{\theta_h}{2}\right) \tag{5.2}$$

where θ_h is half power beam width, λ is wavelength, N is number of antennas in the array, d is distance between array elements, δy is resolution and R is cross range

between the array and devices. For our antenna configurations, the theoretical resolution is 20 degrees for the four-element array and 12 degree for eight-element one.

Figure 5.5 and Figure 5.6 depict the limitations of 4-element and 8-element array for detection of multiple devices placed close to each other. The experimental results agree with the theoretical resolution limit in (5.1). We cannot distinguish between two devices when they are closer than 20-degrees for 4-element antenna. In contrast, the 8-element antenna succeeds in detecting two devices at the 20-degree separation, as shown in Figure 5.7. However, it fails when the devices are closer than 12-degrees, for example in Figure 5.6 we cannot distinguish between two devices at 10-degree separation. In general, the antenna resolution increases with the number of elements.

A 2-dimensional array has been implemented for detection of multiple devices to overcome some of the limitations of detection using phased array processing and 1-dimensional array. Devices placed closer to each other are detected using ESAR. ESAR is capable of differentiating sources placed $\lambda/2$ apart. Figure 5.8 shows detection of 2 devices placed 10^{o} apart ($\frac{\lambda}{2} \approx 0.35\text{m}$) using ESAR based method.

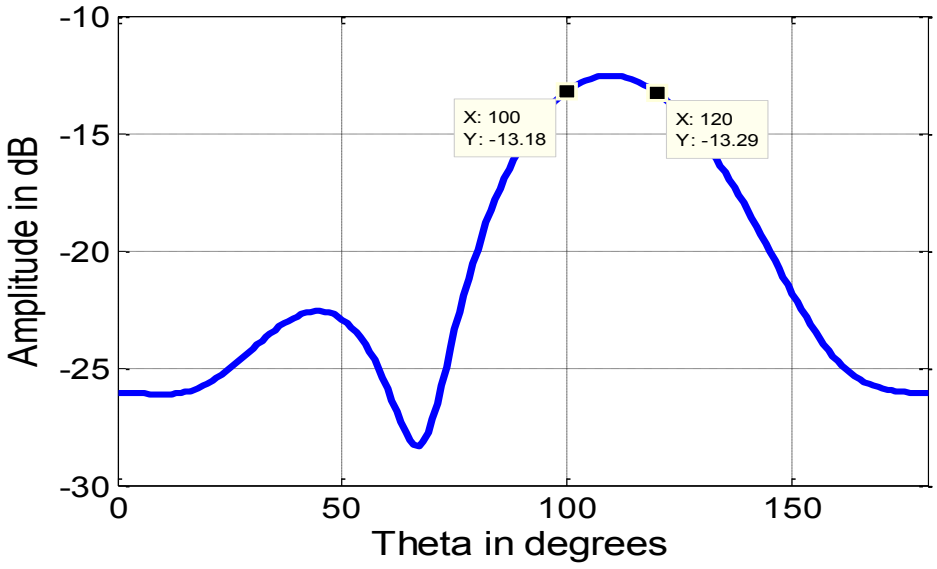

Figure 5. 5. Two walkie-talkies placed closed to each other (0.91m apart at R=3m, 100^{o} and 120^{o}) show as one peak for a 4-element array

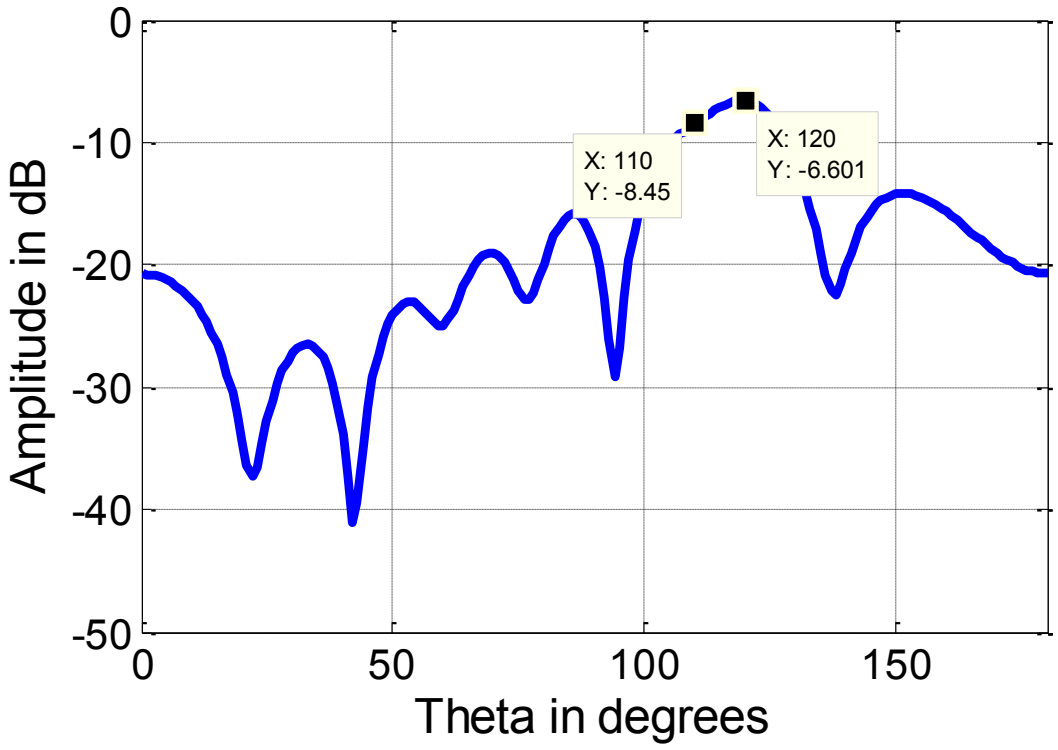

Figure 5. 6. Two walkie-talkies placed close to each other (0.3m apart at R=3m, 110^{o} and 120^{o}) show as one peak for a 8-element array

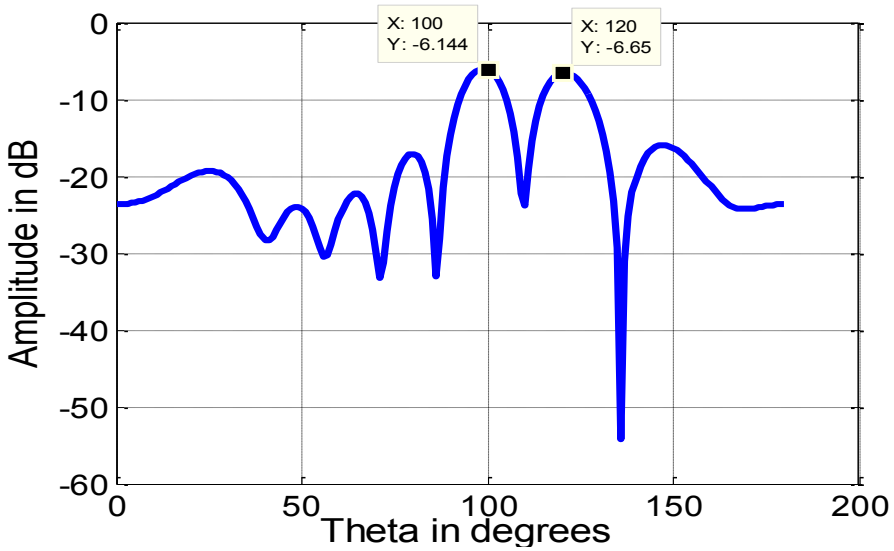

Figure 5. 7. Eight element array detects two peaks where four element array fails (0.91m apart at R=3m, 100^{o} and 120^{o})

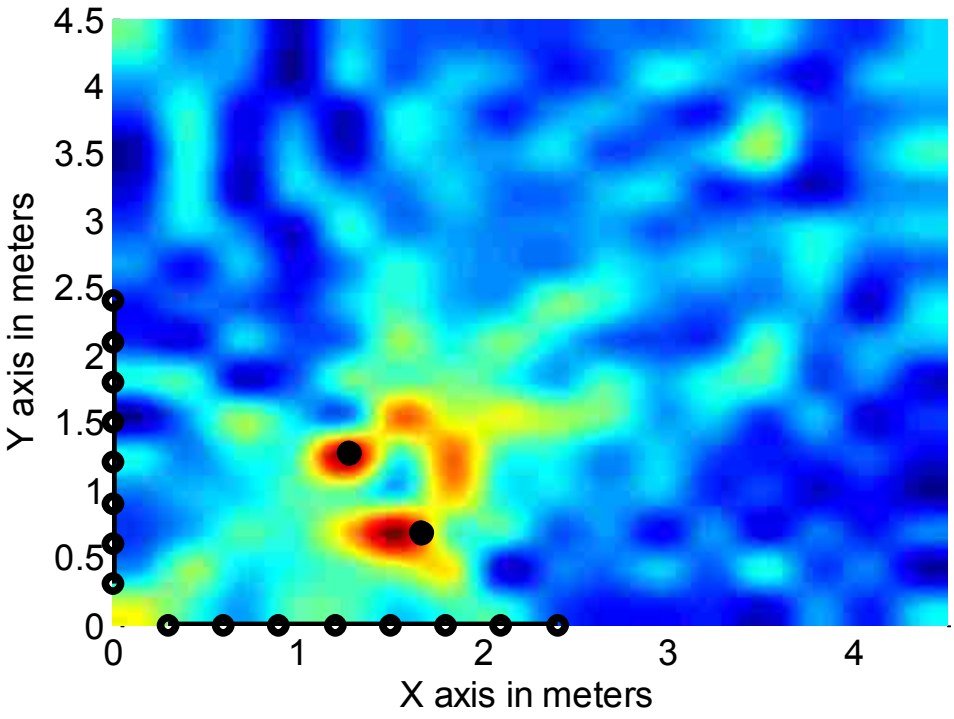

Figure 5. 8. Detection of multiple devices placed close to each other using ESAR and 2-dimensional array

Errors in ESAR method arise due to the following reasons: 1) noise components, 2) finite Fourier transform processing, 3) quantization error due to sampling and 4) incorrect phase estimation. The ESAR method fails when the devices are placed closer than $\frac{\lambda}{2}$. Performance of detection also depends on length of array and distance of objects from arrays. Figure 5.9(a), Figure 5.9(b) and Figure 5.9(c) show failure of E-SAR under different conditions. Estimation of location fails when devices are placed towards the edges of the array. Also, E-SAR cannot differentiate between signals from a source (Line of Sight) and reflector (Non Line of Sight).

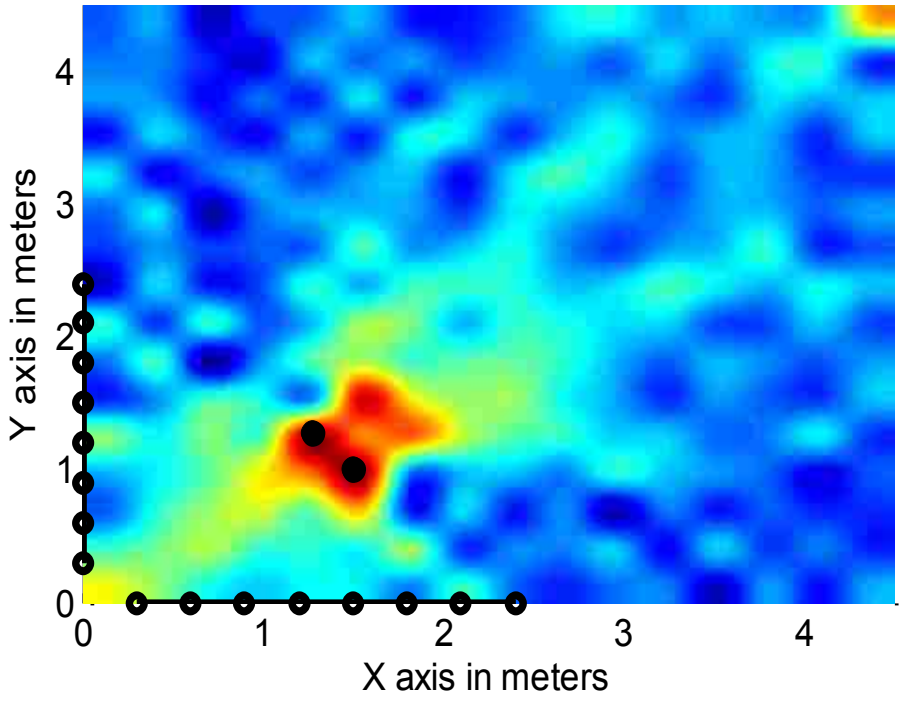

Figure 5.9 (a) Failure of E-SAR method when devices are placed closed to each other

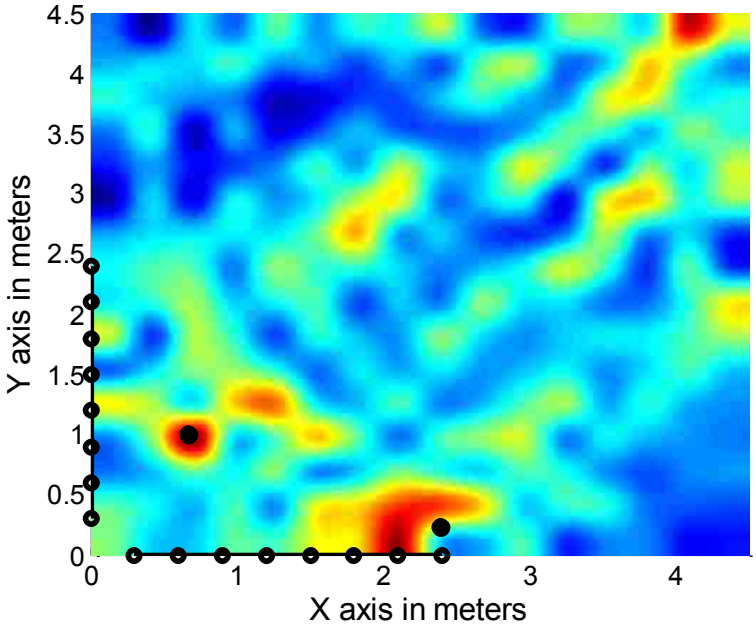

Figure 5.9 (b) Limitations of E-SAR when devices are placed closer to the edge of the array (cont.)

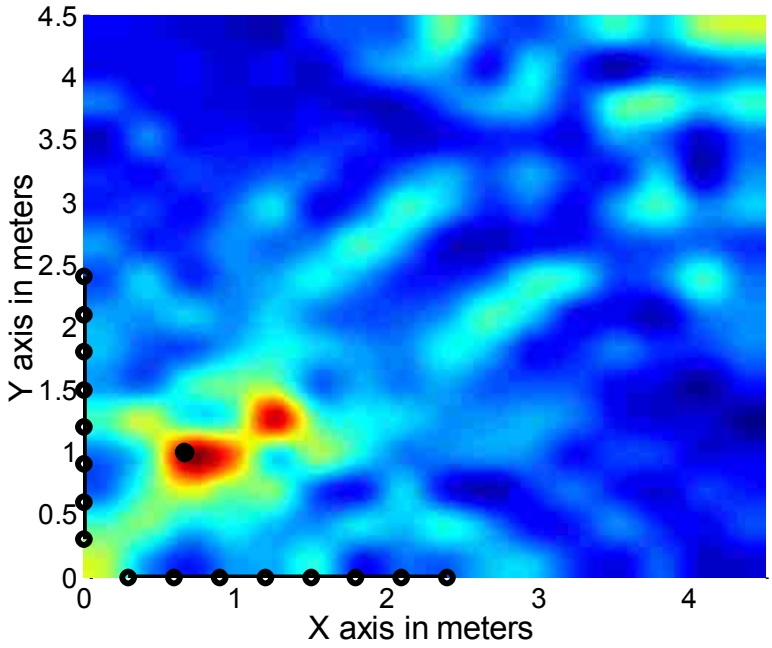

Figure 5.9(c) Reflector placed close to the device shows as a peak resulting in false detection (cont.)

Figure 5. 9: a) Failure of E-SAR method when devices are placed closed to each other, b) Limitations of E-SAR when devices are placed closer to the edge of the array, c) Reflector placed close to the device shows as a peak resulting in false detection

F) Analysis of Localization. The measured angle of arrivals for single device and multiple devices from Section A, B and C can be used to estimate the location of the device. Consider the experimental setup shown in Figure 3.3. Two walkie-talkies at FRS (Family Radio Service) channel 8 (467.5625 MHz) are placed at different locations shown in Table 5.1 and coordinates are estimated using equations 3.1 - 3.4. The error in the measured coordinates is also listed in the table for comparison.

In Table 5.1, 5.2 (X1, Y1), (X2, Y2) represent the actual position of walkie-talkies. The measured coordinates are represented by $(\widehat{X1}, \widehat{Y1})$ and $(\widehat{X2}, \widehat{Y2})$. Error between the measured and actual position of the walkie-talkies is represented by (EX1, EY1) and (EX2, EY2).

The error in the measured location of the walkie-talkies is high for AOA based method. The measurements shown in Table 5.1 are the best-case scenarios for AOA based method. A small error in angle of arrival (AOA) leads to a substantial error in location. The location is estimated as the point where the lines drawn from center of each of the arrays for the given AOA's meet. However, for small error in estimation of AOA, the lines connecting the center of arrays converge at a completely different location resulting in error in localization.

Edge SAR (ESAR) reduces the error in localization compared to the AOA based method. The SAR image generated from both the 4-element arrays placed along X-axis and Y-axis are combined to give a better estimate of the location of the devices. The experimental setup is built based on configuration shown in Figure 3.1. To allow comparison with AoA method the walkie-talkies are placed at the same locations as in Table 5.1.

Table 5. 1. Actual and measured coordinates with error in localization for AOA method (coordinates in m)

(X1,Y1)	**(X2,Y2)**	$(\widehat{X1}, \widehat{Y1})$	$(\widehat{X2}, \widehat{Y2})$	**(EX1,EY1)**	**(EX2,EY2)**
(2.4,1.2)	(1.2,2.4)	(1.6,2)	(2.1,3)	(0.8,0.8)	(0.9,0.6)
(2.4,2.4)	(2.4,2.4)	(3.1,3)	(3.3,1.7)	(0.7,0.6)	(0.9,0.7)
(2.4,2.4)	(2.4,3.6)	(3.2,3.1)	(3.5,4.8)	(0.8,0.7)	(1.1,1.2)
(2.4,2.4)	(3.6,2.4)	(3,3.2)	(5.2,4.1)	(0.6,0.8)	(1.6,1.7)
(0.7,1.7)	(1.5,1.0)	(1.2,2.4)	(2.4,1.6)	(0.5,0.7)	(0.9,0.6)
(0.7,1.0)	(2.4,0.2)	(1.1,1.6)	(3.8,2.1)	(0.4,0.6)	(1.4,1.9)
(0.4,2.0)	(2.0,0.4)	(1.4,3.1)	(3.3,1.1)	(1.0,1.1)	(1.3,0.7)
(1.3,1.3)	(1.7,0.7)	(1.9,1.7)	(2.3,0.2)	(0.6,0.4)	(0.6,0.5)

Table 5. 2. Actual and measured coordinates with error in localization for E-SAR based method (coordinates in m)

(X1,Y1)	**(X2,Y2)**	$(\widehat{X1}, \widehat{Y1})$	$(\widehat{X2}, \widehat{Y2})$	**(EX1,EY1)**	**(EX2,EY2)**
(2.4,1.2)	(1.2,2.4)	(2.5,2.5)	(1.4,2.6)	(0.1,0.1)	(0.2,0.2)
(2.4,2.4)	(2.4,2.4)	(2.3,2.4)	(2.5,2.4)	(0.1,0.0)	(0.1,0.0)
(2.4,2.4)	(2.4,3.6)	(2.2,2.3)	(2.2,3.3)	(0.2,0.1)	(0.2,0.3)
(2.4,2.4)	(3.6,2.4)	(2.6,2.3)	(4.0,2.6)	(0.2,0.1)	(0.4,0.2)
(0.7,1.7)	(1.5,1.0)	(0.8,1.6)	(1.5,0.9)	(0.1,0.1)	(0.0,0.1)
(0.7,1.0)	(2.4,0.2)	(0.7,1.0)	(2.0,0.1)	(0.0,0.0)	(0.4,0.1)
(0.4,2.0)	(2.0,0.4)	(0.4,2.2)	(2..2,0.4)	(0.0,0.2)	(0.2,0.0)
(1.3,1.3)	(1.7,0.7)	(1.4,1.3)	(1.5,0.7)	(0.1,0.0)	(0.2,0.0)

The error in localization is significantly lower for the ESAR method when compared with the angle of arrival-based method. The maximum error in coordinates for ESAR method is 0.4m compared to 1.7m for the AOA based method. SAR based method

is more computationally complex due to employment of Fourier transform, inverse Fourier transform, and reverse mapping. While the ESAR method takes more time and resources to execute than the AOA based method, it improves the localization accuracy. Euclidean error between actual position and measured position of a single device is presented for 4-element and 8-element array in Figure 5.11.

The estimation of the location can further be improved by increasing the number of elements in the array antennas. The error in localization is also a function of position of antennas and range of detection. As the devices are placed farther from the antennas the error in estimation increases for both AOA based and ESAR based localization. Different position of the antennas and number of elements also play a major role in localization error. Figure 5.12(a) and Figure 5.12(b) show the estimate of localization error for different configuration of array antennas.

The error in localization reduces by 84% when the number of elements is increased from four to eight. Figure 5.12(b) uses 8-element array antennas separated by a distance to cover more space resulting in reduction of localization error compared to the setup in Figure 5.12(a). Error in localization is reduced further by 30% when the array antennas are separated by a distance equal to length of array. Increasing the distance much further can result in blind spots due to nulls of the array and cancellation of the signals at those points. Initially as the distance between the arrays increases, the localization error decreases. At distance equal to the length of the array, the localization error decreases by 30% achieving its minimum. Further increase of distance between arrays leads to an increase in error. The maximum error increases by 50% when the distance between arrays is twice of its length.

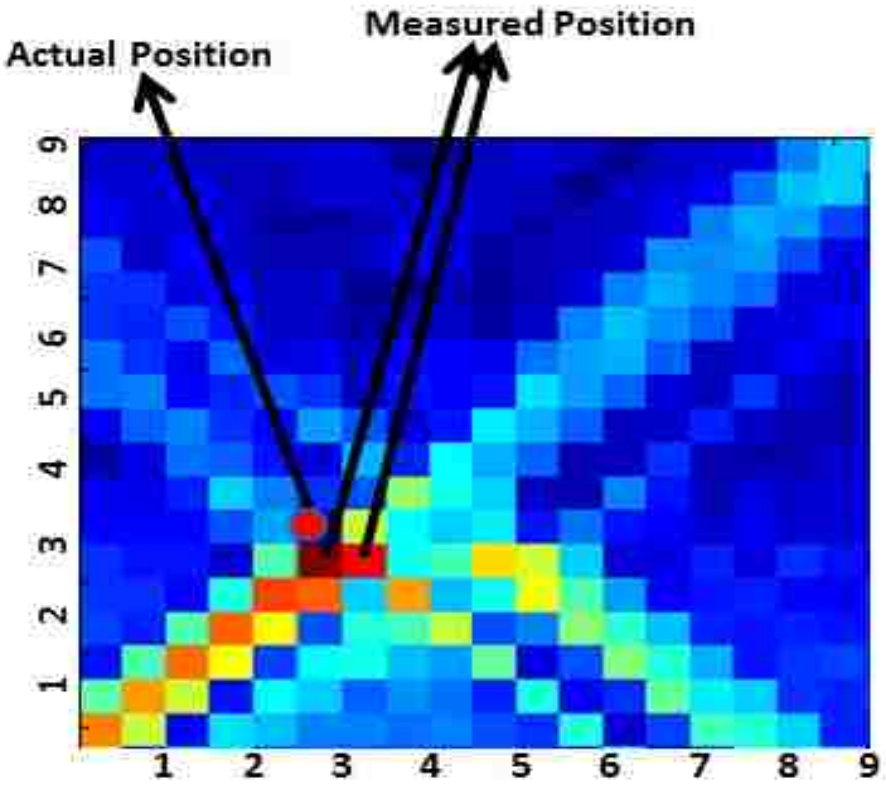

Figure 5. 10. Combined SAR image (X1=Y1=X2=Y2=2.4m)

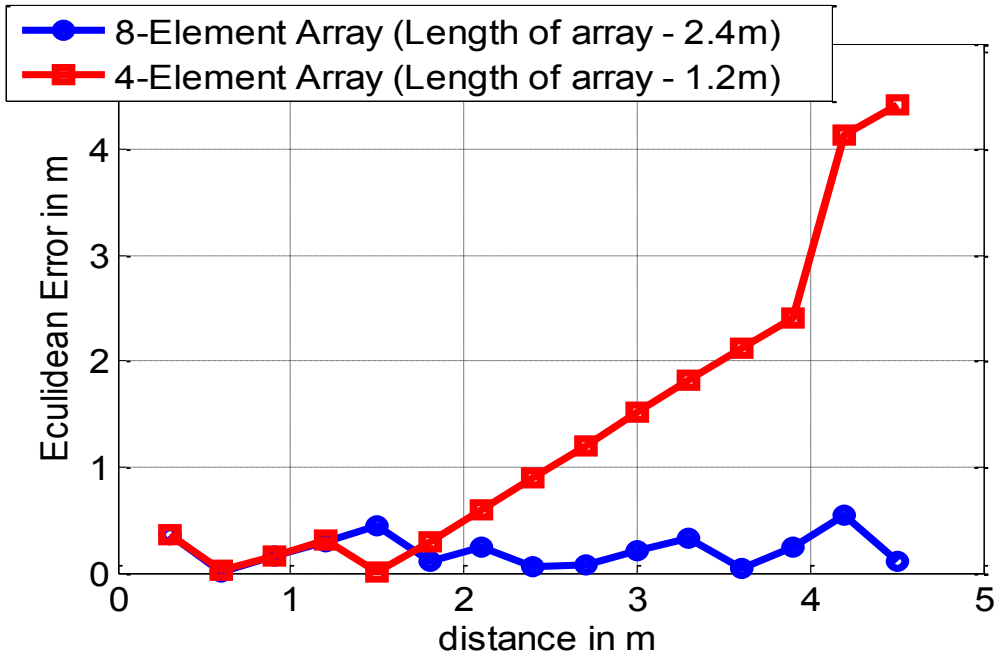

Figure 5. 11. Euclidean error for single device detection

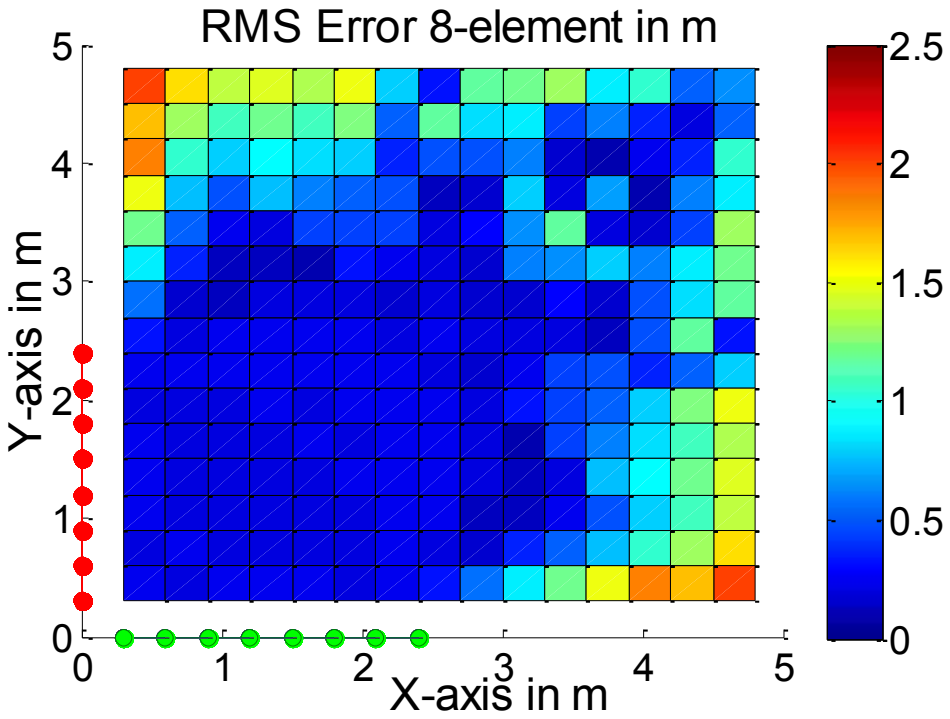

(a) Localization error in meters for 2-D 8-element array

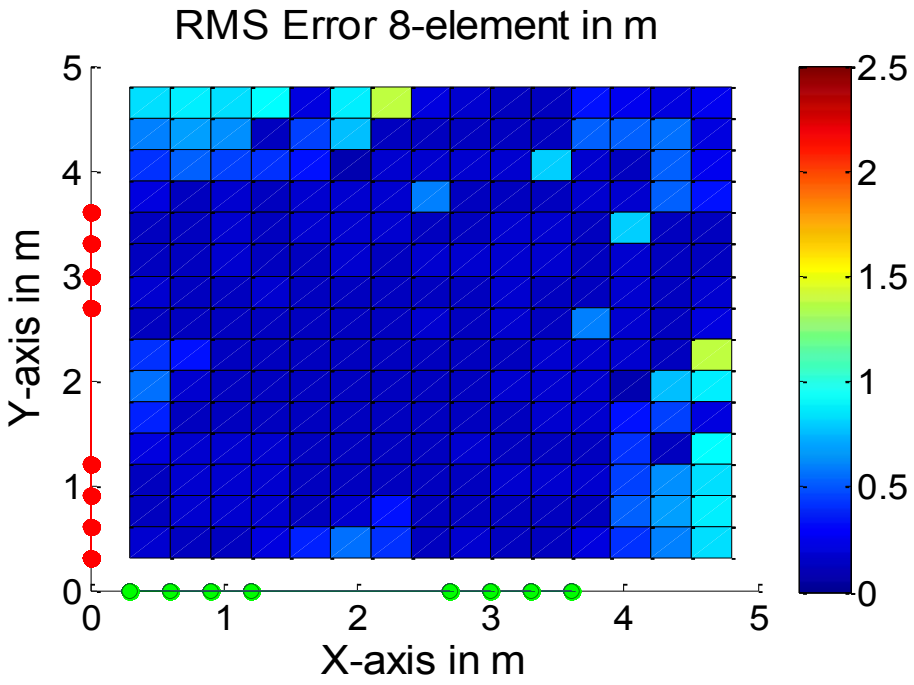

(b) Localization error in meters for 2-D 8-element array in different positions

Figure 5. 12. a) Localization error in meters for 2-D 8-element array, b) Localization error in meters for 2-D 8-element array in different positions

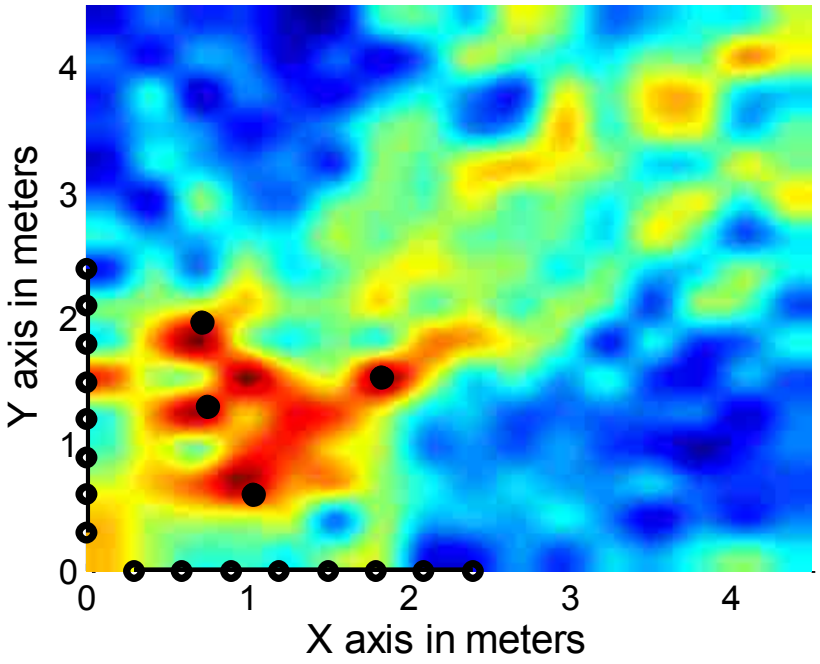

Figure 5. 13. Localization of 4 devices

6. CONCLUSIONS

The proposed architecture achieves a novel, passive detection and localization system of multiple R/C devices. The detection range for the four-element array detector increases by 250% and for the eight-element array detector increases by 450% when compared to the single antenna detector. The estimation of angle and range improves localization accuracy and enables the detection of multiple devices.

Localization has been achieved by using a two dimensional array consisting of two 4-element arrays placed along X-axis and Y-axis. Angle of Arrival (AOA) based estimation and ESAR based estimation have been implemented and compared. Our analysis shows that the Edge SAR method improves detection and localization accuracy when compared with the AOA based one. The proposed Edge SAR method reduces the error in localization by 75% at the expense of computational overhead. The localization error decreases by 84% with an increase in the number of elements from four to eight in each of the arrays. Also position of multiple arrays plays a major role in localization error. Arrays separated by distance equal to length of array results in further, 30% decrease in error. In general, the tradeoff between the localization accuracy and the cost and computational overhead has to be evaluated when selecting a particular array size.

New methods of estimation can be applied for localization both to improve the efficiency and to overcome multipath fading and reflections in a noisy environment. A correlation based method for detection and localization will be evaluated. Finally, detection and localization of more devices as shown in Figure 5.13 will be attempted and improved.

7. REFERENCES

[1]. Thotla, Vivek; Ghasr, M.T.A.; Zawodniok, M.; Jagannathan, S.; Agarwal, S., "Detection and localization of multiple R/C electronic devices using array detectors", Instrumentation and Measurement Technology Conference (I2MTC), 2012 IEEE International , vol., no., pp.1687,1691,13-16May2012.

[2]. Colin Stagner, Andrew Conrad, Christopher Osterwise, Daryl G. Beetner and Steven Grant, "A practical superheterodyne-receiver detector using stimulated emissions", IEEE Transactions on Instrumentation and Measurement, Vol. 60, No. 4, April 2011.

[3]. Shaik, Haixiao Weng, Xiaopeng Dong, T.H. Hubing and D.G. Beetner, "Matched filter detection an identification of electronic circuits based on their unintentional radiated emissions", In Electromagnetic Compatibility, 2006. EMC 2006. 2006 IEEE International Symposium on, volume 3, pages 853-856, August 2006.

[4]. D. Beetner, S. Seguin and H. Hubing, "Electromagnetic emissions stimulation and detection system", U.S. Patent 7 464 005, Dec. 9, 2008.

[5]. Haixiao Weng, Xiaopeng Dong, Xiao Hu, D.G. Beetner, T. Hubing, and D. Wunsch,"Neural network detection and identification of electronic devices based on their unintended emissions," In Electromagnetic Compatibility, 2005. EMC 2005. 2005 International Symposium, volume 1, pages 245-249, August 2005.

[6]. Vivek Thotla ; Mohammad Tayeb Ahmad Ghasr ; Maciej Zawodniok ; S. Jagannathan and Sanjeev Agarwal, "Detection and localization of R/C electronic devices using Hurst parameter",Proc. SPIE 8359, Sensors, and Command, Control, Communications, and Intelligence (C3I) Technologies for Homeland Security and Homeland Defense XI, 835915 (May 1, 2012)

[7]. Jake Hertenstein and S. Jagannathan,,"Detection of unintended electromagnetic emissions from super regenerative receivers," Proc. SPIE 8017, 80170F (2011); doi:10.1117/12.883223.

[8]. Sarah Seguin," Detection of low cost radio frequency receivers based on their unintended electromagnetic emissions and an active stimulation," Ph.D dissertation, Missouri University of Science and Technology, Rolla, MO 2009.

[9]. Ghasr, M.T.; Thotla, Vivek; Zawodniok, M.J.; Sarangapani, J., "Detection of Super Regenerative Receiver using Amplitude Modulated Stimulation," Instrumentation and Measurement, IEEE Transactions on , vol.PP, no.99, pp.1,1,0.

[10]. Jeffery B. Schodorf and Douglas B. Williams,"Array processing techniques for multiuser detection," IEEE Transactions on Communications, VOL. 45, NO. 11, November 1997

[11]. J. Beran, Robert Sherman, Murad S. Taqqu, and Walter Willinger, “Long-Range Dependence in Variable Bit-Rate Video Traffic”. IEEE Transaction on Communications, Vol. 43, No. 2/3/4, February/March/April 1995.

[12]. J. Beran. “Statistics for Long-Memory Processes”, Chapman and Hall, 1994.

[13]. C. Balanis, “Antenna Theory Analysis and Design”, John Wiley and Sons, 2nd ed. 1997.

[14]. McCorkle, J.W., "Focusing of synthetic aperture ultra wideband data," Systems Engineering, 1991., IEEE International Conference on , vol., no., pp.1,5, 1-3 Aug. 1993.

[15]. Wiley, C.A., “Synthetic Aperture Radars-A Paradigm for Technology Evolution,” IEEE Transactions on Aerospace and Electronic Systems, vol. AES-21, no. 3, pp. 440-443, May 1985.

[16]. Mark A. Richard, James A. Scheer, William A. Holm, “Principles of Modern Radar: Basic Principles”, SciTech Publishing, Edison, NJ, 2010.

[17]. Gerry, M.J.; Potter, L.C.; Gupta, I.J.; Van Der Merwe, A., "A parametric model for synthetic aperture radar measurements," Antennas and Propagation, IEEE Transactions on , vol.47, no.7, pp.1179,1188, Jul 1999.

[18]. Samczynski, P.; Kulpa, K., "Passive SAR imaging using a satellite pulsed radar as an illuminator of opportunity," Radar Symposium (IRS), 2012 13th International , vol., no., pp.157,161, 23-25 May 2012

[19]. Haraty, M.; Mohammadi, A.; Alimadady, M.; Sheikholvaezin, S., "Localization in wireless imaging sensor networks using SARtechniques," Telecommunications (IST), 2012 Sixth International Symposium on , vol., no., pp.560,565, 6-8 Nov. 2012.

[20]. Parr, A.; Miesen, R.; Vossiek, M., "Inverse SAR approach for localization of moving RFID tags," RFID (RFID), 2013 IEEE International Conference on , vol., no., pp.104,109, April 30 2013-May 2 2013.

[21]. De Maio, Antonio; Fornaro, G.; Pauciullo, A., "Detection of Single Scatterers in Multidimensional SAR Imaging," Geoscience and Remote Sensing, IEEE Transactions on , vol.47, no.7, pp.2284,2297, July 2009.

[22]. Soumekh, M., "Bistatic synthetic aperture radar inversion with application in dynamic object imaging," Signal Processing, IEEE Transactions on , vol.39, no.9, pp.2044,2055, Sep 1991.

[23]. Bohme, J.F.; Kraus, D., "On least squares methods for direction of arrival estimation in the presence of unknown noise fields," Acoustics, Speech, and Signal

Processing, 1988. ICASSP-88., 1988 International Conference on , vol., no., pp.2833,2836 vol.5, 11-14 Apr 1988.

[24]. Stoica, Petre; Nehorai Arye, "MUSIC, maximum likelihood, and Cramer-Rao bound," Acoustics, Speech and Signal Processing, IEEE Transactions on , vol.37, no.5, pp.720,741, May 1989.

III. DETECTION OF MULTIPLE R/C DEVICES USING MVDR AND GENETIC ALGORITHMS

ABSTRACT

Reflections, multipath propagation, and scattering create phantom sources of signal. Additionally, reliable detection of radio controlled (RC) devices in the presence of multiple, actual devices is a challenging task. RC devices employing super regenerative receivers (SRR) and super heterodyne receivers (SHR) emit unintended radiations in their ON state. This paper introduces a novel detection scheme that combines self-similarity and received signal strength indicator (RSSI) based detection with minimum variance distortion-less response (MVDR) method. Also, detection accuracy is improved using multi-constrained genetic algorithms. RSSI method detects multiple devices from received signal strength and Hurst parameter identifies self-similar SRR devices. Regularized MVDR improves detection of multiple devices by jamming unwanted signals and signals from known angle of arrival (AOA). Regularization reduces variation in detection due to environmental noise. Multi-constrained genetic algorithm is implemented in cases where MVDR fails. Experimental results for detection have also been presented for multiple SRR receivers (door bells at 315 MHz).

1. INTRODUCTION

Detection and identification of multiple R/C (radio controlled) electronic devices through their unintended emissions have a vital role in security applications. RC devices are low cost and can be reconfigured to cause security concerns. Typical radio controlled receivers are 1) super heterodyne receiver (SHR) and 2) super regenerative receiver (SRR). These receivers emit unintended radiations in both their active and inactive state. Unfortunately, these emissions are weak and thus hard to detect. A stimulated signal has been used previously to enhance the unintended radiations to improve detection and identification [1-6].

UE (unintended emissions) from super heterodyne receivers are usually single tone and vary based on frequency channel of operation of the receiver [2]. A low cost mobile array detector has been proposed in [2] for detection and localization of multiple SHR's. Received signal strength (RSS) method was utilized for detection of these devices. Some of the major challenges for detection of multiple devices using RSS are 1) multiple reflections, 2) multipath, 3) correlated sources and, 4) closely spaced devices. RSS method fails in the presence of strong reflections and multipath.

Super regenerative receivers are usually found in RC cars, wireless door bells, garage door openers etc. These receivers are cheap and available off the shelf. SRR's have a feedback loop in their circuit that acts like a quench oscillator resulting in a shaped response. Unintended emissions from the SRR are due to noise and filter response in SRR. When a stimulating signal is used the internal quench oscillator modulates the signal resulting in enhanced emissions. Shaped response of the emissions, act as a signature for detection and identification of the receiver [3][4]. A mathematical model of

SRR has been simulated and analyzed in previous work [3]. Unintended emissions from SRR have a second order self-similar property that can be used for detection. Hurst parameter was used in [3] and [4] as measure of self-similarity for detection and identification of SRR's. Mandelbrot (1965), Mandelbrot and Wallis (1969) originally introduced the concept of self-similarity and its estimation [2], [8], [9]. Rescaled range (R/S) method was used in [3] for estimation of Hurst parameter. This method fails in the presence of multiple receivers, reflections and multipath.

Previously, various adaptive array-processing techniques have been used for detection of multiple entities [10-13]. A partition linear interference canceller (PLIC) was used in [11] for multiuser detection. PLIC used a constrained optimization technique to array signal processing. A generalized minimum variance distortion-less response (MVDR) method is used in [12] for active source localization. An incoherent minimization has been used contrary to the conventional matched field based MVDR [14-16]. An auto-focusing algorithm using steepest descent (SD) has been suggested in [13]. Steepest descent has been used for iteratively changing the focusing angles for beamforming and MVDR is used to null stationary and non-stationary interferences. Also, gain from a particular angle of arrival can be enhanced. Nulls applied to jam signals from a particular direction can be used to reduce interference. Previous methods assume different noise models and use received signal strength for detection of active sources. These methods fail in the presence of multiple coherent sources and closely spaced sources. MVDR fails when direction of main beam is closer to the direction of null.

Genetic algorithms (GA) [16-21] are search and optimization algorithms which have been used for array synthesis. For fixed uniform linear arrays, excitation amplitude

of individual elements can be configured to obtain desired radiation patterns. Multi-constrained genetic algorithms can be used to increase the directivity in one direction while jamming signal from another direction.

The proposed approach combines mobile array detectors, Hurst parameter based detection, MVDR to detect multiple SRR's and GA to improve detection accuracy. Phased array processing is used with received signal strength for detection of sources, multipath and reflections. Hurst parameter is used to identify SRR's, MVDR is used to null known signals and interferences and multi-constrained GA is used to address multiple array design requirements. The Hurst parameter method has been shown to detect SRR devices [3]. However, this approach cannot be successfully combined with antenna array processing to perform localization of multiple devices. Even single self-similar source will be "detected" using Hurst parameter at multiple angles due to self-similar statistical properties of the signal. Consequently, presence and number of multiple devices could not be accurately determined. Also, MVDR fails under certain null conditions and when the devices are placed closed to each other. The proposed approach addresses these challenges by employing multi-constrained GA. In [1], MVDR has been used with Hurst parameter to detect multiple SRR's and identify them. A detailed analysis of this method has been presented in this paper with point of failure analysis and estimation of ROD (range of detection) for different scenarios. Detection error in AOA (angle of arrival) has been presented for different frequencies for the given fixed uniform array. Also, Genetic algorithm has been implemented to optimize the array again and improve resolution of detection when compared to the method in [1].

The main contributions of the proposed work include: (1) study of major challenges in detection of multiple SRR's, (2), analysis of failure for MVDR based detection, (3) developing a novel detection scheme that combines RSS, Hurst parameter, MVDR and GA and, (4) analysis of detection for the proposed approach under different conditions. Experimental results for real time data are also included.

2. METHODOLOGY

Overview of the proposed approach is shown in Figure 2.1. A uniform six-element array connected to a data acquisition unit (oscilloscope) acts as the detector. Each of the elements in the array is connected to 20dB low noise amplifiers (LNA) to amplify the signal. Wireless doorbells employing super regenerative receiver are used as device under test (DUT). These SRRs work at 315MHz with a quench signal at 550KHz.

Phased array processing is used for RSS based detection. The experimental setup of a 6-element array is shown in Figure 2.2. For an N element array antenna, consider the received signal $\boldsymbol{R}_{in}$, $in=1,2,3,4,5,6...N$ from individual antennas $\boldsymbol{A}_{in}$, $in=1,2,3,4,5,6,....N$ respectively [1],[2],[23].

$$\boldsymbol{S}(t,\theta) = \sum_{n=1}^{\mathrm{N}} \boldsymbol{R}_{in}(t) e^{j(in-1)\Psi} \tag{2.1}$$

where θ is the steering angle, $\Psi = K * d * \cos\theta$ represents the progressive phase of each antenna referenced to the previous one, $K = 2\pi/\lambda$, $d = \lambda/2$, and $\theta \in [0, \pi]$ [1]. $\boldsymbol{S}(t,\theta)$, gives the time series signal at the steering angles.

Rescaled range method (R/S method) is used to estimate the Hurst parameter of the signal. When Hurst parameter value H of the frequency spectrum of signal, satisfies 0.5< H < 1 it is said self-similar. For a process 'X', the rescaled range R/S over an interval 'NN' is given by [2-3]:

$$\frac{R}{S} = \frac{\max_{1\le j\le NN}\left[\sum_{k=1}^{j}(X_k - M(NN))\right] - \min_{1\le j\le NN}\left[\sum_{k=1}^{j}(X_k - M(NN))\right]}{\sqrt{\frac{1}{NN}\sum_{k=1}^{NN}(X_k - M(\mathrm{NN}))^2}} \tag{2.2}$$

where X_K is a sample of the process and $M(NN) = \frac{1}{NN}\sum_{j=1}^{NN} X_j$ is a sample mean over the period NN. The slope of the first order curve fitting for a plot of $log[R/S]$ versus NN on a log-log graph determines the value of H (Hurst Parameter).

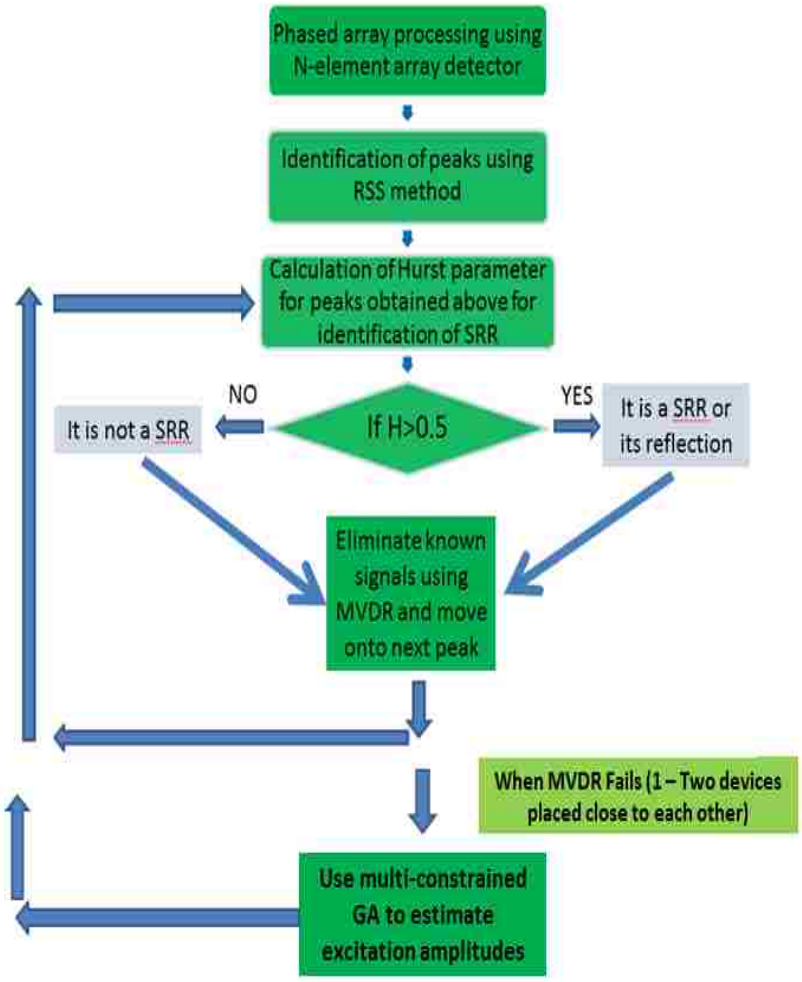

Figure 2. 1. Overview of the proposed approach

2.1 MINIMUM VARIANCE DISTORTIONLESS RESPONSE BEAMFORMER (MVDR).

MVDR is a form of linearly constrained minimum variance (LCMV) beamformer [15]. It minimizes the variance of a beamformer output while maintaining a distortionless response. Also, nulls can be placed at different steering angles as required. Consider a liner array with 'M' sensors as shown in Figure 2.2, with planar waves at an angle of 'Φ_0'. Let the time series signal at 1st sensor be:

$$\boldsymbol{U}_0(t) = e^{j\omega_0 t} \tag{2.3}$$

where ω_0 is the frequency of the capture signal and t is the time.

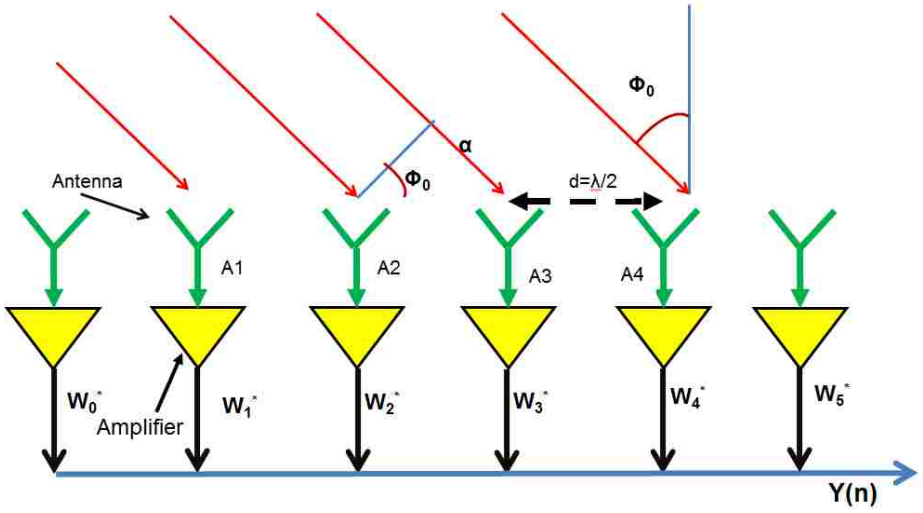

Figure 2. 2. Setup for six element phased array processing and MVDR

Signal at the k[th] sensor is given by:

$$\boldsymbol{U}_k(t) = \boldsymbol{U}_0(t-\tau_k) = e^{j\omega_0(t-\frac{kd\sin\boldsymbol{\Phi}}{c})} \tag{2.4}$$

where τ_k is the time delay to reach the k[th] sensor and c is the speed of the emissions (3e8 m/s). Sampling the signal we get:

$$\boldsymbol{U_k(t)}_{\boldsymbol{t=\frac{n}{F_s}=\frac{2\pi n}{w_s}}} = \boldsymbol{e^{jw_0(\frac{2\pi n}{w_s}-\frac{kd\sin\Phi}{c})}} = \boldsymbol{e^{jw_0 n}e^{-jk\theta}} \tag{2.5}$$

where $\theta = \frac{2\pi d\sin\boldsymbol{\Phi}}{\lambda}$, is the electrical angle, n is the total number of samples, F_s or ω_s is the sampling frequency. The range of 'θ' is restricted to (-π, π) to prevent spatial aliasing. Output signal of the array for given set of weights is given by:

$$\boldsymbol{Y_s}(n) = \sum_{k=0}^{M-1} \boldsymbol{W}_k^* e^{jwn} e^{-jk\theta_0} \tag{2.6}$$

$$\boldsymbol{Y}_s(n) = \boldsymbol{U_0}(n)\boldsymbol{W^H S}(\theta_0) \tag{2.7}$$

where $\boldsymbol{W} = \begin{bmatrix} \boldsymbol{W_0} \\ \boldsymbol{W_1} \\ \cdot \\ \cdot \\ \boldsymbol{W_{M-1}} \end{bmatrix}$ and $\boldsymbol{S(\theta_0)} = \begin{bmatrix} 1 \\ e^{-j\theta_0} \\ \cdot \\ \cdot \\ e^{-j(M-1)\theta_0} \end{bmatrix}$.

MVDR can also be used for jamming signals from another direction 'θ_j', for example from an already located source.

$$\boldsymbol{Y_j(n) = U_j(n) W^H S(\theta_j)} \tag{2.8}$$

The total output is given as:

$$\boldsymbol{Y}_T(n) = \boldsymbol{Y}_s(n) + \boldsymbol{Y}_j(n) \tag{2.9}$$

To find the weights for MVDR, LCMV is first derived to minimize undesired output energy. The cost function is expressed with Lagrange multiplier as:

$$\boldsymbol{J} = E\{|\boldsymbol{Y_T}(n)|^2\} + Re\{\lambda[\boldsymbol{W^H S}(\theta_0) - g]\} \tag{2.10}$$

where g=1 is the gain in direction $\theta_0(\Phi_0)$ for MVDR.

Solving for '$\boldsymbol{W}_0$' with $\nabla J = 0$ and 'g' as constant gives:

$$\boldsymbol{W}_0 = \frac{R_T^{-1}\boldsymbol{S}(\theta_0)}{\boldsymbol{S}(\theta_0)^H R_T^{-1}\boldsymbol{S}(\theta_0)} \tag{2.11}$$

where $\boldsymbol{R_T^{-1}} = -\frac{1}{2}\lambda * \boldsymbol{S}(\theta_0)$. Equation (2.11) gives the final solution of weights for conditions mentioned above resulting in MVDR.

In the proposed method, phased array processing is applied first to determine the peaks based on received signal strength (RSS). Hurst parameter is then applied to the frequency spectrum of the signal at the peaks to identify SRR's and interference signals. Known interference signals and signals from SRR are jammed to search for other sources of peaks using MVDR.

Figure 2.3 depicts the different cases for detection of multiple SRR's. The presence of multiple devices and reflection can be detected using received signal strength. SRR's can be identified using Hurst parameter and MVDR can be used to create nulls for signal coming from other devices and strong signals that mask the emissions from SRR's.

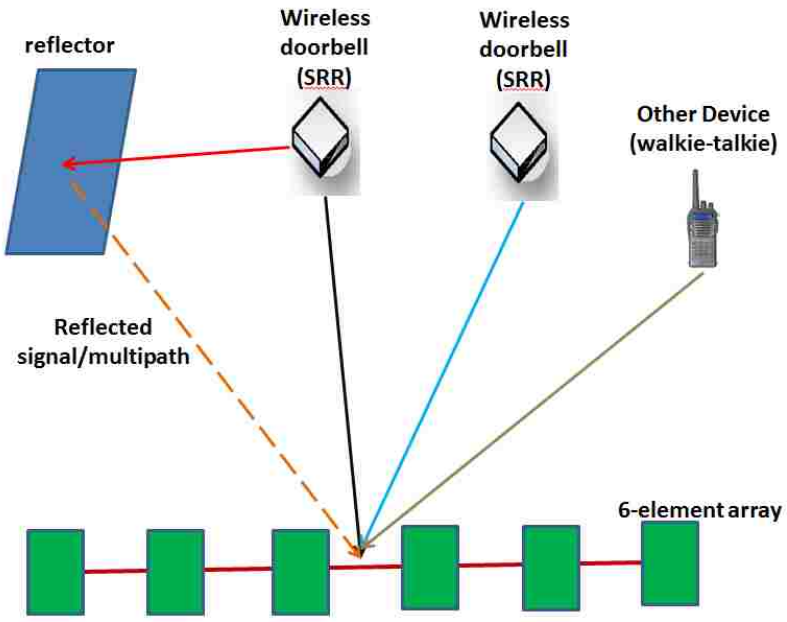

Figure 2. 3. Experimental setup – different cases for detection of multiple devices

2.2 GENETIC ALGORITHM OPTIMIZATION.

Genetic algorithm (GA) is a powerful optimization method based on natural selection and evolution. GA's are computationally simple and provide various search techniques in complex data spaces. With a given initial population, they effectively utilize the information to smartly guess new searches for improved performance. At every stage of generation GA maintains populations of individual entities (chromosomes) that represent a solution for the given cost function. The solutions are evaluated by the cost function or objective function (called Fitness function or Misfit function) of the corresponding optimization problem. GA selects individuals from the current population (parents) and modifies them to produce children for the next generation. In the successive reproductions, the children evolve to an optimized solution. The reproduction consists of three major steps: 1) selection, 2) crossover and, 3) mutation. In the selection process, GA chooses population with highest fitness. Reproduction generates new individuals by

crossover operation from existing parents. Mutation modifies the existing individuals that allow creating new individuals. The basic genetic algorithm steps have been depicted in Figure 2.4. One of the major aspects of implementing GA is relating to the real world. Setting up cost function or misfitness (MF) determines the optimization problem. In this paper, the performance of a uniformly placed and non-uniformly excited array is optimized using a combination of genetic algorithm and minimum variance distortion-less response (GA-MVDR).

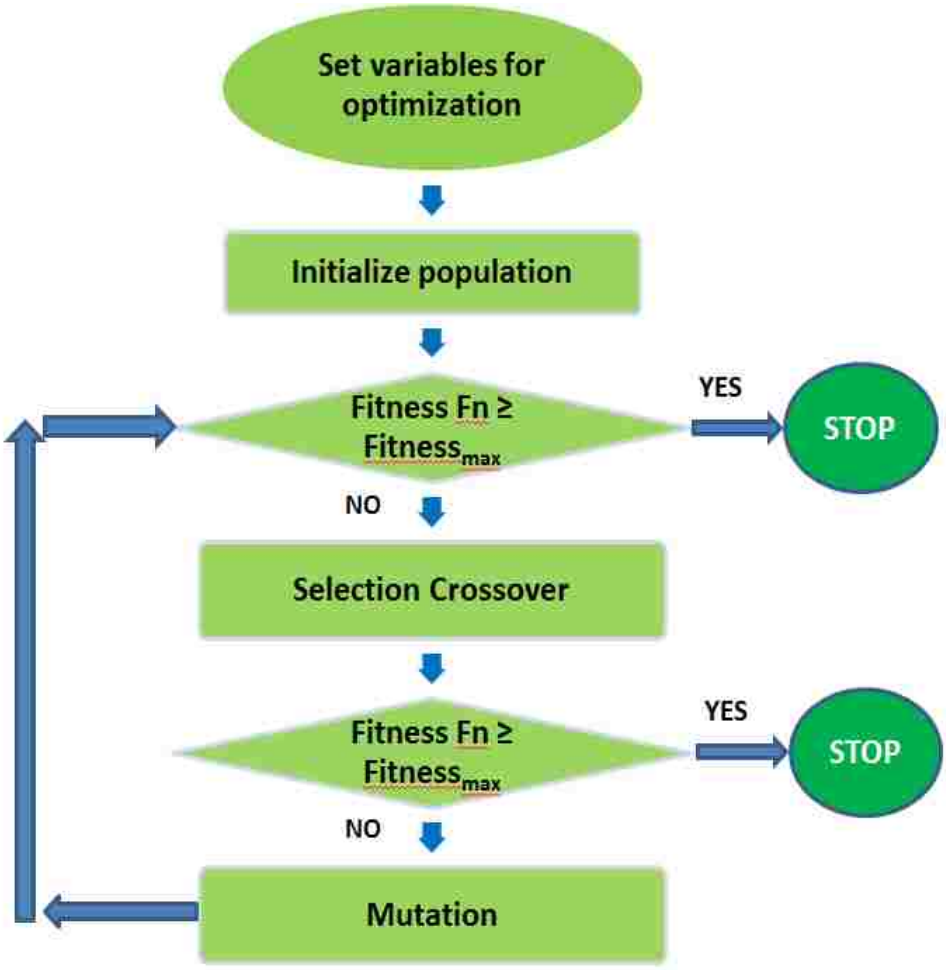

Figure 2. 4. Basic steps of GA

Genetic algorithm is used to estimate the excitation amplitudes of elements in the six-element array to obtain peak at a desired angle and null at another angle. Array factor (AF) of an array determines the gain at different angles of arrival. The array acts as a spatial filter for incoming signals. Position of elements in the array, excitation amplitudes of the elements and angle of arrival determine the position of main beams and nulls in the AF. Array factor can be optimized based on design requirements using GA. Though genetic algorithms can be computationally expensive, an offline implementation can be performed to create a database of weights for all possible detection cases based on the application. A lookup table can then be employed for faster real time applications.

Consider the array factor of a six-element linear uniformly spaced array shown in Figure 2.2.

$$\boldsymbol{AF} = \sum_{m=1}^{6} \boldsymbol{W}_{m-1} exp(jk(m-1)d\cos\theta) \tag{2.12}$$

where, W_{m-1} is the excitation amplitude of m^{th} element, $K = 2\pi/\lambda$, $d = \lambda/2$, and θ $\in [0, \pi]$. Consider θ_{da} -desired angle and θ_{ja} – jamming angle. $AF(\theta_{da})$ and $AF(\theta_{ja})$ determine gain at desired angle and jamming angle respectively. We need to maximize $AF(\theta_{da})$ and minimize $AF(\theta_{ja})$. The misfitness (MF) function in our case is defined as shown below:

$$\boldsymbol{MF} = \frac{|\boldsymbol{AF}(\theta_{ja})|}{|\boldsymbol{AF}(\theta_{da})|} \tag{2.13}$$

Minimization of MF for $\{(\theta_{ja}),(\theta_{da}) \in [0, \pi]\}$ results in optimized AF for desired requirements. Steps of GA as implemented for optimization of excitation amplitudes for the given array design are:

1. Initialization of chromosome population based on number of excitations for the array design.
2. Evaluation of misfit function for each solution.
3. Selection of sets that result in optimizing MF.
4. Crossover and mutation for generation of new sets.
5. Updating GA table
6. Continue until minimum value of MF is obtained.

3. RESULTS AND DISCUSSIONS

The uniform linear array with six elements, as shown in Figure 2.2 and Figure 2.3 is used for experimental setup, for collecting real time data in the presence of a doorbell (SRR), interference signal from another source and reflector. The array is designed to operate at 315 MHz with a spacing of $d = \lambda/2$ between the elements. The antenna elements are omnidirectional, lightweight, unobtrusive, and wideband antennas with an operating bandwidth in the range of 225 – 2500 MHz. Low-noise amplifiers (HILNAG2VIR, NuWaves - 20dB) are connected to the elements and output of the amplifier is connected to an oscilloscope. The oscilloscope acts as a receiver and data acquisition unit. Two of the Agilent MSO6104A oscilloscopes that act as receivers are used and an Agilent N5182A signal generator is used to send the stimulating signal. The oscilloscope is controlled from a laptop using LabView interface to acquire and store data. A stimulating signal at a frequency 315 MHz and amplitude of -40dBm is used to enhance the signals from the doorbell. Initially the devices are placed 10ft away on the ground for measurements. It is assumed that the exact frequency of the doorbell is unknown. Detection error for angle of arrival is calculated at different frequencies using phased array processing given in equation (2.1). Array designed at 315 MHz is tested at different frequencies for a fixed angle of arrival. Error in angle of arrival is due to non-coherent summation at other frequencies. The fixed uniform array still works for detection due to minor difference in wave length. Figure 3.1 shows the variation in detection error w.r.t frequency of detection. Frequency band of measurement for an error less than 5^o is more than 100 MHz.

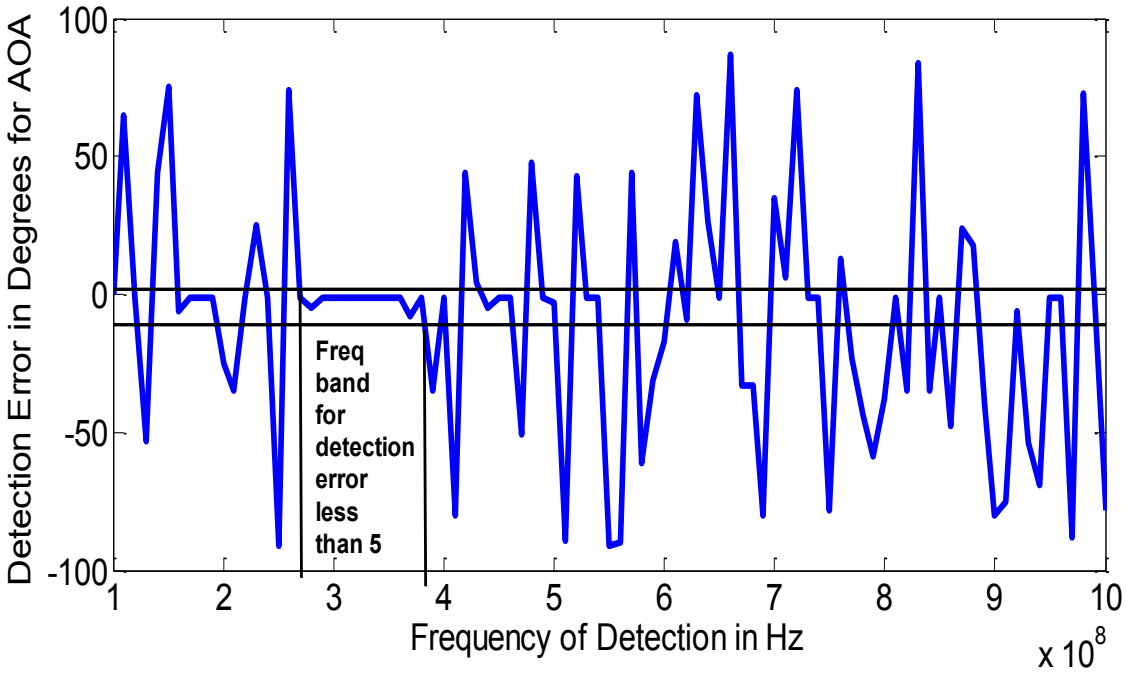

Figure 3. 1. Detection error vs frequency

B. MVDR WITH HURST PARAMETER

A) Detection of multiple sources with MVDR. A combination of doorbells (self-similar) and other sources (non-self-similar) are used for analysis. Initially a doorbell is placed at 40^0 and another source is placed at 140^0. Figure 3.2(a) shows amplitude vs angle using the basic RSS based method. Hurst parameter can be used to differentiate between the sources. The effectiveness of MVDR can be analyzed by placing at null at 40^0, as shown in Figure 3.2(b). After MVDR has been applied the signal from the doorbell is suppressed. Figure 3.2(c) shows the difference in Hurst parameter value before and after MVDR. The MVDR suppressed the signal from that direction while preserving the signals at other angles.

Doorbells have been placed at 135^o, 100^o and, another source at 60^o as shown in Figure 3.2(d). First, received signal strength of the emissions is plotted using phased array processing. Figure 3.2(e) shows the peaks due signal strength at different angles. Hurst parameter is then applied to frequency spectrum of signal from 55^o. Frequency spectrum of the signal at 55^o is analyzed and its Hurst parameter is estimated. A null is now placed at 55^o using MVDR and measurement is performed again with new weights. The new array factor after MVDR is shown in Figure 3.2(f). Figure 3.3 shows the frequency spectrum of self-similar emissions from the doorbell placed at 100^o.

Values of Hurst parameter for signals from different angles are tabulated in Table 3.1. It shows that signal from 55^o is not self-similar ($H < 0.5$). The effect of interference signal from 55^o is eliminated using MVDR. H parameter values at 100^o and 135^o confirms the presence of SRR's.

The maximum number of independent sources that can be detected for a given number of elements in an array is given by *N-1*, where N is the number of elements. A detailed analysis of the performance of different array antennas for detection and localization of multiple devices has been presented in [23].

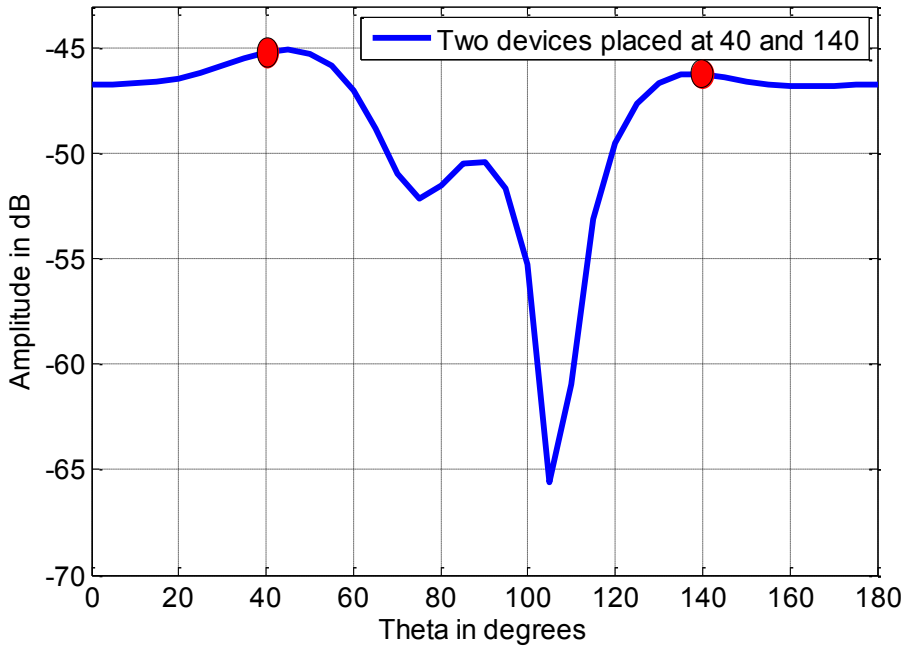

Figure 3.2 (a) Amplitude vs angle for RSS based method for 2 sources

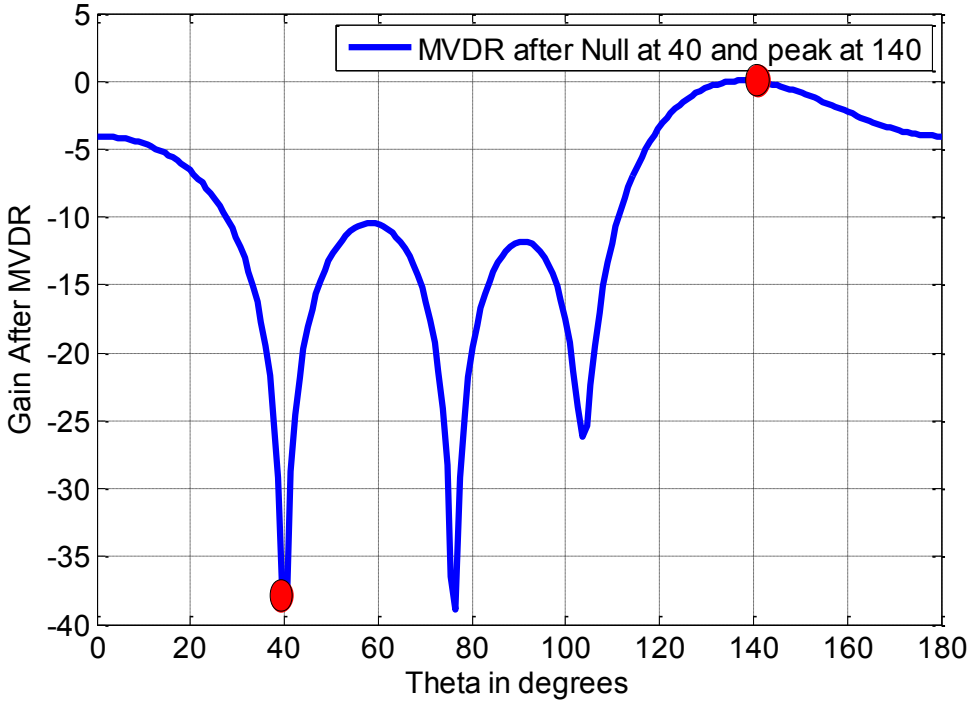

Figure 3.2 (b) MVDR beamformer with null at 40 and peak at 140 (cont.)

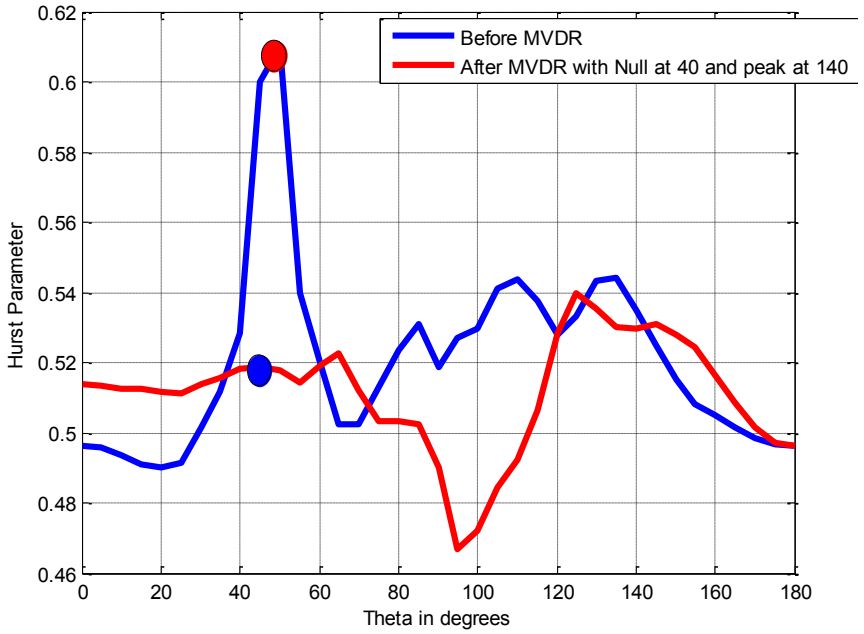

Figure 3.2 (c) Hurst Parameter based detection after applying MVDR (cont.)

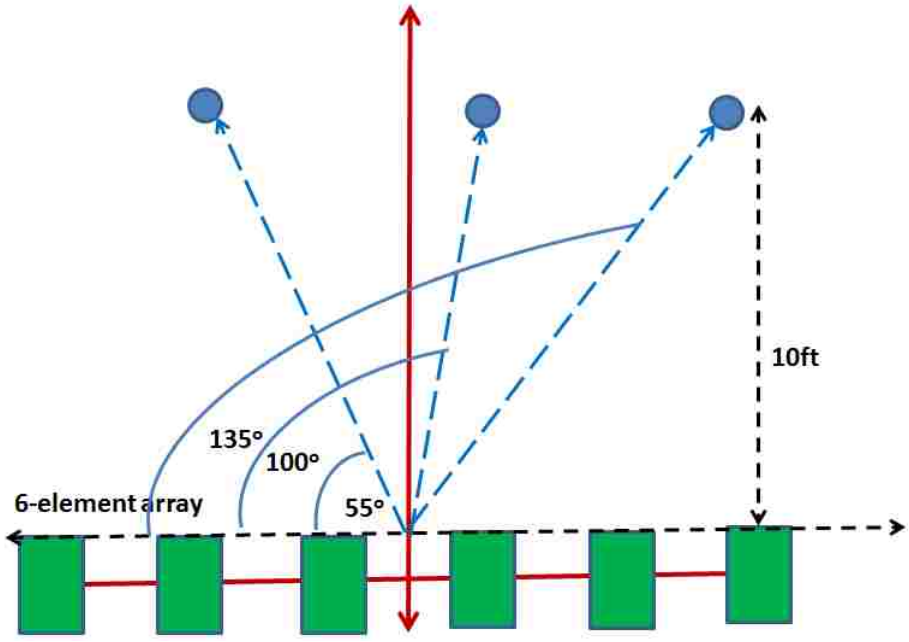

Figure 3.2 (d) Schematic for placement of devices (cont.)

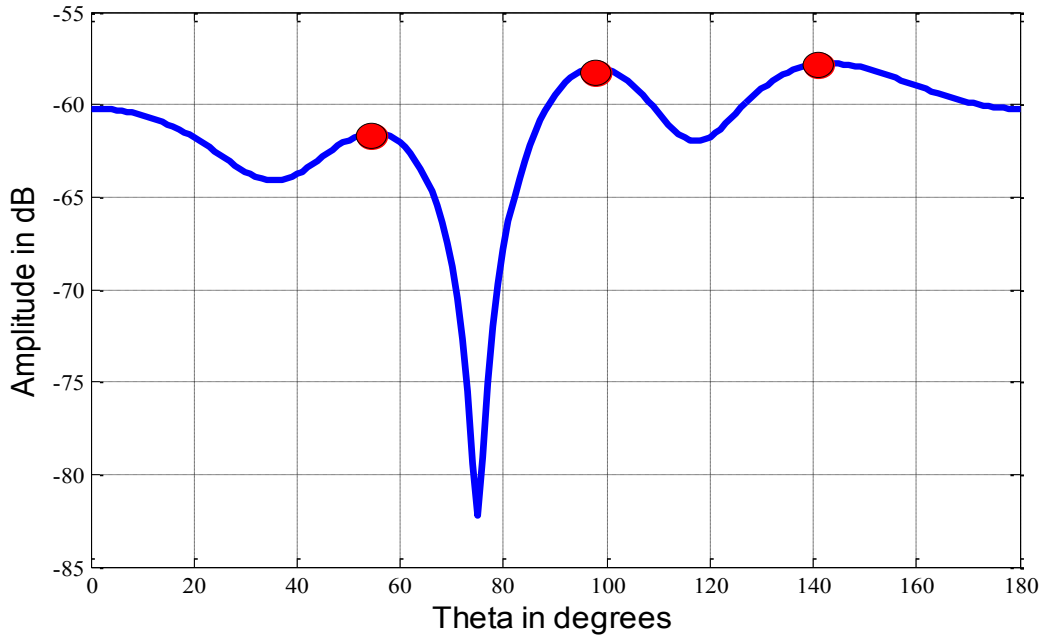

Figure 3.2 (e) Amplitude vs angle for RSS based method (cont.)

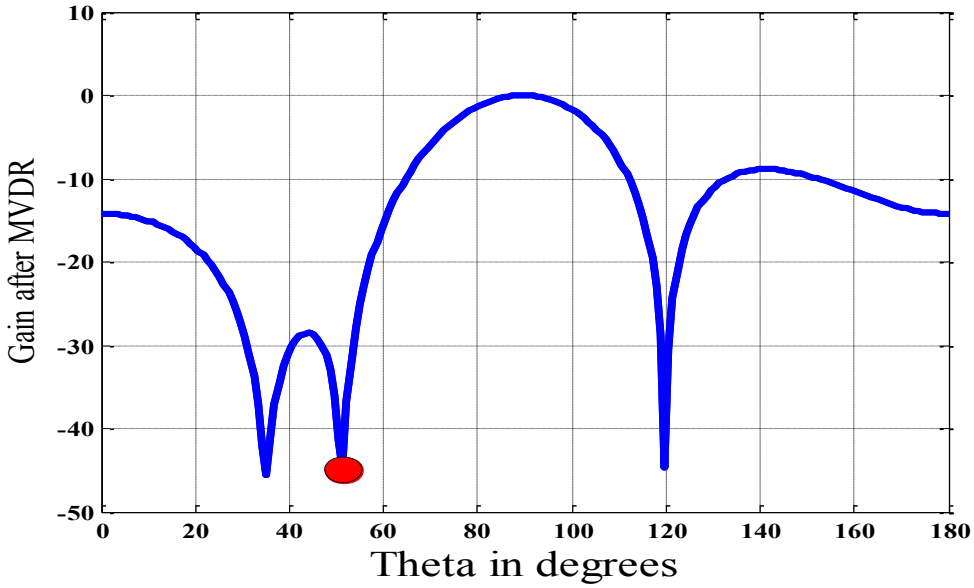

(f) MVDR beamformer with null at 55^{o} (cont.)

Figure 3. 2. (a) Amplitude vs angle for RSS based method for 2 sources (b) MVDR beamformer with null at 40 and peak at 140 (c) Hurst parameter based detection after applying MVDR (d) Schematic for placement of devices (e) Amplitude vs angle for RSS based method for 3 sources (f) MVDR beamformer with null at 55

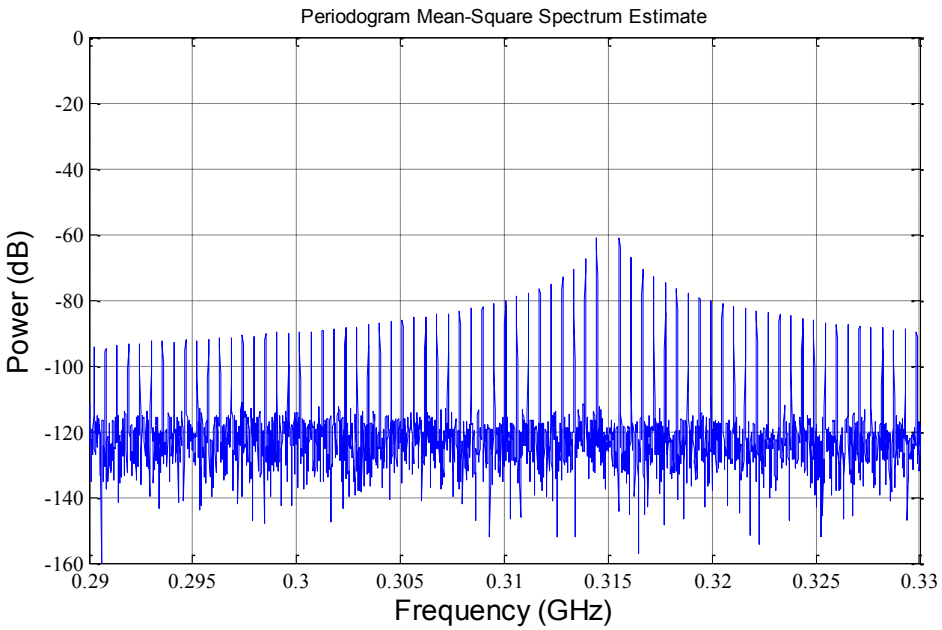

Figure 3. 3. Frequency spectrum of signal at 95^{o}

Table 3. 1. Hurst Parameter at peaks shown in Figure 3.6(a)

	Hurst Parameter (H)
Signal at 55^{o}	0.35
Signal at 100^{o}	0.68
Signal at 135^{o}	0.79

B) Failure of Phased Array Processing. A doorbell is placed at 40^{o} and reflector at 90^{o}. The amplitude vs angle of arrival is plotted using phased array processing. Phased array processing fails to differentiate between line of sight signal and reflected signal as shown in Figure 3.4. Hurst parameter also fails to differentiate between line of sight signal and reflected signal as shown in Figure 3.5(a). MVDR is used to eliminate the reflected signal by placing a null at 90^{o}, as shown in Figure 3.5(b).

C) Failure of the simple MVDR. Two doorbells are placed at 70^{o} and 90^{o}. MVDR is applied to place null at 70^{o} and peak at 90^{o}. Figure 3.6 shows the failure of

MVDR when devices are placed close to each other. The resolution of detection for MVDR for six-element array is 20^{o}.

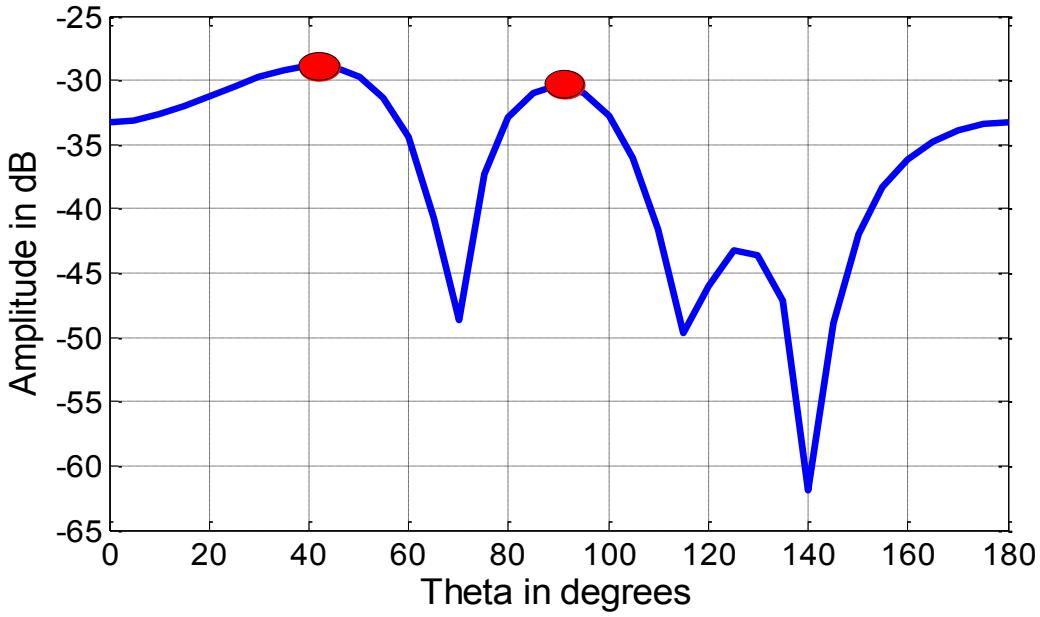

Figure 3. 4. Amp vs AOA for line of sight signal and reflected signal

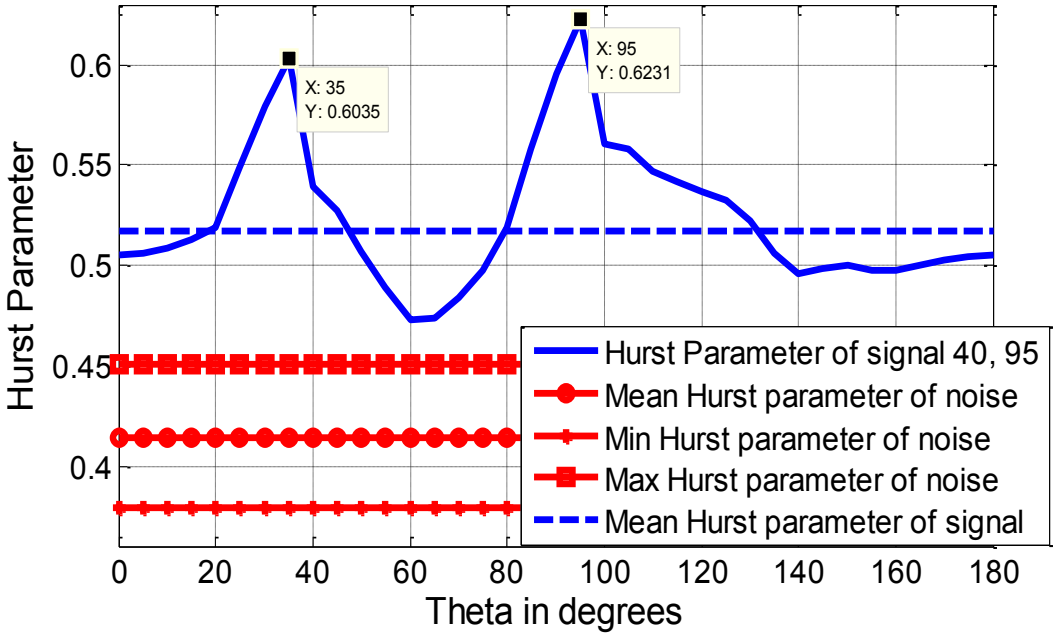

Figure 3. 5. (a) Hurst parameter vs AOA for line of sight signal and reflected signal

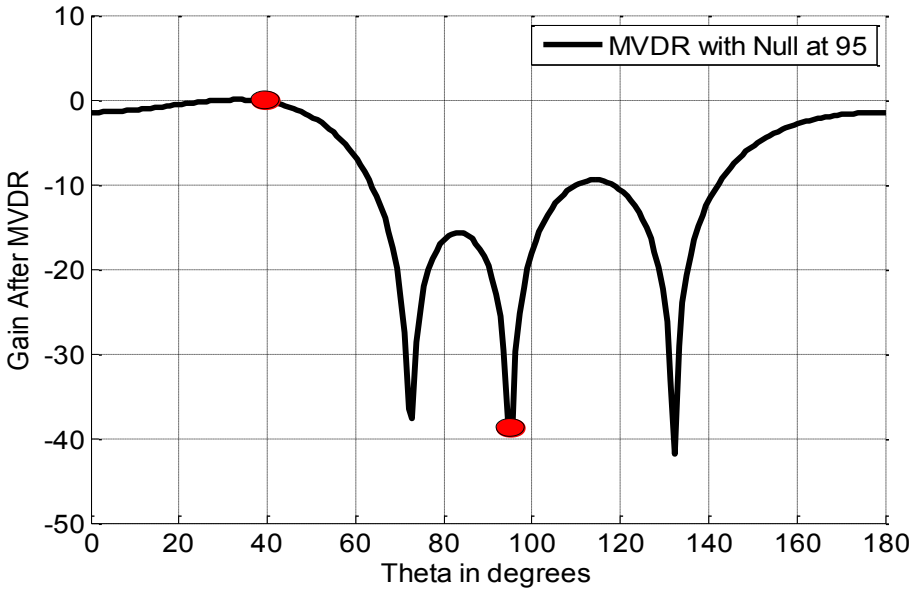

(b) MVDR to jam the signal from reflector (cont.)

Figure 3. 5. (a) Hurst parameter vs AOA for line of sight signal and reflected signal; (b) MVDR to jam the signal from reflector

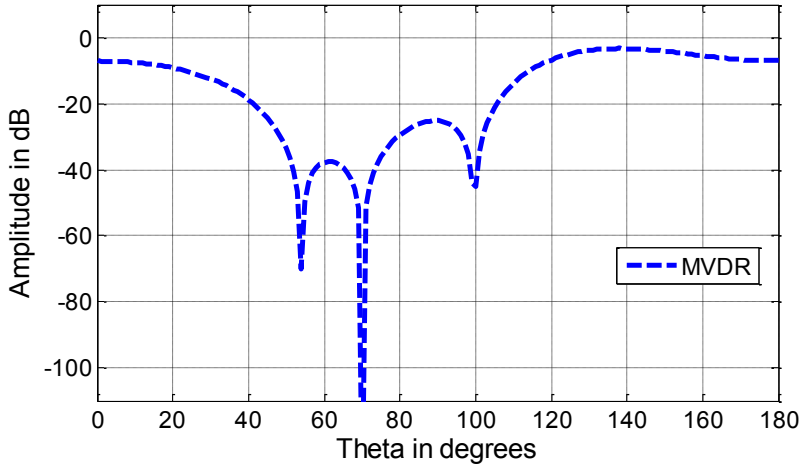

Figure 3. 6. MVDR with Null at 70^{o} and peak at 90^{o}

D) Range of estimation. Another major aspect for detection of multiple devices is range estimation. Two doorbells are placed at 40^{o} and 90^{o} respectively and measurements are made at different distances to estimate range of detection. Also,

MVDR is applied to reduce the interference between the devices. Figure 3.7 shows the improvement in range of detection after applying MVDR.

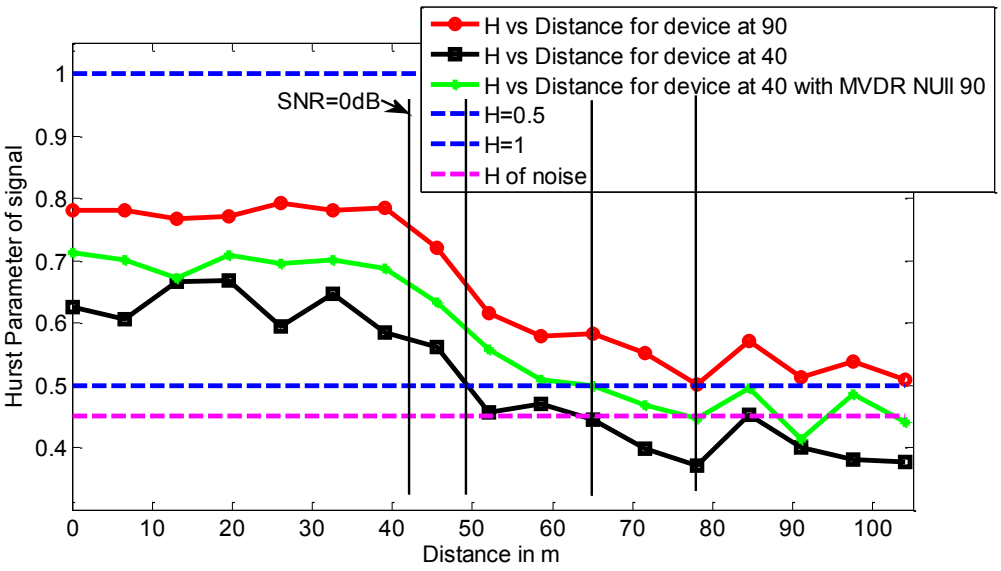

Figure 3. 7. Hurst parameter vs distance for estimation of range

C. OPTIMIZATION USING GENETIC ALGORITHM

A) Doorbells placed at 40^o and 90^o. Two doorbells are placed at 40^o and 90^o. GA is used to place a null at 40^o and peak at 90^o. Optimized weights for the given case are obtained through GA. Figure 3.8 shows the amplitude vs angle after optimization. Table 3.2 shows a comparison for difference in amplitude for null and peak directions for MVDR and GA. The difference in amplitude is similar when the devices are placed far from each other as shown in cases where nulls are placed at 20^0 and 50^0 respectively. As the devices are placed closer MVDR fails to give a significant peak.

B) Doorbells placed at 70^o and 90^o. Doorbells place at 70^o and 90^o. GA is applied to obtain optimized weights for null at 70^o and peak at 90^o. The difference

between amplitudes at null and peak directions is almost the same for MVDR and GA. GA performs better than MVDR in producing a significant peak as shown in Figure 3.9.

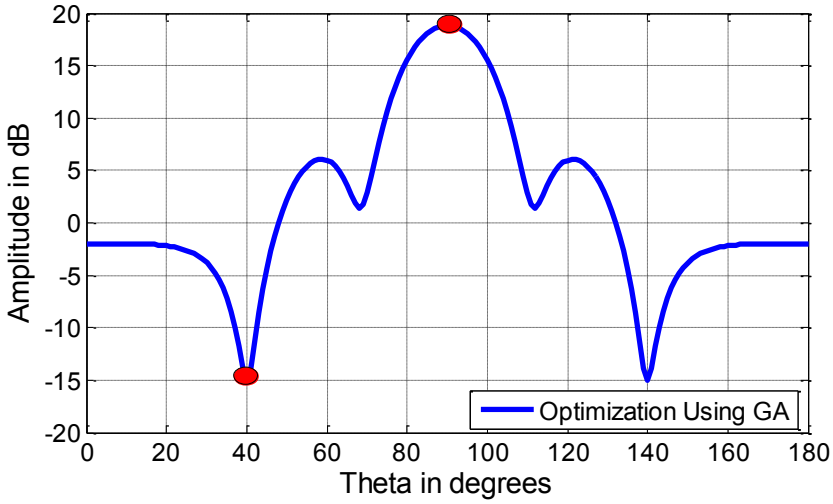

Figure 3. 8. Array gain vs AOA using GA

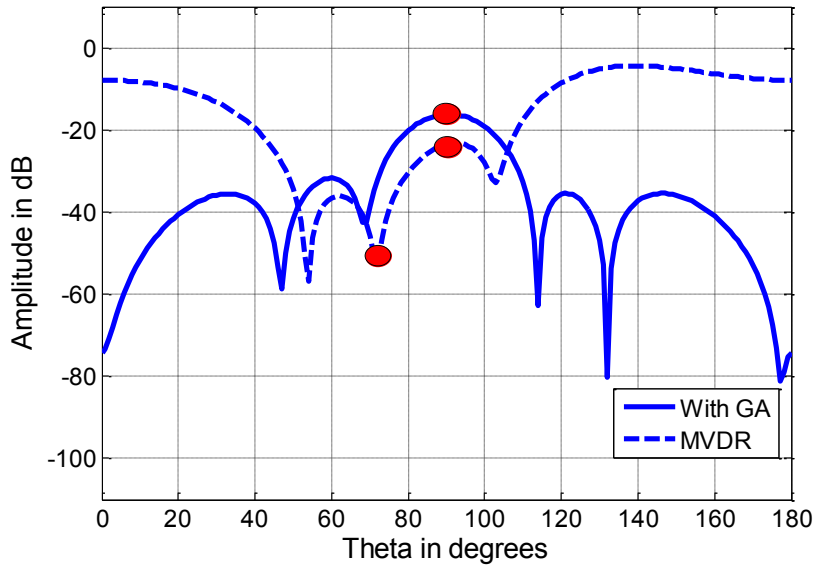

Figure 3. 9. MVDR vs GA for null at 70 and peak at 90^{o}

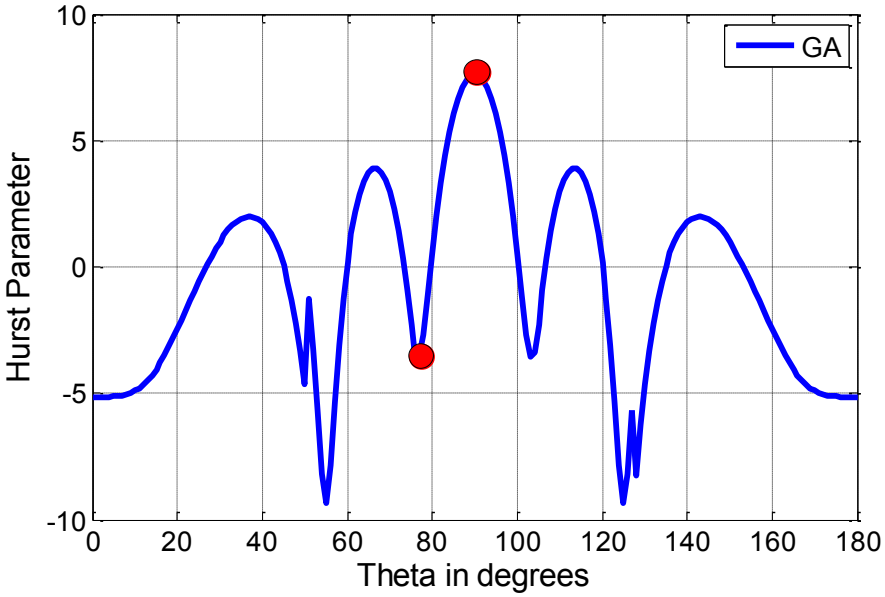

Figure 3. 10. GA for null at 80^{o} and peak at 90^{o}

GA improves the accuracy of detection and resolution of the array. For the six element array, the resolution reduces to 10^{o} as shown in Figure 3.10, compared to 20^{o} with MVDR. An overview of computational details for ten iterations is presented in Table 3.3. Computational complexities increase for bigger arrays and more complex constraints. An offline processing of these scenarios can be implemented to reduce run time in real world applications.

Table 3. 2. MVDR vs GA for different cases

Null direction in degrees	Peak direction in degrees	Difference in amplitude for MVDR in dB	Difference in amplitude for GA in dB
20	90	20.09	19.87
40	90	19.94	21.47
70	90	22.4	23.56
80	90	3.1	11.2

Table 3. 3. Computational details for GA

Null direction in degrees	Peak direction in degrees	Number of Generations	Function Count	Computation time for detection process in secs
20	90	104	21001	3.420353
40	90	102	20601	3.517744
70	90	106	21401	3.155911
80	90	103	20801	3.570194
40,140	90	116	23401	4.147534

4. CONCLUSIONS

The proposed novel combination GA-MVDR improves detection and identification of multiple SRR's. GA-MVDR is a combination of received signal strength, Hurst parameter, MVDR and GA optimization. RSS method and Hurst parameter method fail in the case of strong reflections close to another device. MVDR has been successfully used to jam the "interference" signal and detect the SRR's. Range of detection increases by 30% when MVDR and GA are used. However, this method fails to differentiate between strong reflected signal and line of sight signal. Also, MVDR fails when devices are placed close to each other. Genetic algorithm is used to improve the resolution of detection by 10^{o}. Multiple sources separated by more than 5^{o} can be distinguished using the novel method. But the method fails to differentiate between line of sight and non-line of sight signals, which will be addressed in future work.

5. REFERENCES

[1] Thotla, Vivek; Zawodniok, M.;, "Hurst parameter based detection of multiple super regenerative receivers (SRR) using MVDR," Instrumentation and Measurement Technology Conference (I2MTC), 2014 IEEE International, 12-15 May 2014

[2] Thotla, Vivek; Ghasr, M.T.A.; Zawodniok, M.; Jagannathan, S.; Agarwal, S.;, "Detection and localization of multiple R/C electronic devices using array detectors," Instrumentation and Measurement Technology Conference (I2MTC), 2012 IEEE International , vol., no., pp.1687-1691, 13-16 May 2012.

[3] Jake Hertenstein and S. Jagannathan,,"Detection of unintended electromagnetic emissions from super regenerative receivers," Proc. SPIE 8017, 80170F (2011); doi:10.1117/12.883223.

[4] Thotla, Vivek.; Ghasr, M.T.A.; Zawodniok, M.J.; Jagannathan, S.; Agarwal, S., "Detection of Super-Regenerative Receivers Using Hurst Parameter," Instrumentation and Measurement, IEEE Transactions on , vol.62, no.11, pp.3006,3014, Nov. 2013.

[5] Ghasr, M.T.; Thotla, V.; Zawodniok, M.J.; Sarangapani, J., "Detection of Super Regenerative Receiver Using Amplitude Modulated Stimulation," Instrumentation and Measurement, IEEE Transactions on , vol.62, no.7, pp.2029,2036, July 2013.

[6] H. Zargarzadeh ; David Nodland ; Thotla Vivek ; S. Jagannathan; S. Agarwal;, "Neural-network-based navigation and control of unmanned aerial vehicles for detecting unintended emissions". Proc. SPIE 8387, Unmanned Systems Technology XIV, 83870H , May 1, 2012.

[7] D. Beetner, S. Seguin and H. Hubing, "Electromagnetic emissions stimulation and detection system," U.S. Patent 7 464 005, Dec. 9, 2008.

[8] J.Beran, R. Sherman, Murad S. Taqqu, and W. Willinger, " Long-Range Dependence in Variable Bit-Rate Video Traffic," IEEE Transaction on Communications, Vol. 43, No. 2/3/4, February/March/April 1995.

[9] Jan Beran,"Statistics for Long-Memory Processes," Chapman and Hall, p. 81, 1994.

[10] C. Balanis, "Antenna Theory Analysis and Design", John Wiley and Sons, 2nd ed. 1997.

[11] Jeffery B. Schodorf and Douglas B. Williams,"Array processing techniques for multiuser detection," IEEE Transactions on Communications, VOL. 45, NO. 11, November 1997.

[12] Krolik, J.; Lynch, J.; Swingler, D., "A robust incoherent matched field processor for source localization in uncertain multipath fields," Acoustics, Speech, and Signal Processing, 1989. ICASSP-89., 1989 International Conference on , vol., no., pp.2637,2640 vol.4, 23-26 May 1989.

[13] Churng-Jou Tsai; Jar-Ferr Yang, "Auto-focusing and tracking techniques for enhancement of coherent signal-subspace methods," Statistical Signal and Array Processing, 1992. Conference Proceedings., IEEE Sixth SP Workshop on , vol., no., pp.370,373, 7-9 Oct 1992.

[14] Zoltowski, M.D., "On the performance analysis of the MVDR beamformer in the presence of correlated interference," Acoustics, Speech and Signal Processing, IEEE Transactions on , vol.36, no.6, pp.945,947, Jun 1988.

[15] Alam, M.J.; O'Shaughnessy, D.; Kenny, P., "A novel feature extractor employing regularized MVDR spectrum estimator and subband spectrum enhancement technique," Systems, Signal Processing and their Applications (WoSSPA), 2013 8th International Workshop on , vol., no., pp.342,346, 12-15 May 2013.

[16] Simon Haykin, "Adaptive Filter Theory", Prentice-Hall Inc., 4th Edition 2002.

[17] D. E. Goldberg, "Genetic Algorithms in Search, Optimization and Machine Learning". Reading, MA: Addison-Wesley, 1989.

[18] P. K. Murthy and A. Kumar, "Synthesis of Linear Antenna Arrays," IEEE Trans. Antennas Propagat., Vol. AP-24, pp. 865-870, November 1976.

[19] F. Hodjat and S. A. Hovanessian, "Non-uniformly spaced linear and planar array antennas for sidelobe reduction", IEEE Trans, on Antennas and Propagation, vol. AP-26, No.2, pp. 198-204, March 1978.

[20] Keen-Keong Yan and Yilong Lu, "Sidelobe Reduction in Array-Pattern Synthesis Using Genetic Algorithm", IEEE Transactions on Antennas and Propagation. Vol 45, No. 7, July 1997, pp. 1117-1122.

[21] Franciso J. Ares-Pena, Juan A. Rodriguez-Gonzalez, Emilio Villanueva-Lopez and S. R. Rengarajan, "Genetic Algorithms in the Design and Optimization of Antenna Array Patterns", IEEE Transactions on Antennas and Propagation., Vol. 47, No. 3, March 1999, pp. 506-510.

[22] Diogenes Marcano and FIlinto Duran, “Synthesis of Antenna Arrays using Genetic Algorithms”, IEEE Antennas and Propagation Magazine, Vol. 42, No. 3, June 2000, pp. 1688-1691.

[23] Thotla, V.; Zawodniok, M.J.; Jagannathan, S.; Ghasr, M.T.A.; Agarwal, S., "Detection and Localization of Multiple R/C Electronic Devices Using Array Detectors," Instrumentation and Measurement, IEEE Transactions on , vol.PP, no.99, pp.1,1 doi: 10.1109/TIM.2014.2331432.

IV. UAV BASED DETECTION OF R/C ELECTRONIC DEVICES USING CORRELATION

ABSTRACT

Reliable detection of RC electronic devices is very important in compromised environments with a short response time. Unmanned aerial based vehicles (UAV) have been used for surveillance and many other security applications. It is predicted that the use of UAV's for different applications will be dominant in the near future. One of the major advantages of UAV's is the low risk factor in its applications. UAV's can be guided remotely and can be used for sensitive applications involving detection and identification.

A 4-element array antenna mounted on a UAV setup is presented in this paper. Detection of device placed above ground and on the ground is compared. The detection accuracy of the devices decreases as the devices are placed closer to the ground. Also, best results are obtained when the UAV is placed exactly above the device. A time based correlation method is proposed for array detectors to identify the line of sight (LOS) and non-line of sight (N-LOS) signals. A normalized error correlation function has been implemented to improve the estimation of angle of arrival (AOA) in the presence of strong non-line of sight (N-LOS) signals. Also, analysis of an effective 12- element array is presented for future work.

1. INTRODUCTION

Radio controlled (RC) devices emit unintended radiations in their active and passive state. Standardized radio controlled (RC) receivers are either super-heterodyne [1-3] or superregenerative [4 - 7]. Unintended emissions from superheterodyne and super-regenerative receivers can be utilized for detection of RC devices [1-12]. However, these emissions are weak and are further affected by environmental noise and reflections. The power of emissions and their properties also vary with the position of device and sensor.

Recent studies [8, 10, and 12] have proven that unintended emissions from a super-heterodyne receiver can be enhanced by a sinusoidal simulated source. These enhanced emissions have been used with a matched filter and neural network for detection of RC devices [9-11]. Matched filter detection method utilizes Fourier transform and IF filter to identify the signal. Whereas, the neural network method utilizes a set of known emissions from RC devices to compare with emissions from the device under test (DUT). The performance of these methods degrades in the presence of multiple devices, reflections/multipath and strong environmental noise.

In preceding work [1, 2] major challenges like multiple device detection, ranging and detection of devices at different frequency of operation have been addressed. In [1] a four element cost-effective mobile array detector has been proposed to spatially discriminate emissions for detection and localization of multiple RC electronic devices. Also the array detector employed wide band antennas to detect emissions from different frequencies. It has been proven that the array detector has improved gain over single antenna detectors. Array antenna also provides angle of arrival (AOA) information of the signal which is utilized for detection and identification. A two dimensional array was also

proposed with a novel edge synthetic aperture radar based method (E-SAR). Also, in [4] the statistical properties of a super regenerative receiver have been used to detect and identify the presence of a super-regenerative receiver.

However, these methods fail in realistic environment where multipath fading and reflections create virtual, false sources of emissions. Consequently, the AoA estimation often contains significant error due to multipath and reflected signals. Due to multipath signals, the receiver obtains the Line of sight (LOS) and delayed version of the signals causing a drop in the signal strength. It is difficult to separate the multipath components from the original signal. The presence of obstacles on the ground causes errors with the sensor on ground. Therefore, a better technique for detection is explored in this paper.

The four element array used previously for detection of multiple devices and to obtain angle of arrival information is used in an effective way to overcome the problem of error due to obstacles and improve the ease of detection. An Unmanned Aerial Vehicle (UAV) is proposed to carry the array antenna for detection and localization.

UAV is an aircraft that can be controlled remotely or can be completely autonomous based on complex aerodynamic algorithms. Initially UAV's were built to be used in hostile territories for surveillance and to prevent loss of human life. UAV's are currently used for many applications including remote sensing, aerial surveying of agricultural lands, aerial filmmaking, inspecting power lines, wildlife surveillance, delivering medical supplies to remote areas, search and rescue operations. The possibilities for new developments and applications are ever expanding.

The UAV can easily be used to do a first step surveillance over a given area. Detection using a UAV eliminates many reflections due obstacles on the ground and have

a higher probability for line of sight (LOS) detection. Initially, angle of arrival (AOA) using phased array processing is used for detection of devices. However, the AoA estimation often contains significant error due to multipath and reflected signals. Due to multipath signals, the receiver obtains the Line of sight (LOS) and delayed version of the signals causing a drop in the signal strength. It is difficult to separate the multipath components from the original signal.

Previously, correlation methods have been used for spectrum sensing and detection of audio signals [15, 16] when multipath components are present. Auto correlation and cross correlation has been applied for frequency spectrum of known signals and signal under test. A cross correlation between two signals gives the similarity between them. However, to the best knowledge of the authors, correlation methods have not been actively applied to detect unintended emissions from passive devices.

The overarching objective of this paper is to analyze the detection of devices using a UAV and detect multiple RC devices in the presence of reflections and multipath. Further, correlation of time series signal at different angles of arrival is proposed for detection of line of sight (LOS) signals. The overview of the proposed method is shown in Figure 2.1.

2. METHODOLOGY

A. UAV BASED DETECTION.

A uniform 4-element array is employed to receive unintended emissions, as shown in Figure 2.2. Phased-array processing is used to process the data resulting in constructive interference. Depending on distance from the objects, near-field and far-field models for array processing are employed. The widely accepted threshold for the far-field is equal to $\mathbf{2} * \boldsymbol{d^2/\lambda}$, where d is the longest dimension of the antenna. Measurements for the 4-element array antenna attached to the UAV are assumed to be far field.

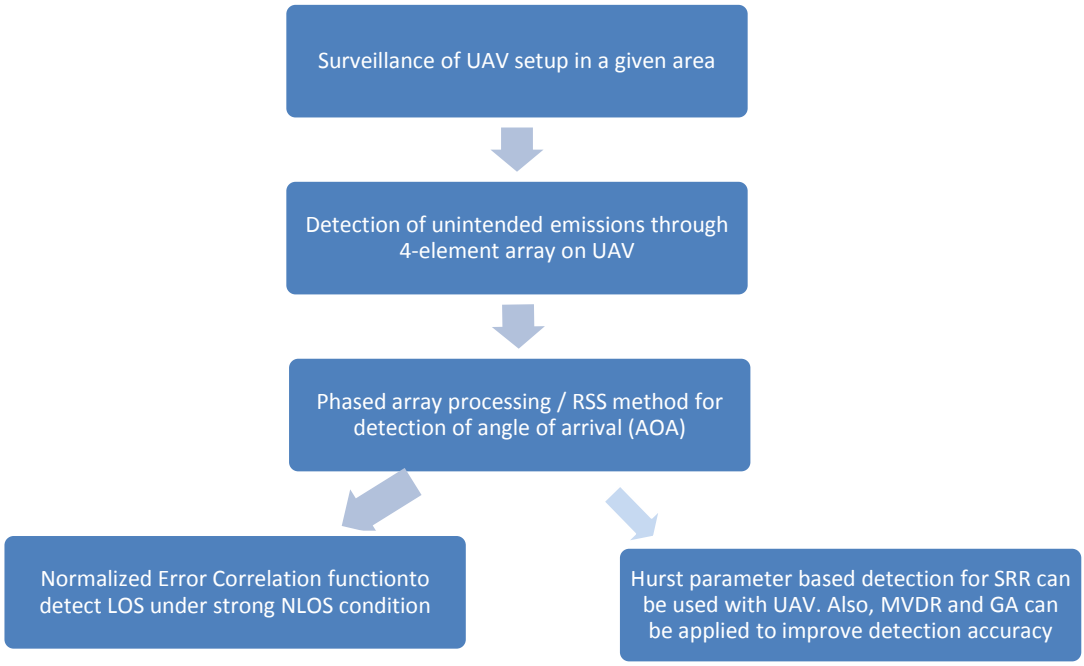

Figure 2.1. Overview of UAV based detection

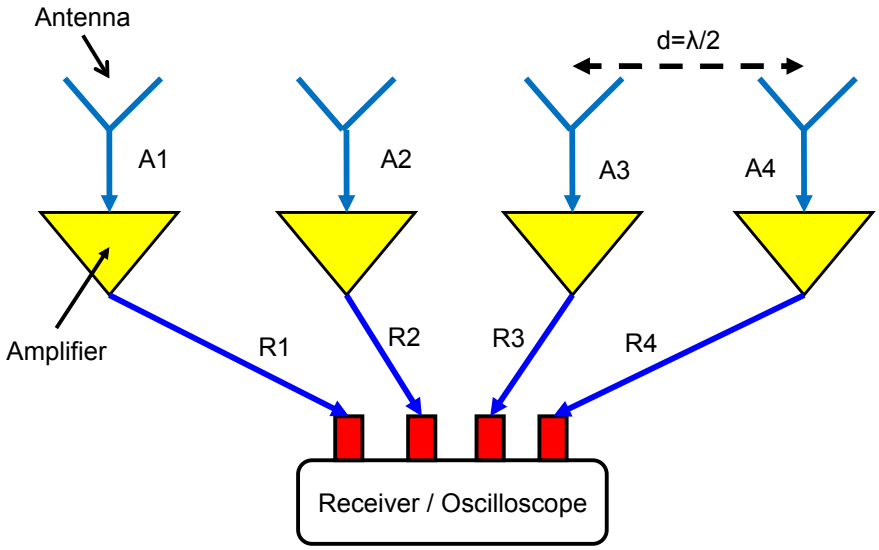

Figure 2.2. Four element array antenna for phased array processing

Consider a signal R_i from the antenna element A_i, where $i=1,2,3,..,N$ is antenna number. Phased array processing provides for a coherent summation of the received signals from each individual array element R_i:

$$S(t,\theta) = \sum_{i=1}^{N} R_i(t) e^{j(i-1)\Psi} \tag{2.1}$$

where θ is the angle at which the antenna beam is directed for signal measurement and Ψ represents the progressive phase of each array element referenced to the previous one.

$$\Psi = Kd\cos\theta \tag{2.2}$$

where $K = 2\pi/\lambda$, $d = \lambda/2$ is the distance between the antennas, and $\theta \in [0, \pi]$. The signal power is obtained by integrating the signal at the frequency of interest over a period of time T and is given by:

$$P(\theta) = \int_0^T S(t,\theta) e^{-j2\pi ft}\, dt \tag{2.3}$$

The experimental setup for UAV based detection is presented in Figure 2.3. The array antenna is attached to the UAV. A data acquisition unit is used for measurements and the processing is performed in a base station. A similar environmental setup has

been created due to restrictions of flying a UAV. The first environmental setup for antenna placed on the UAV is shown in Figure 2.4. The array antenna was placed 12ft above ground and measurements have been made for multiple devices. When the devices are buried or in the presence of obstacles detection becomes difficult with the array antenna/sensor placed on the ground. This is due to the absence of line of sight communication. With the array antenna/sensor attached to the UAV, detection can be improved in such cases by flying the UAV over the area under surveillance.

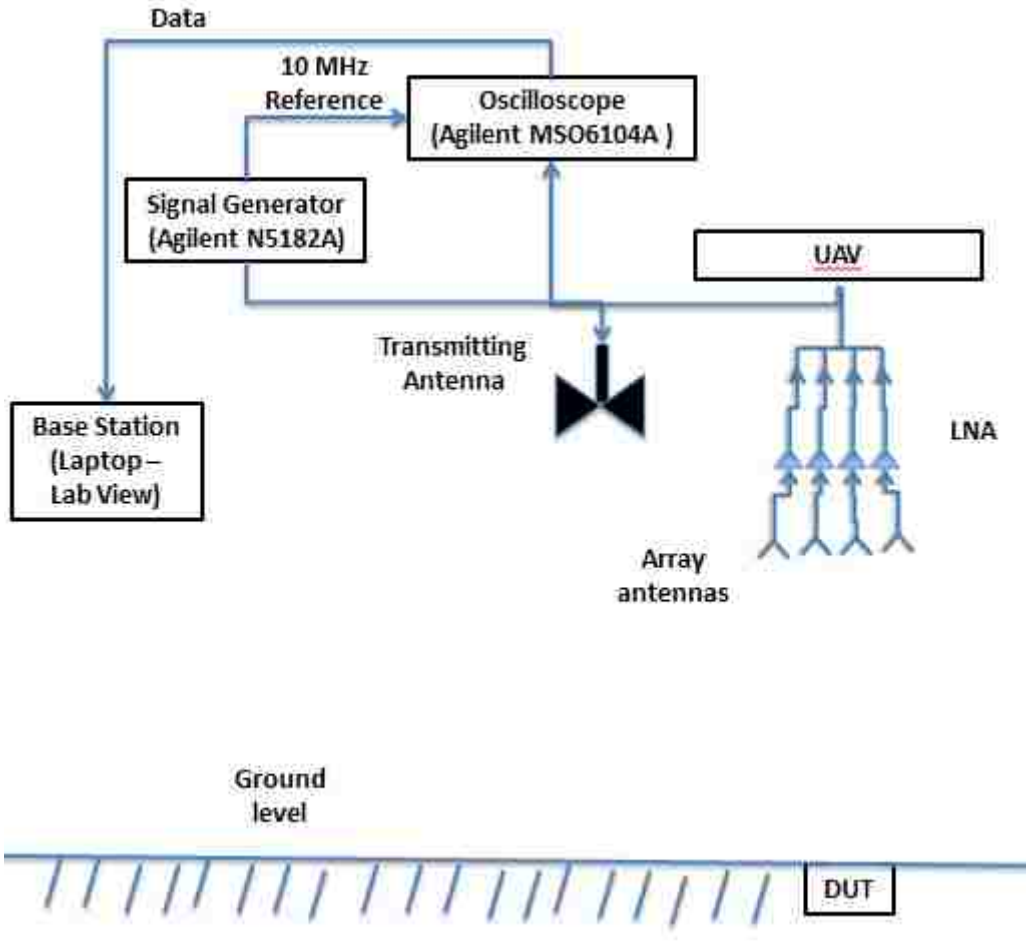

Figure 2.3. Overview of the proposed approach

The emissions as seen at a far-field sensor from a source with a half-wave dipole antenna are simulated using CST. The emission patterns for different scenarios representing the distance of the source in multiples of λ (operating wavelength) from the ground are presented in Figure 2.5.

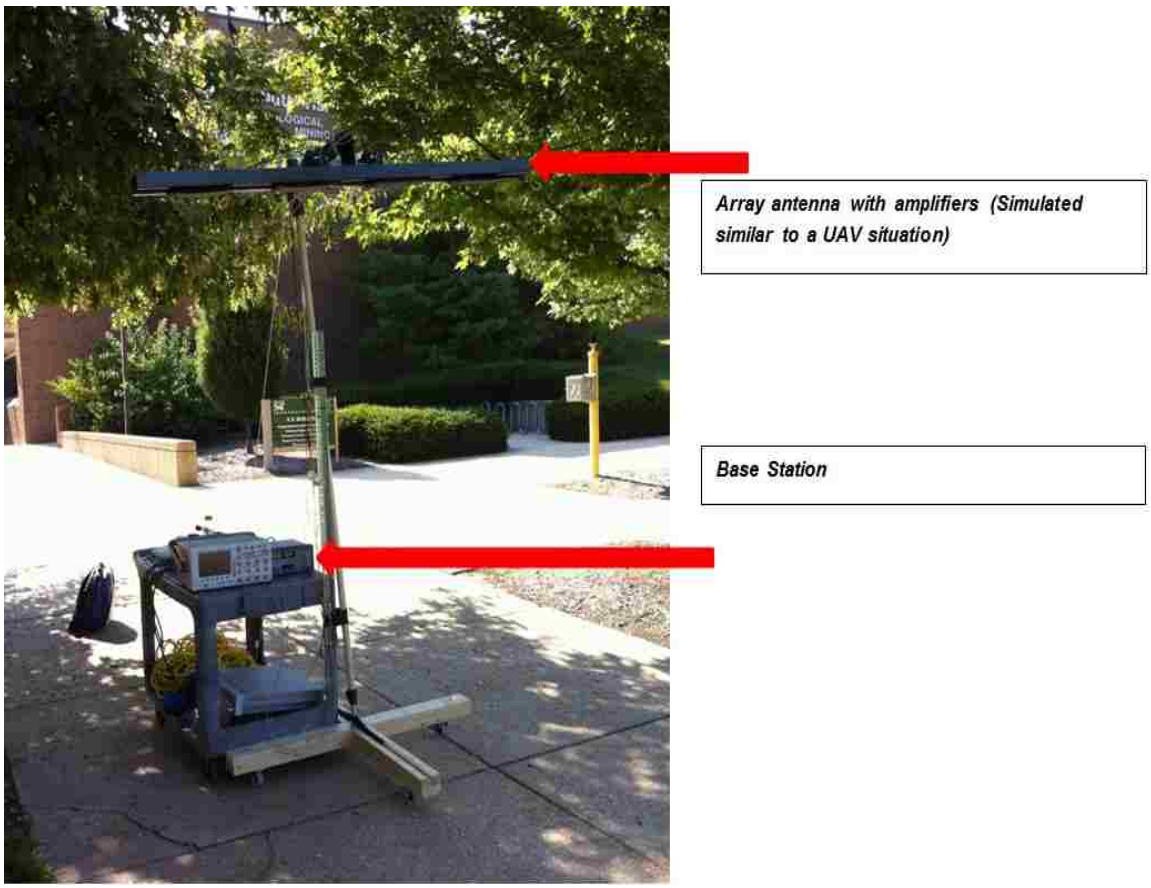

Figure 2.4. Experimental setup for real time measurements

The simulations clearly show the decrease in gain when the source moves closer to the ground and drops drastically when placed on the ground. Also, the best position for placement of the sensor for detection of the source is right above the device at max gain.

The overview of measurements taken at different positions is shown in Figure 2.5. The experimental setup is moved to different locations to act as a UAV. Initially, the

device is fixed at the origin and the setup is moved around to analyze detection of the device at different positions. The position shown in Figure 2.6 represents the center of the array mounted on the UAV.

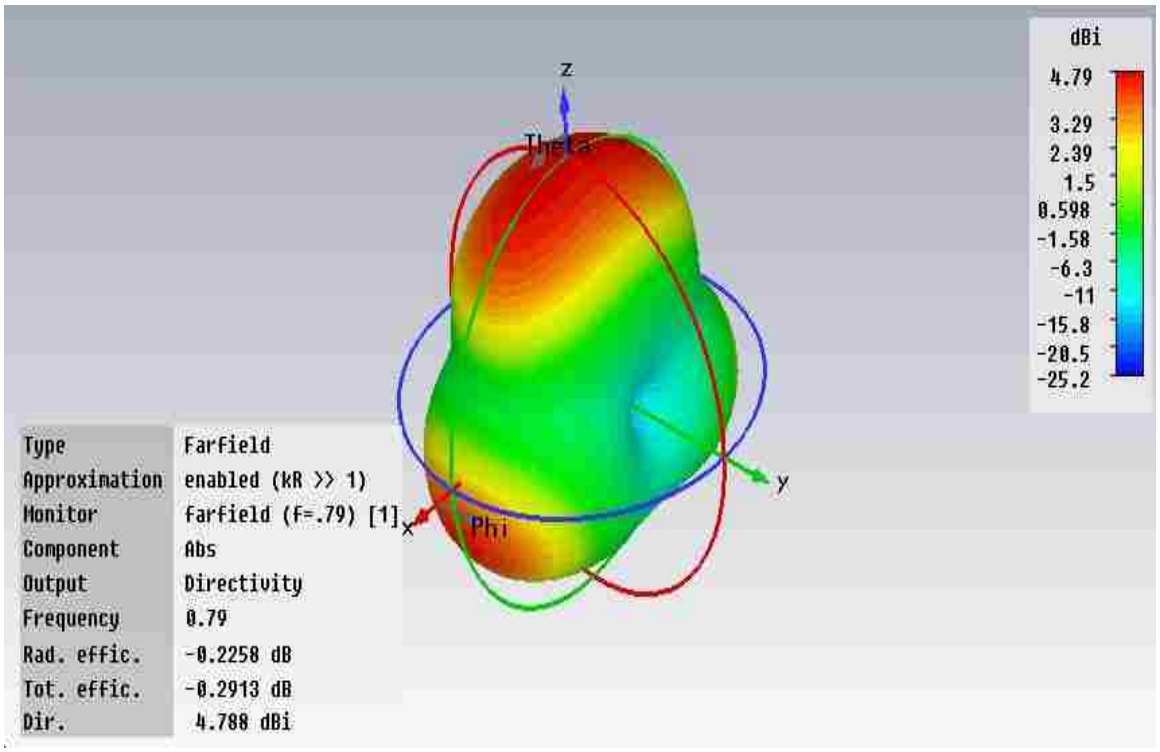

Figure 2.5 (a) Emission pattern for source placed λ (operating wavelength) above ground

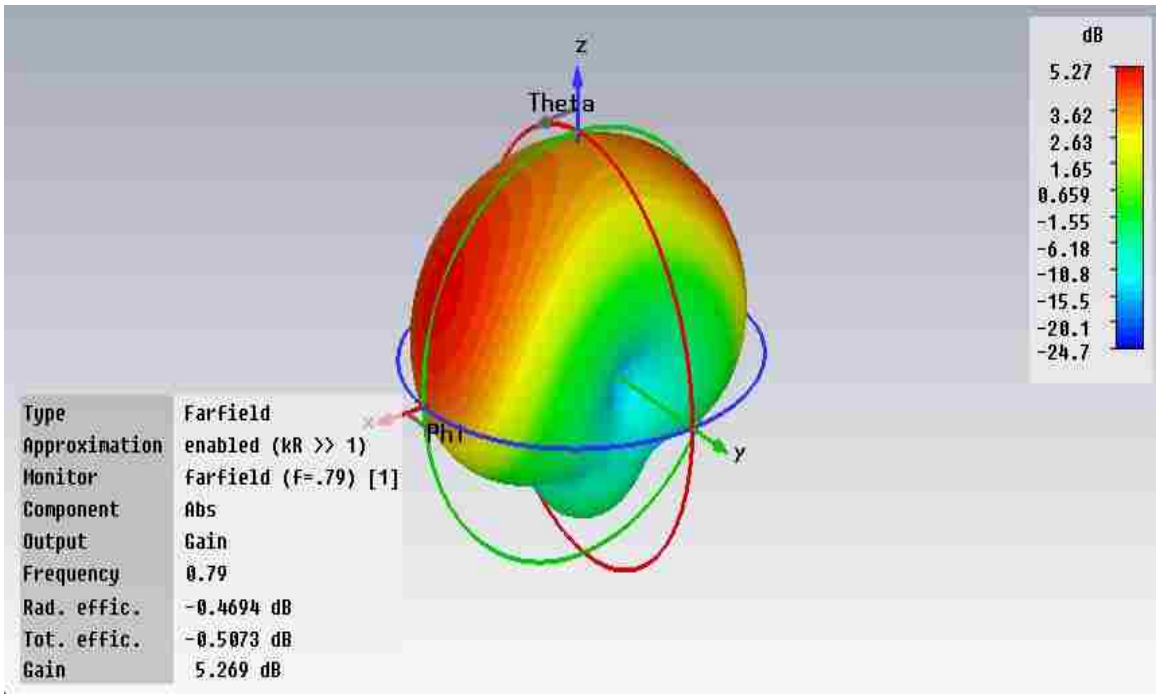

Figure 2.5 (b) Emission pattern for source placed $\lambda/2$ (operating wavelength) above ground (cont.)

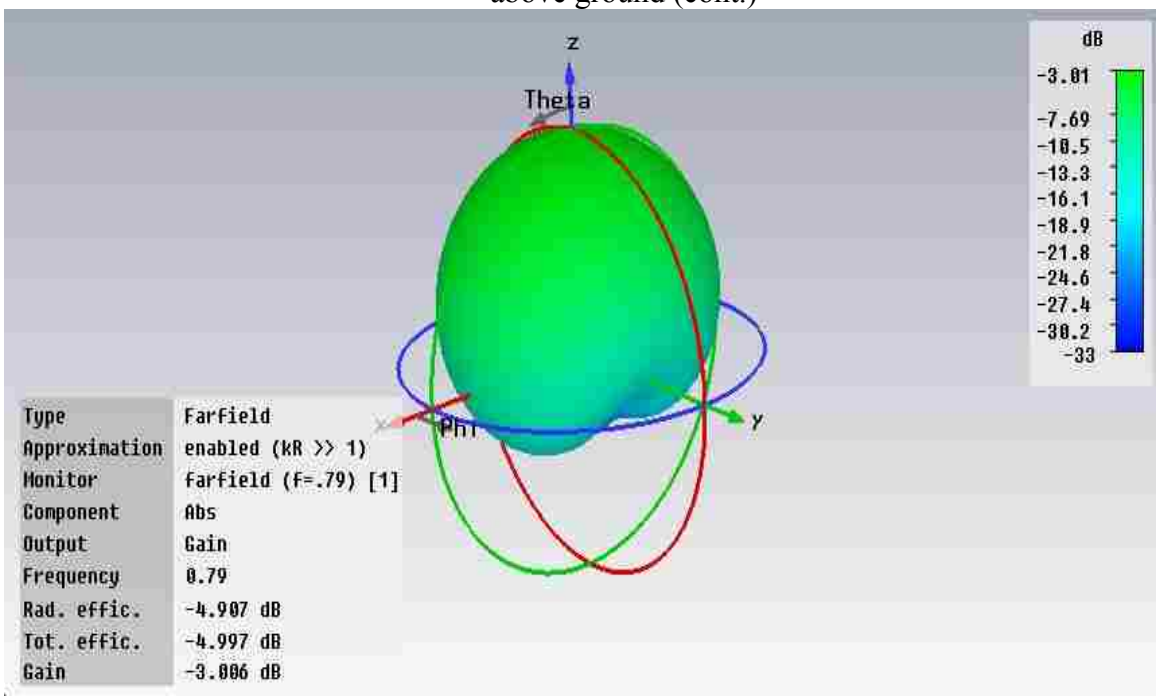

Figure 2.5 (c) Emission pattern for source placed $\lambda/20$ (operating wavelength) above ground (cont.)

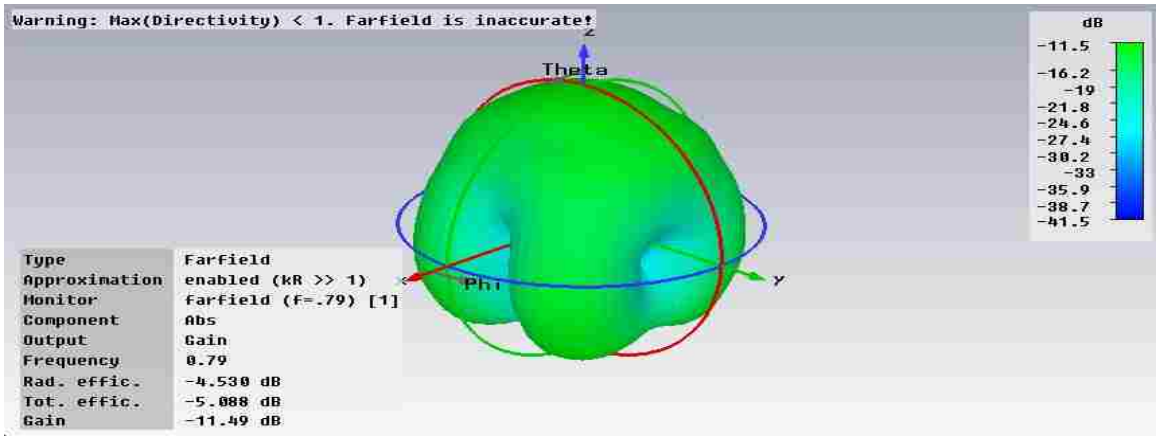

(d) Emission pattern for source placed on the ground

Figure 2.5. (a) Emission pattern for source placed λ (operating wavelength) above ground; (b) Emission pattern for source placed $\lambda/2$ (operating wavelength) above ground; (c) Emission pattern for source placed $\lambda/20$ (operating wavelength) above ground; (d) Emission pattern for source placed on the ground.

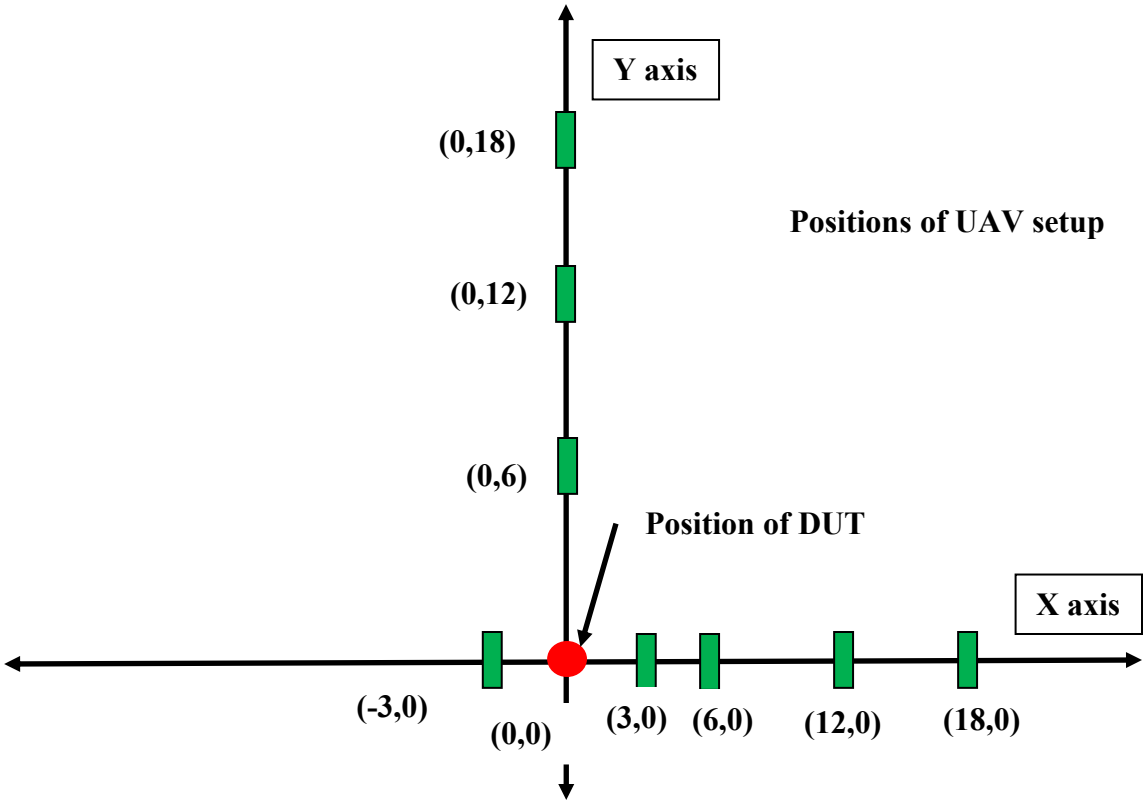

Figure 2.6. Measurement setup for UAV based detection. Position of the device is fixed at the origin and the UAV is moved to different positions for measurement. (Note: All distances in feet)

An effective 12-element array is also simulated and measurements have been made as shown in Figure 2.7.

B. CORRELATION METHOD.

The major challenges in accurately detecting and locating multiple devices, in particular from their unintended emissions, are (a) multipath fading, (b) reflections which create false source of signal, and (c) presence of multiple uncorrelated devices. Power analysis of the received signal, which was employed in previous works [1-9] at different angles cannot be used to differentiate between signal from a source or line of sight (LOS) signal and reflections / multipath or non-line of sight (NLOS) signal.

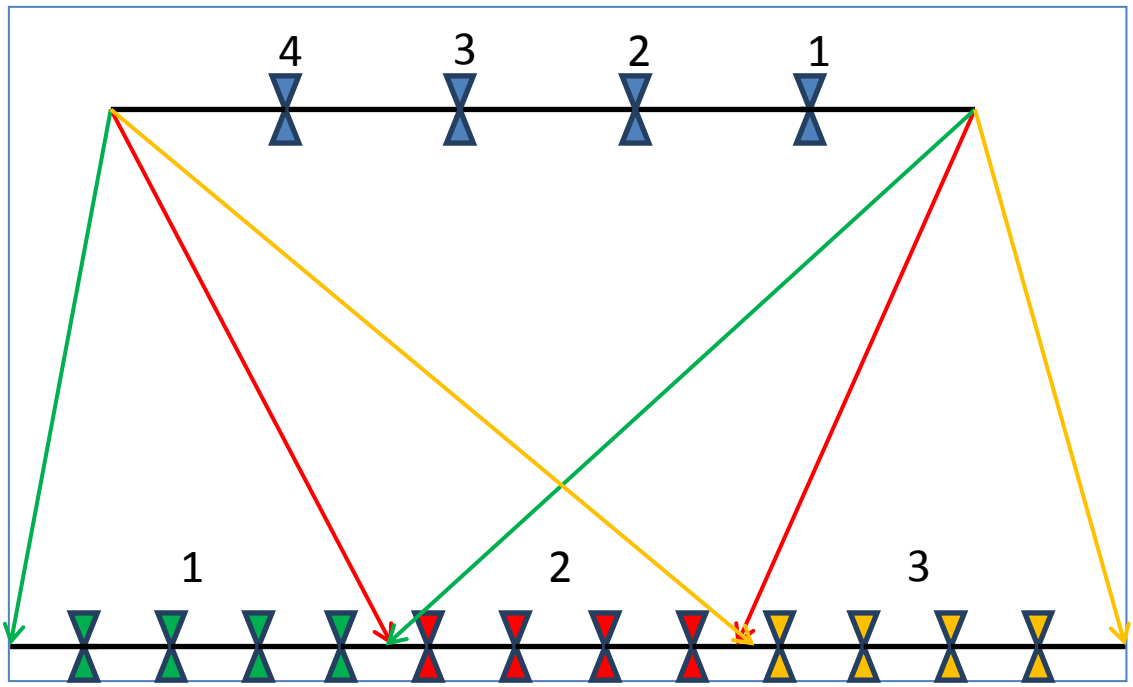

Figure 2.7. UAV setup for effective 12-element array

Line of sight and non-line of sight signals are shifted in time due to the distance signals have to travel. LOS signal is the direct signal and NLOS is caused due to

reflection or multipath due to reflectors or different objects in the environment as shown in Figure 2.8. Such signals have a higher degree of correlation than signals from different source. The level of correlation between the LOS and NLOS signals from the same source varies with the channel paths the signals took. Hence, we employ a cross correlation between the time series signals to differentiate between sources and between LOS and NLOS signals.

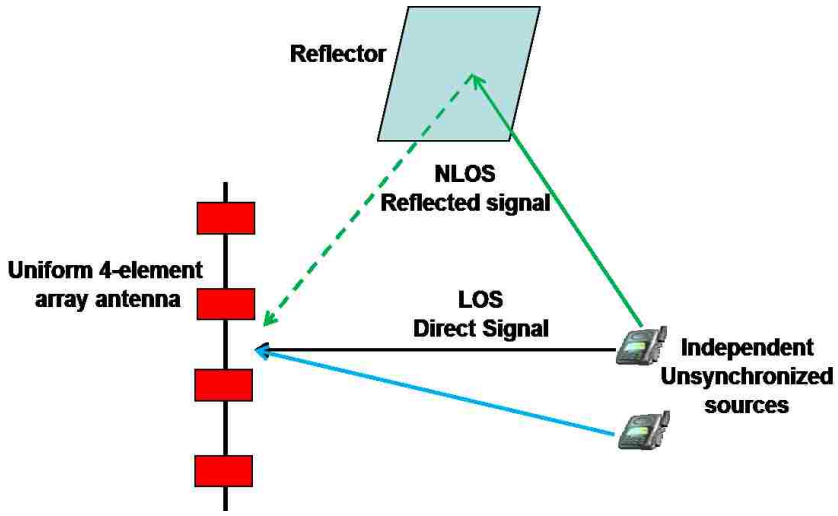

Figure 2.8. LOS and NLOS scenarios

Cross correlation is a measure of similarity of two signals (continuous or discrete). It is calculated as a function of time lag between the two signals. For discrete signals f(n) and g(n), the cross correlation is given by:

$$(f * g)[n] = \sum_{a=-\infty}^{\infty} f^*[a] * g[n+a] \tag{2.4}$$

The autocorrelation coefficient of time series signal of equation (4.1) is given by:

$$(S(:,\theta) * S(:,\theta))[n] = \sum_{a=-\infty}^{\infty} S(a,\theta) * S(n+a,\theta) \;|_{\theta=0\ to\ \pi} \tag{2.5}$$

The cross correlation coefficient of time series signal between two angles of arrival θ_1 and θ_2 is given by:

$$(S(:,\theta_1) * S(:,\theta_2))[n] = \sum_{a=-\infty}^{\infty} S(a,\theta_1) * S(n+a,\theta_2) \quad (2.6)$$

$$S_{an} = (S(:,\theta) * S(:,\theta))[n]/(S(:,\theta_{actual}) * S(:,\theta_{actual})) \quad (2.7)$$

$$S_{cn} = (S(:,\theta_1) * S(:,\theta_2))[n]/(S(:,\theta_{actual}) * S(:,\theta_{actual})) \quad (2.8)$$

$$E_n = S_{cn} - S_{an} \quad (2.9)$$

where, S_{an} is the normalized auto correlation coefficient, S_{cn} is the normalized cross correlation coefficient and E_n is the normalized correlation coefficient error.

The autocorrelation coefficient for actual position of the device under zero lag is used for normalizing both the auto correlation and cross correlation coefficients. Difference between the normalized auto correlation and cross correlation coefficients gives the normalized correlation error function. The normalized error correlation function is plotted against the angle of arrival to differentiate between line of sight (LOS) and non-line of sight (NLOS) signals.

3. RESULTS AND DISCUSSION

A. UAV BASED DETECTION.

The uniform linear array as shown in Figure 2.2 is used for measurements. Each of the antennas is omni-directional, lightweight, unobtrusive, and wideband with an operating bandwidth in the range of 225 – 2500 MHz (Pharad lightweight wearable antennas). These antennas are connected to 40dB low noise amplifiers and then to a data acquisition unit which is a 4-channel Agilent MSO6104A oscilloscope. The array is designed to operate at 450MHz, with a uniform spacing of $\lambda/2$ between the elements. The walkie-talkie is operated at FRS channel 8. Agilent N5182A signal generator is used to send the stimulating signal at a frequency of 467.5625 MHz and amplitude of -40 dBm to enhance the emissions from the walkie-talkie. The oscilloscope is controlled from a laptop using LabView interface to acquire and store data. Angle of arrival measurements have been made using the setup shown in Figure 2.4 and Figure 2.6. The antenna is placed at height of 12ft above ground.

A) Device placed above ground. Initially, the device is placed 18 inches above ground at the origin. The UAV setup is then placed at different locations along X=0, X= -3 and X= 12 axes. Detection of the device is analyzed at varying distances on each of the axes.

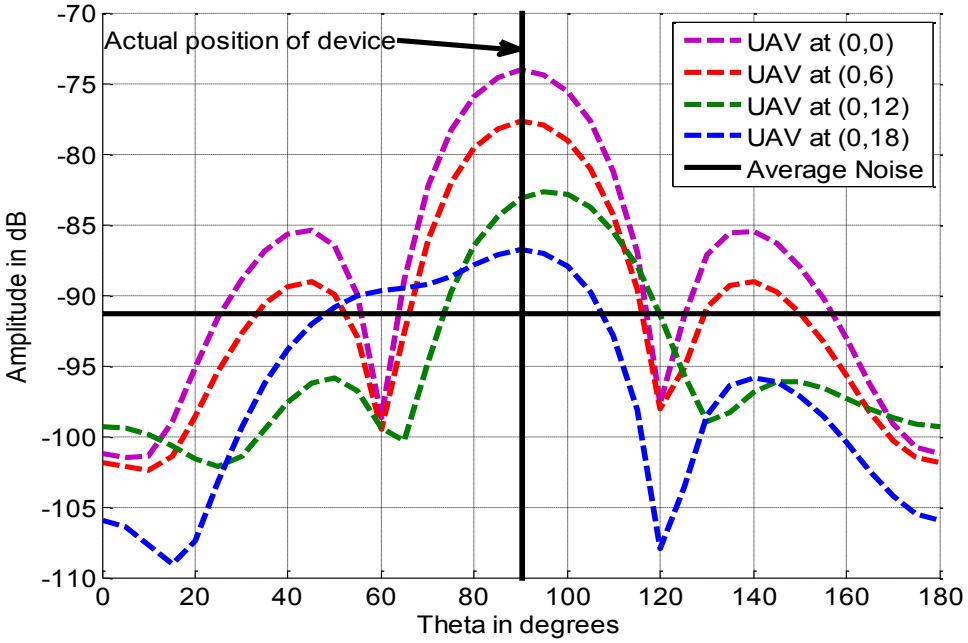

Figure 3.1 (a) Detection of device at (0,0) with UAV setup along X=0

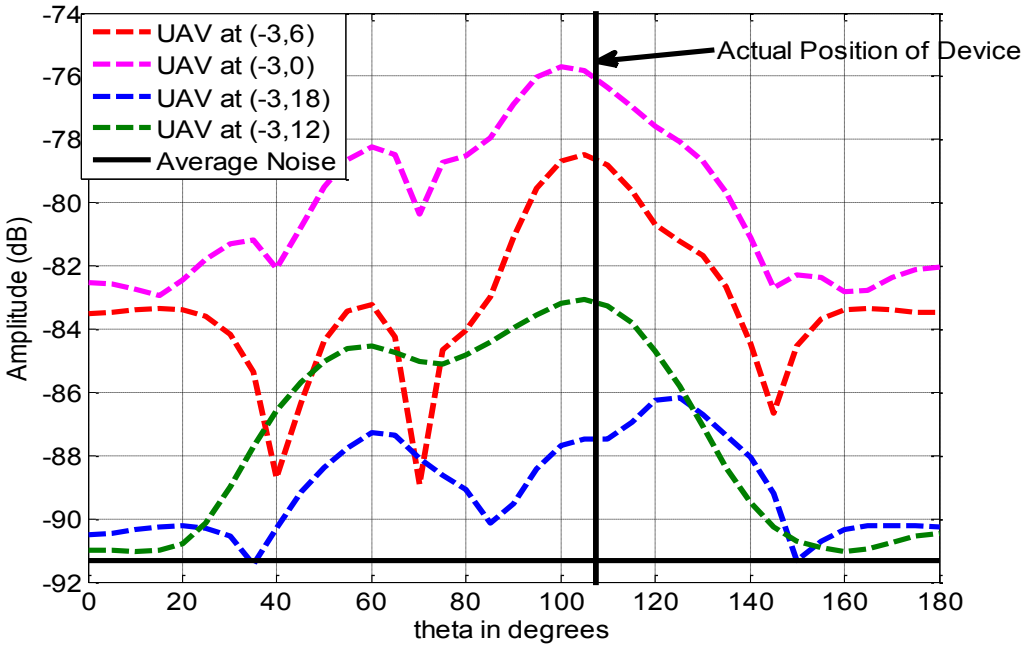

Figure 3.1 (b) Detection of device at (0,0) with UAV setup along X= -3 (cont.)

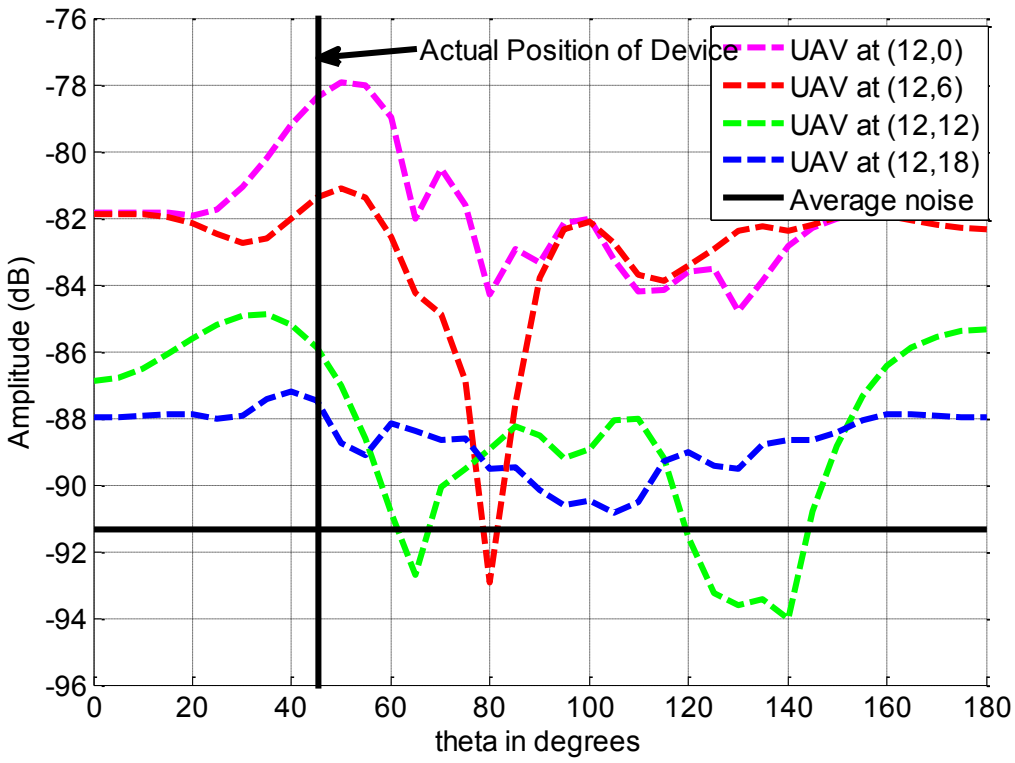

Figure 3.1 (c) Detection of device at (0,0) with UAV setup along X= 12

Figure 3.1. Detection of device placed above ground (a) Detection of device at (0,0) with UAV setup along X= 0; (b) Detection of device at (0,0) with UAV setup along X= -3; (c) Detection of device at (0,0) with UAV setup along X= 12. Note: All coordinates in ft

Detection of the device at origin for different positions on X=0 is shown in Figure 3.1(a). Detection accuracy decreases as the UAV moves away from the device. Figure 3.1(b) shows the detection accuracy for the UAV on X= -3 and Figure 3.1(c) shows the detection accuracy for the UAV on X = 12. The error in AOA is depicted in Table 3.1. AOA error increases as the UAV is moved away from the device. Also, there is no dominant peak for detection as the UAV is moved further than 12ft on Y axis.

Table 3. 1. Error in Angle of Arrival in degrees for device placed above ground

X,Y	Y = 0	Y = 6	Y = 12	Y = 18
X = 0 AOA = 90^o	0	0	5	0 (no dominant peak)
X = -3 AOA= 106^o	6	1	1 (no dominant peak)	19 (no dominant peak)
X = 12 AOA = 42^o	3	3	12 (no dominant peak)	7 (no dominant peak)

B) Device placed on the ground. The walkie-talkie is placed on the ground at the origin for analysis of detection for device on the ground. Gain of the antenna decrease drastically when a source is placed on the ground as shown in Figure 3.2. Similar analysis of detection has been made for different positions along X=0, X= -3 and X=12 axes.

Detection of the device placed on the ground at origin for different positions on X=0 is shown in Figure 3.2(a). Detection accuracy decreases as the UAV moves away from the device. Figure 3.2 (b) shows the detection accuracy for the UAV on X= -3 and Figure 3.2 (c) shows the detection accuracy for the UAV on X = 12. Reduce in gain of the antenna effects the detection accuracy when the device is placed on the ground. Also, the max height for detection decreases with decrease in emitted power. The error in AOA is depicted in Table 3.2.

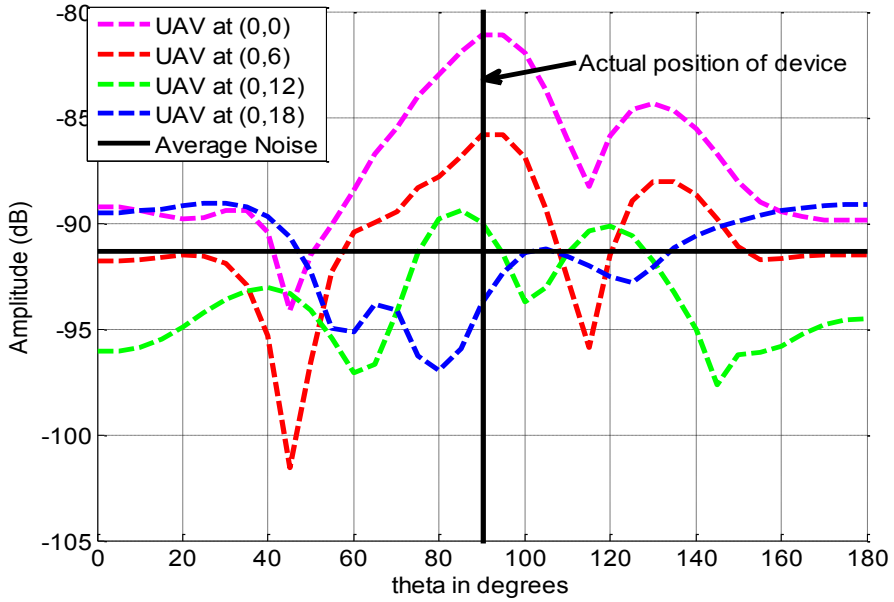

Figure 3.2 (a) Detection of device at (0,0) with UAV setup along X= 0

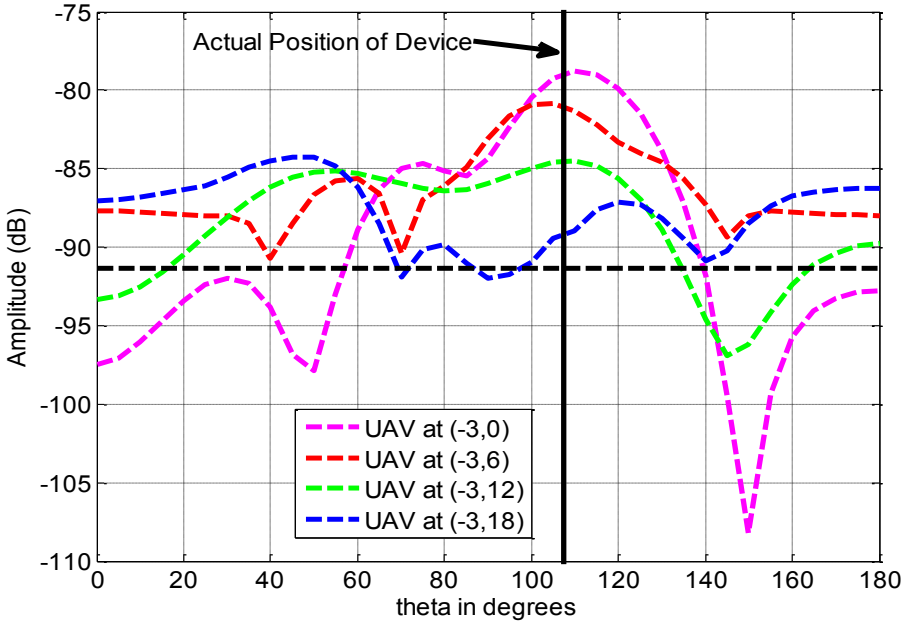

Figure 3.2 (b) Detection of device at (0,0) with UAV setup along X= -3 (cont.)

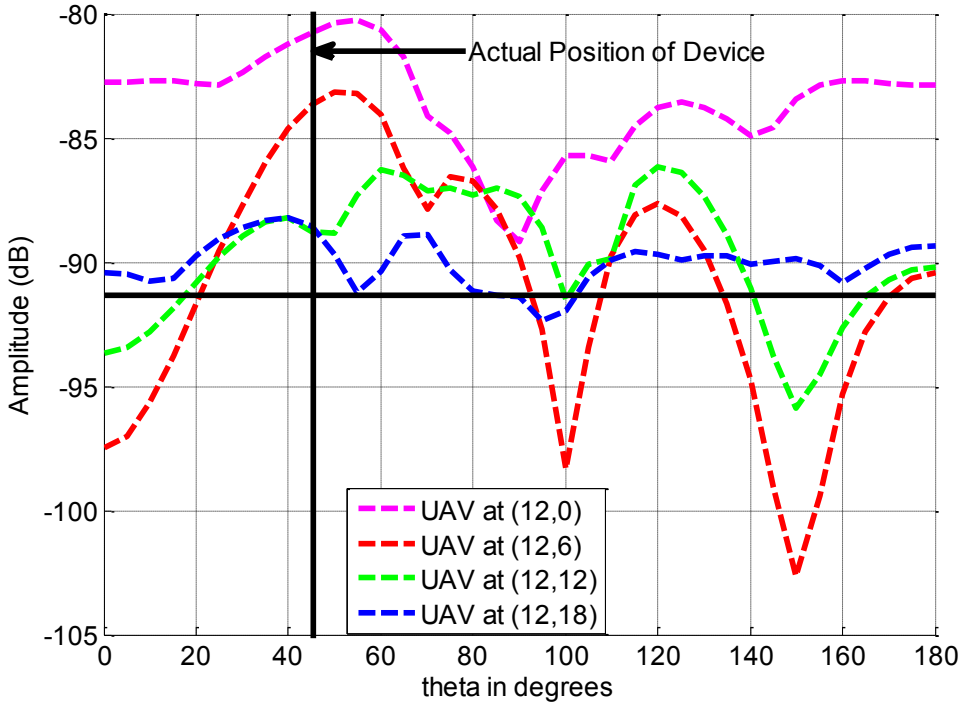

(c) Detection of device at (0,0) with UAV setup along X= 12

Figure 3.2. Detection of device placed on the ground (a) Detection of device at (0,0) with UAV setup along X= 0; (b) Detection of device at (0,0) with UAV setup along X= -3; (c) Detection of device at (0,0) with UAV setup along X= 12. Note: All coordinates in ft

Table 3.2. Error in Angle of Arrival in degrees for device placed on the ground

X,Y	Y = 0	Y = 6	Y = 12	Y = 18
X = 0 AOA = 90^o	5	5	5 (no dominant peak)	60 (no dominant peak)
X = -3 AOA= 104^o	6	4	6 (no dominant peak)	59 (no dominant peak)
X = 12 AOA = 45^o	10	10	15 (no dominant peak)	5 (no dominant peak)

C) Effective 12-element array. As shown in Figure 2.7, UAV setup with the 4-element array is moved to position 1, 2 and 3 and measurements are recorded. These measurements are combined at the base station resulting in an effective 12-element array. The array pattern of the effective 12-element array is shown in Figure 3.3.

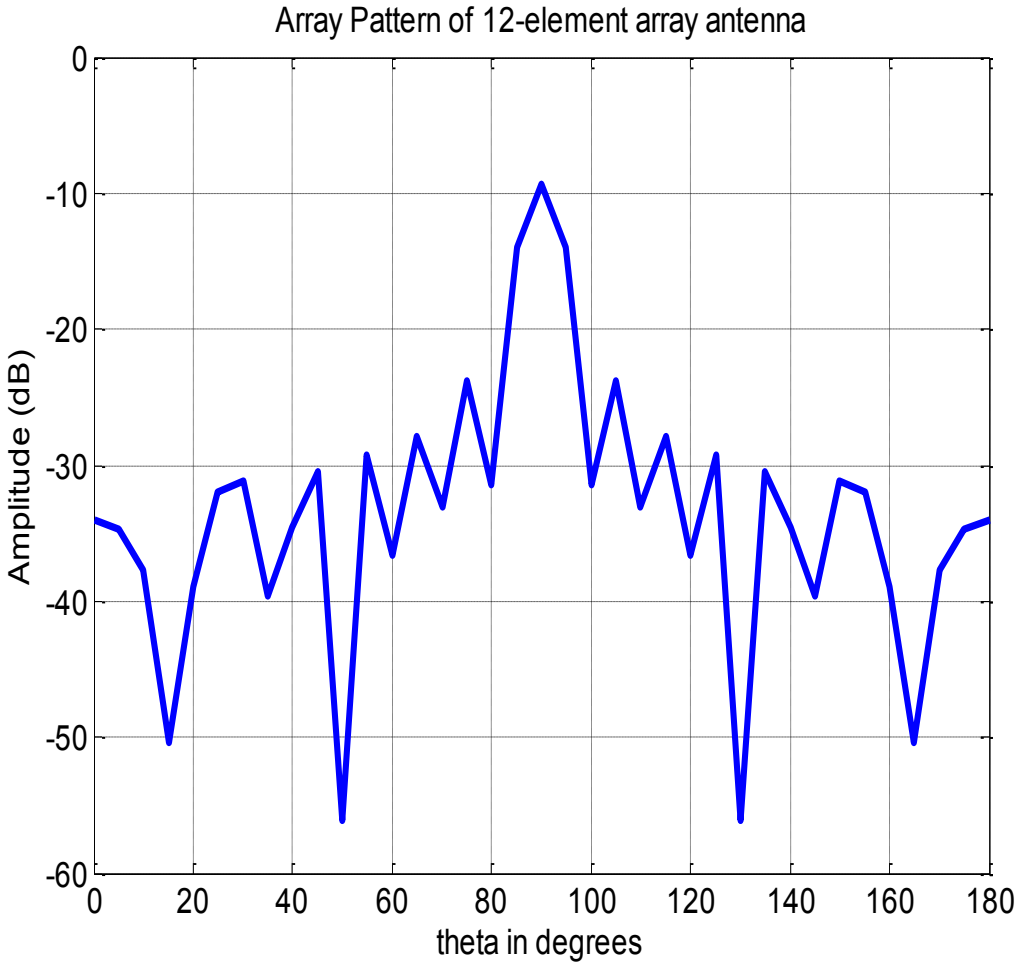

Figure 3.3. 12-element array gain pattern

For testing the effective 12-element array, a device is placed at the Origin on the ground and the center of the effective array is placed at (-3,0) and (12,0). Figure 3.4 shows the power vs AOA relation. The detection accuracy of AOA for the effective array

increases when compared to the 4-element array. Also, increase in power due to higher gain enable detection from higher altitudes. Reflections from the ground are one of the major challenges for detection of unintended emissions using array/sensor on UAV. In the future different positions of the 4-element UAV can be considered to build an effective 2-D array for detection.

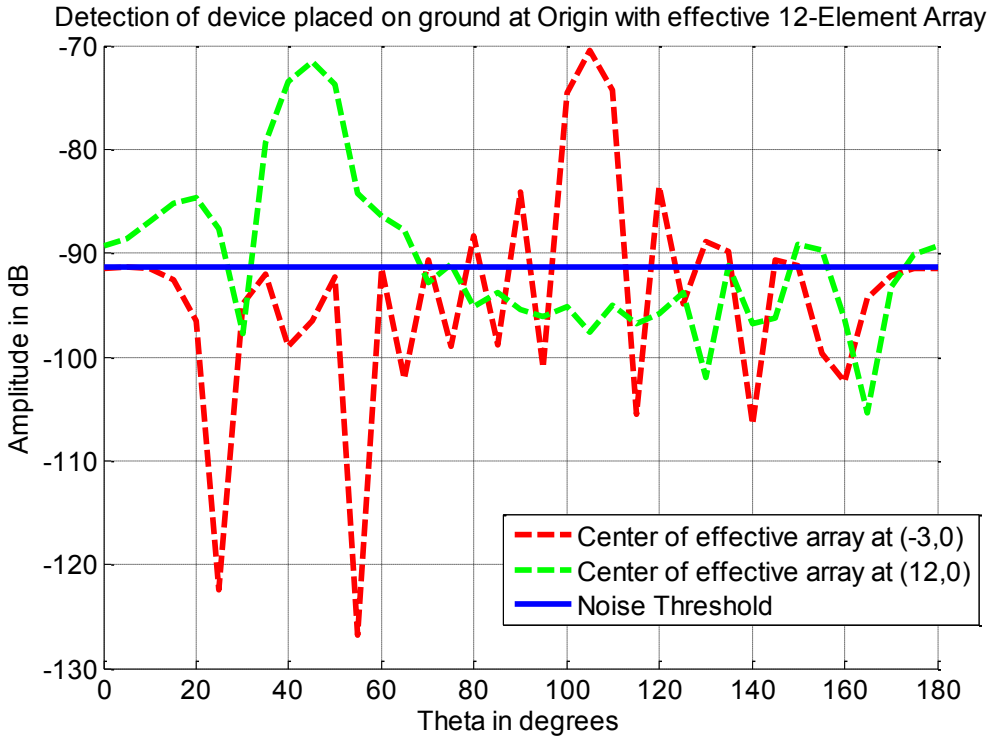

Figure 3.4. Detection of device placed on the ground at Origin (0,0)

B. CORRELATION METHOD

A) Mathematical simulations. A simulation with time shifted sinusoidal signals has been performed to show the difference in auto correlation and cross correlation coefficients. Initial simulation of two time shifted ideal sinusoidal signals is shown in

Figure 3.5. The signals are shifted by (1/3)*T, where T is the time period of sinusoidal signal.

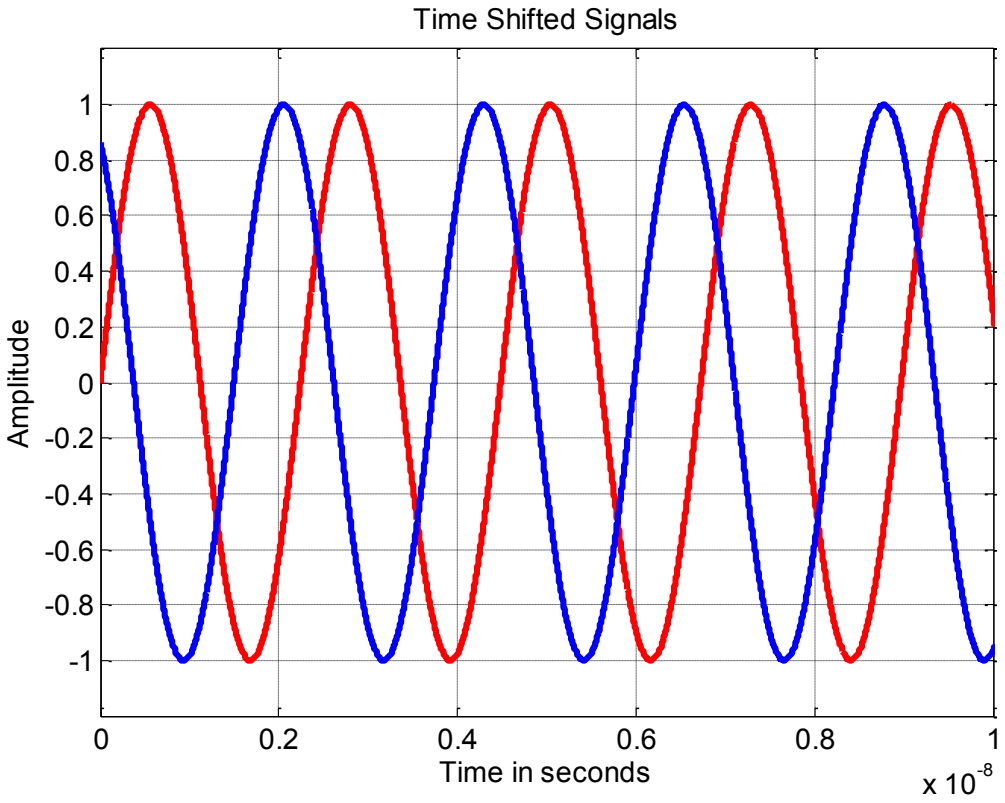

Figure 3.5. Ideal Sinusoidal Signals shifted in time

Correlation coefficients for different lags are plotted in Figure 3.6 for signals shown in Figure 3.5. Table 3.3 shows the correlation coefficients and comparison of time lag for maximum correlation coefficient. Time lag for maximum of cross-correlation matches exactly with time difference between the signals. The difference in correlation coefficient is very less due to the ideal nature of the signals. In real time scenarios different paths have different signal fading resulting in lower cross correlation. The effect of varying noise in multipath propagation can be used to differentiate between LOS and NLOS.

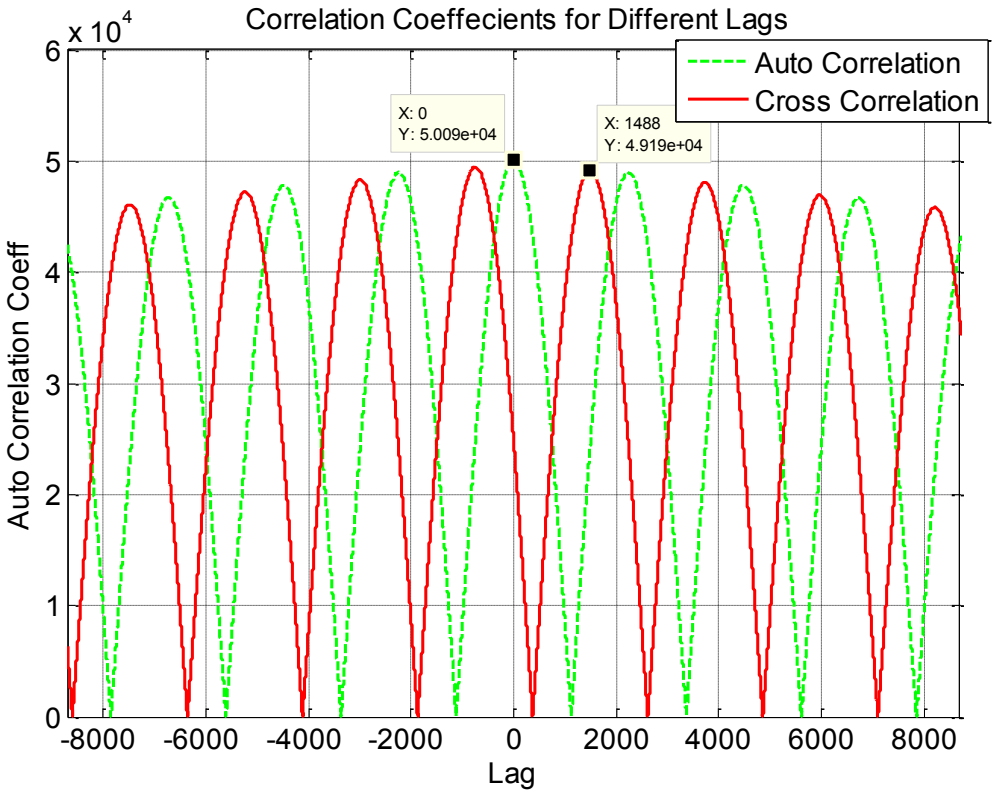

Figure 3.6. Correlation coefficients for different lags

Table 3.3. Correlation Coefficients

	Correlation Coefficient	Time Lag in seconds for Max Correlation Coefficient in seconds
Auto Correlation Coefficient for Signal 1	5.0093e+04	0
Auto Correlation Coefficient for Signal 2	4.9668e+04	0
Cross Correlation Coefficient for Signal 1 and Signal 2	4.9194e+04	7.4350e-10

Figure 3.7 shows the relationship between time shifts for ideal signals and time lag for max cross correlation coefficients.

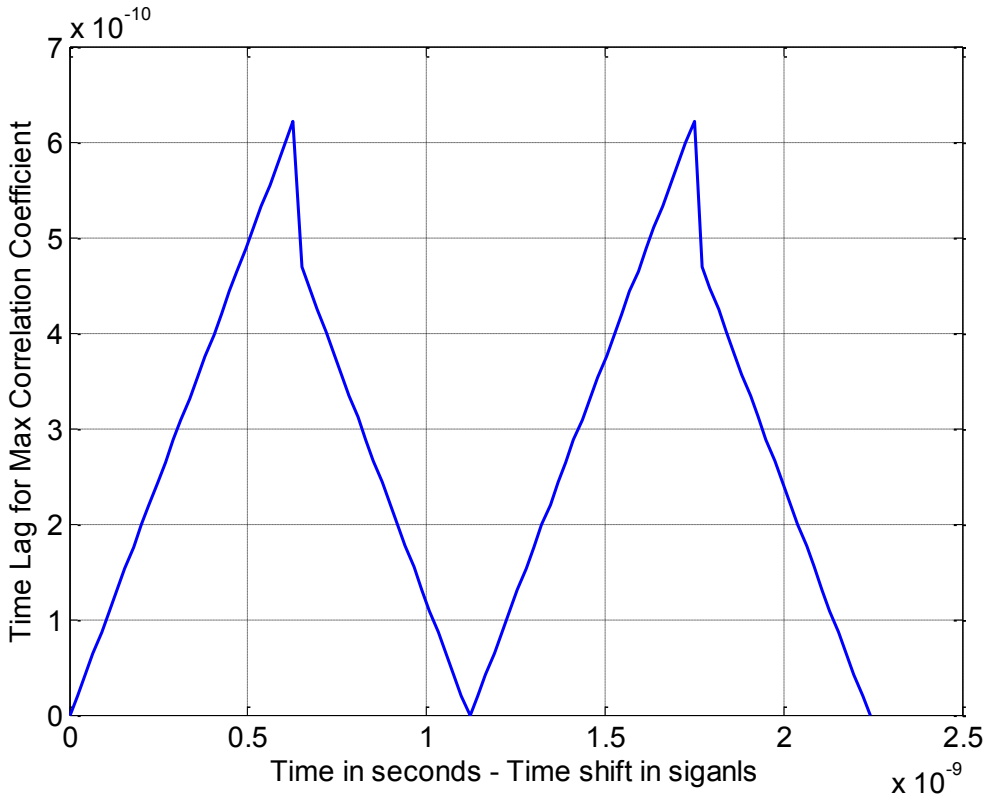

Figure 3.7. Time lag for max cross correlation vs time shifts between signals

Secondly, two time shifted signals with added uncorrelated noise is simulated to duplicate the real time environment. Figure 3.8 shows two time shifted sinusoidal signals with uncorrelated noise (SNR = 40dB) added to it. Figure 3.9 shows the relationship between time shifts of signals and time lag for max cross correlation coefficients. The relationship does not follow a particular format similar to Figure 3.7 due to uncorrelated noise components.

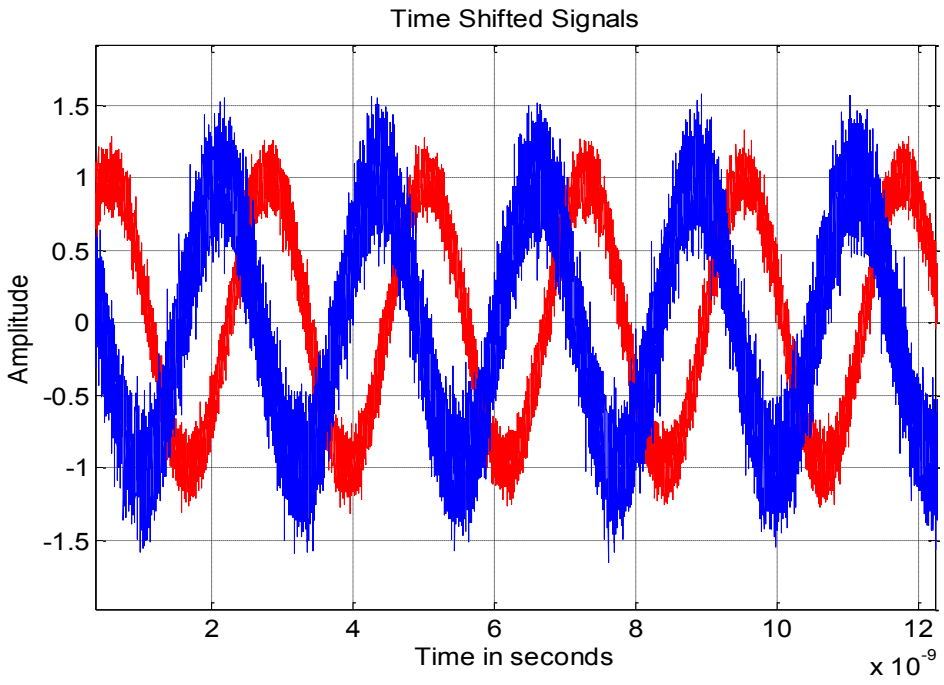

Figure 3.8. Real time sinusoidal signals shifted in time

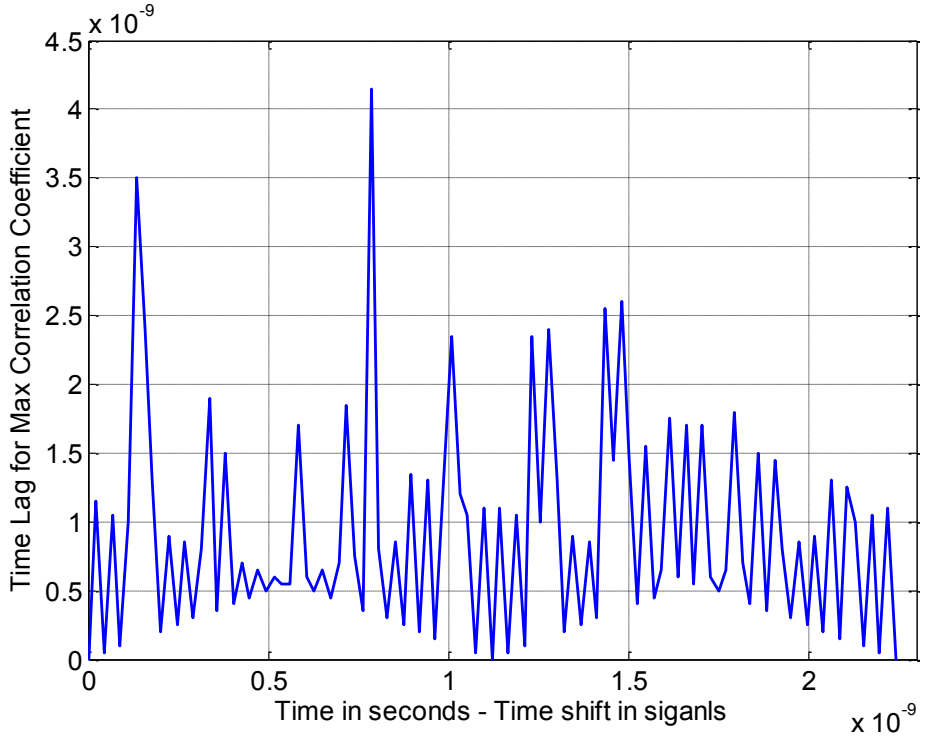

Figure 3.9. Time lag for max cross correlation vs time shifts between signals

Also, a simulation for difference in correlation coefficients is presented for signals with varying frequencies. Figure 3.10 shows the relationship between error in correlation and frequency shift. The correlation decreases exponential with increase in difference between frequencies of signals.

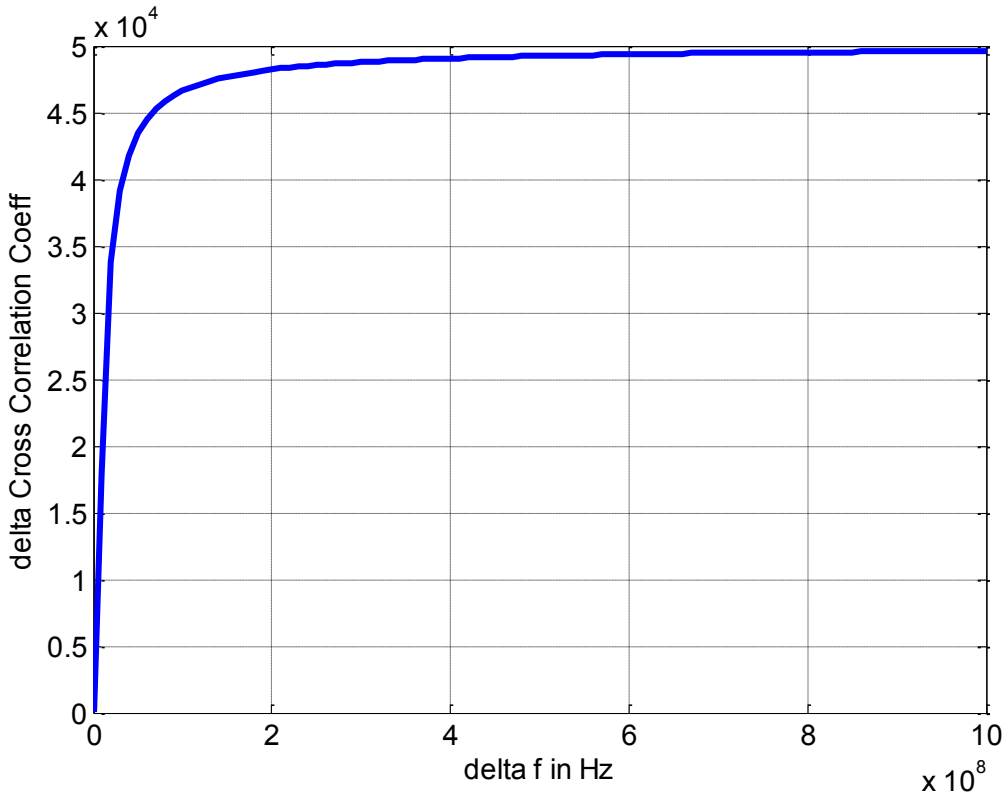

Figure 3.10. Error in Cross Correlation Coeff vs Difference in Frequencies

B) Amplitude of LOS signal greater than NLOS signal. Walkie talkie is placed at 90^{o} and passive emissions from the walkie-talkie are measured. Figure 3.11 shows the relation of power with angle of arrival.

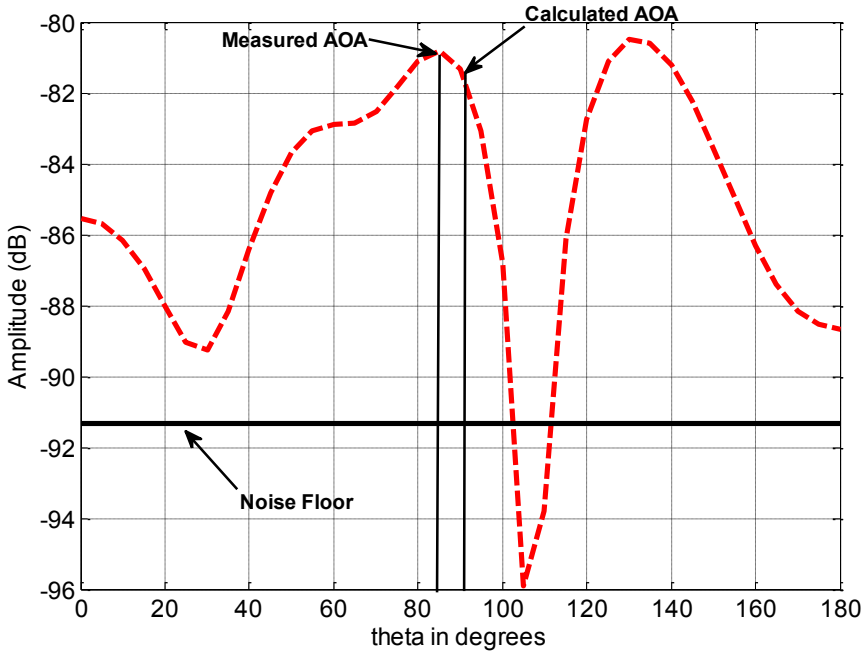

Figure 3.11. Power vs AOA for device at 90

The error for AOA is less in the case of high power from LOS. Figure 3.12 shows the plot of correlation functions. Normalized error correlation function gives less error compared to the power based AOA estimation.

C) Amplitude of LOS less than NLOS signal. Walkie-talkie is placed at 65^{o}. Power due to the presence of reflector/multipath is more than LOS signal. Figure 3.13 clearly shows the drawback of power based AOA when detecting a walkie-talkie where the LOS signal experiences fading and the power of the reflected signal is significantly higher than the LOS. Consequently, the power based AoA method falsely estimates the measured AoA. Figure 3.14 shows the normalized error correlation function, which detects (maximum of the difference) the actual AOA with an error less than the resolution of processing and measurements.

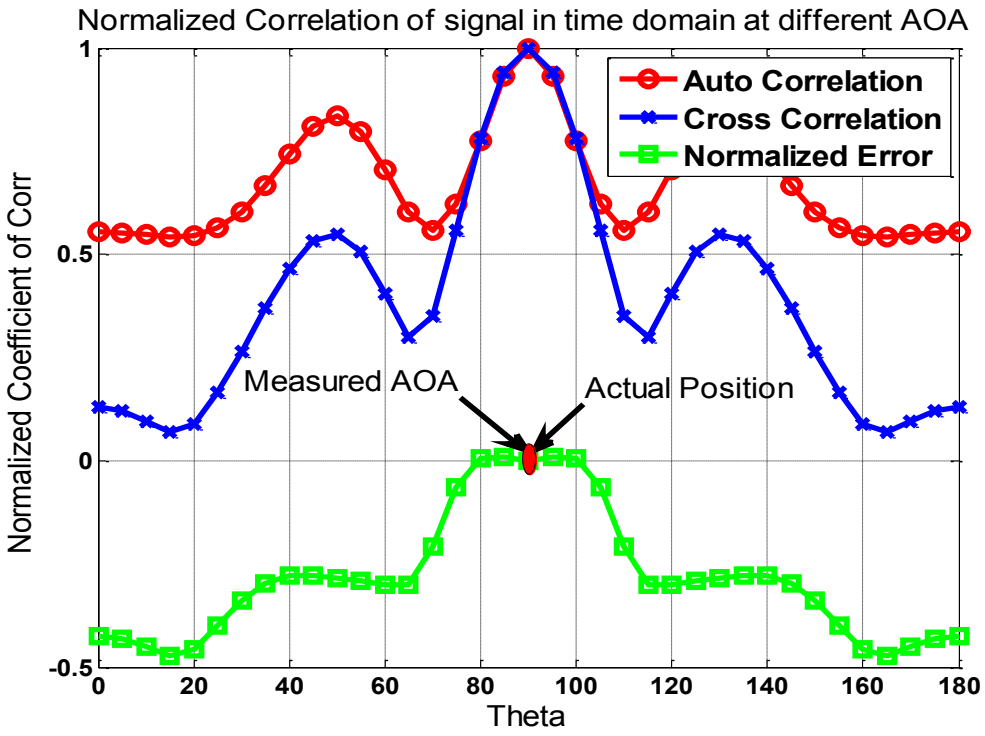

Figure 3.12. Normalized Error Correlation Function vs AOA

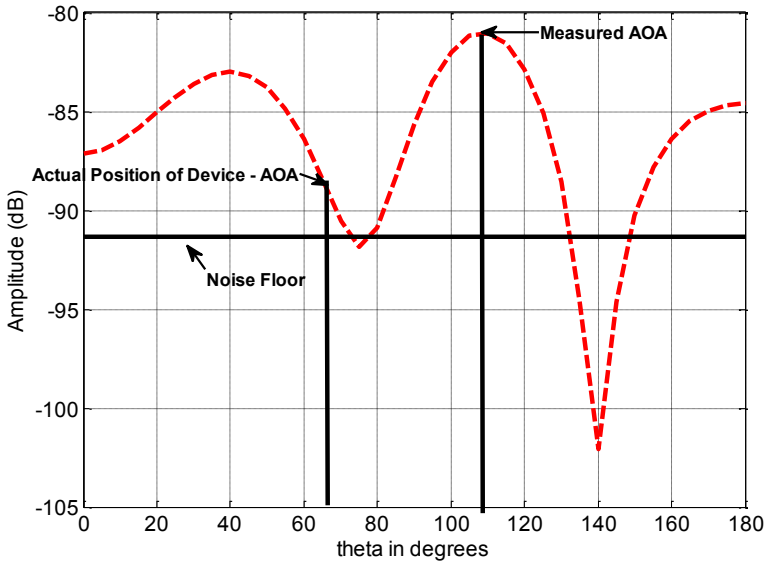

Figure 3.13. Power vs AOA (AOA = 65^{o})

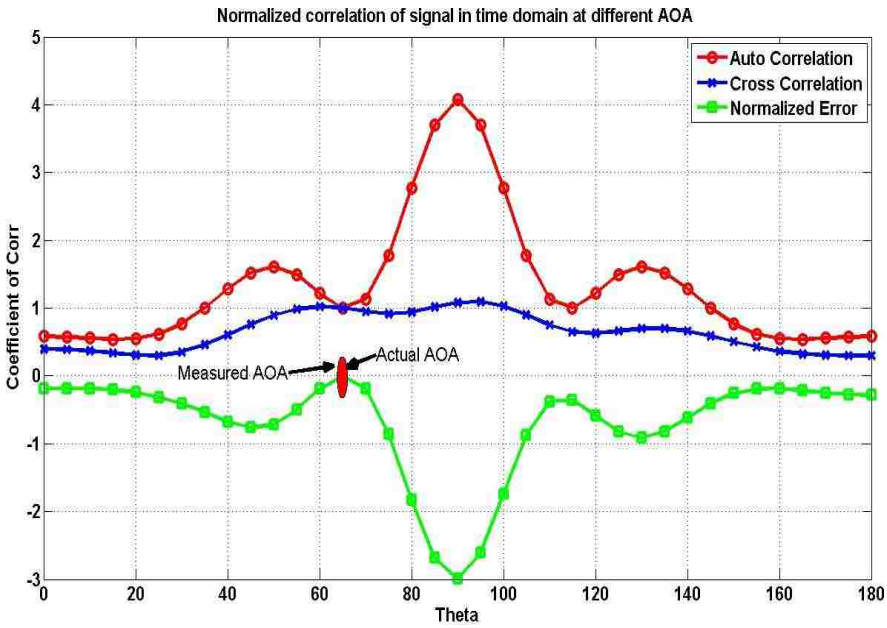

Figure 3.14. Correlation coefficient vs AOA (AOA = 65^{o})

4. CONCLUSION

Array detectors connected to a UAV can be used for detection of devices under certain environmental conditions. When devices are buried under ground or in presence of obstructions, UAV based detection works best. The error of AOA detection increases as the UAV moves away from the device. A 4-element array connected to a UAV can be used to simulate a bigger 1-D array or a 2-D array. Initial results for detection of angle of arrival for different locations have been presented and also the use of a mobile UAV setup for creating bigger 1D array and 2D arrays has been explored.

The proposed normalized error correlation function shows reduced error in estimation the angle of arrival (AoA) when compared with the power-based AOA method. In case of reflections/multipath, the power based AOA fails to detect the device and often mistakes the reflected AoA as the actual direction to the source. Detection with correlation method overcomes the effect of multipath and reflection and improves the AoA estimation accuracy with an error less than the resolution of processing and measurements. The proposed correlation based approach can potentially be used to differentiate two independent sources as well.

5. REFERENCES

[1] Thotla, V.; Zawodniok, M.J.; Jagannathan, S.; Ghasr, M.T.A.; Agarwal, S., "Detection and Localization of Multiple R/C Electronic Devices Using Array Detectors," *Instrumentation and Measurement, IEEE Transactions on* , vol.64, no.1, pp.241,251,Jan.2015.

[2] Thotla, Vivek; Ghasr, M.T.A.; Zawodniok, M.; Jagannathan, S.; Agarwal, S.;, "Detection and localization of multiple R/C electronic devices using array detectors," Instrumentation and Measurement Technology Conference (I2MTC), 2012 IEEE International , vol., no., pp.1687-1691, 13-16 May 2012.

[3] Thotla, Vivek; Zawodniok, M.;, "Hurst parameter based detection of multiple super regenerative receivers (SRR) using MVDR," Instrumentation and Measurement Technology Conference (I2MTC), 2014 IEEE International, 12-15 May 2014.

[4] Thotla, V.; Zawodniok, M.; Jagannathan, S.; Agarwal, S., "Correlation based detection and localization of R/C electronic devices using array detectors," *Instrumentation and Measurement Technology Conference (I2MTC), 2013 IEEE International* , vol., no., pp.1636,1639, 6-9 May 2013.

[5] Jake Hertenstein and S. Jagannathan,,"Detection of unintended electromagnetic emissions from super regenerative receivers," Proc. SPIE 8017, 80170F (2011); doi:10.1117/12.883223.

[6] Thotla, Vivek.; Ghasr, M.T.A.; Zawodniok, M.J.; Jagannathan, S.; Agarwal, S., "Detection of Super-Regenerative Receivers Using Hurst Parameter," Instrumentation and Measurement, IEEE Transactions on , vol.62, no.11, pp.3006,3014, Nov. 2013.

[7] Ghasr, M.T.; Thotla, V.; Zawodniok, M.J.; Sarangapani, J., "Detection of Super Regenerative Receiver Using Amplitude Modulated Stimulation," Instrumentation and Measurement, IEEE Transactions on , vol.62, no.7, pp.2029,2036, July 2013.

[8] H. Zargarzadeh ; David Nodland ; Thotla Vivek ; S. Jagannathan; S. Agarwal;, "Neural-network-based navigation and control of unmanned aerial vehicles for detecting unintended emissions". Proc. SPIE 8387, Unmanned Systems Technology XIV, 83870H , May 1, 2012.

[9] Colin Stagner, Andrew Conrad, Christopher Osterwise, Daryl G. Beetner and Steven Grant, "A practical superheterodyne-receiver detector using stimulated emissions," IEEE Transactions on Instrumentation and Measurement, Vol. 60, No. 4, April 2011.

[10] Shaik, Haixiao Weng, Xiaopeng Dong, T.H. Hubing and D.G.Beetner," Matched filter detection an identification of electronic circuits based on their unintentional radiated emissions," In Electromagnetic Compatibility, 2006. EMC 2006. 2006 IEEE International Symposium on, volume 3, pages 853-856, August 2006.

[11] D. Beetner, S. Seguin and H. Hubing, "Electromagnetic emissions stimulation and detection system," U.S. Patent 7 464 005, Dec. 9, 2008.

[12] Haixiao Weng, Xiaopeng Dong, Xiao Hu, D.G. Beetner, T. Hubing, and D. Wunsch,"Neural network detection and identification of electronic devices based on their unintended emissions," In Electromagnetic Compatibility, 2005. EMC 2005. 2005 International Symposium, volume 1, pages 245-249, August 2005.

[13] Sarah Seguin," Detection of low cost radio frequency receivers based on their unintended electromagnetic emissions and an active stimulation," Ph.D dissertation, Missouri University of Science and Technology, Rolla, MO 2009.

[14] Jeffery B. Schodorf and Douglas B. Williams,"Array processing techniques for multiuser detection," IEEE Transactions on Communications, VOL. 45, NO. 11, November 1997.

[15] Goerlich, J.; Bruckner, D.; Richter, A.; Strama, O.; Thoma, R.S.; Trautwein, U.; , "Signal analysis using spectral correlation measurement," Instrumentation and Measurement Technology Conference, 1998. IMTC/98. Conference Proceedings. IEEE , vol.2, no., pp.1313-1318 vol.2, 18-21 May 1998

[16] Sharma, R.K.; Wallace, J.W.; , "Improved autocorrelation-based sensing using correlation distribution information," Smart Antennas (WSA), 2010 International ITG Workshop on , vol., no., pp.335-341, 23-24 Feb. 2010

2. CONCLUSION

A series of novel methods for detection of multiple R/C electronic devices has been presented. A Hurst parameter based detection method for super-regenerative receivers (SRR) has been used for detection in the first paper. Second paper presents a novel detection and localization scheme of multiple RC electronic devices called Edge-Synthetic Aperture Radar (Edge-SAR). Third paper improves detection of multiple devices by proposing a dynamic antenna-array processing method called VIVEK-MVDR-GA. Finally, a 4-element array mounted on an unmanned aerial vehicle (UAV) is proposed to overcome multipath and reflection due to environmental surroundings and improve the response time in compromised scenarios. Also, a time based correlation method is proposed for array detectors to identify the line of sight (LOS) and non-line of sight (N-LOS) signals. A normalized error correlation function has been implemented to improve the estimation of angle of arrival (AOA) in the presence of strong non-line of sight (N-LOS) signals.

VITA

Vivek Thotla was born in Hyderabad, India in 1988. His initial schooling took place at Atomic Energy Central School (DAE), Hyderabad India. He earned his bachelor's degree in Electronics and Communication Engineering from Sreenidhi Institute of Science and Technology (JNTU – Jawaharlal Nehru Technology University) at Hyderabad in 2005. He was the president of ISTE (Indian Society of Technical Education) and a member of IEEE in his bachelor's. He also received a TEQIP (Technical Education Quality Improvement Program) fellowship for his work on the Telemedicine project.

Vivek came to the United States of America in January 2010 to start his Doctorate of Philosophy in Electrical Engineering at Missouri University of Science and Technology. In May 2015 he earned his PhD in Electrical Engineering from Missouri S&T. He worked as a research assistant with Dr. Maciej Zawodniok and Dr. Jagannathan Sarangapani. His work was based on developing an algorithm for Detection, Identification and Localization of Multiple RC Electronic Devices through their Unintended Emissions. He was also responsible for implementing the concept in hardware and testing it real-time. He also earned his CLAD (Certified LabView Associate Developer) certification during his time at MS&T.